UNIVERSITY OF CATANIA
DEPARTMENT OF BIOMEDICAL AND BIOTECHNOLOGICAL SCIENCES
International Ph.D. in Basic and Applied Biomedical Sciences
XXXVI Cycle

Ph.D. Thesis

ALESSANDRO LAVORO

Role of DNA methylation in the regulation of *SLC22A17* in cutaneous melanoma

Ph.D. Tutor:
PROF. SAVERIO CANDIDO

Ph.D. Coordinator:
PROF. STEFANIA STEFANI

ACADEMIC YEAR 2022-223

ABSTRACT

Cutaneous melanoma represents one of the deadliest forms of skin cancer due to its high invasiveness and metastatic tendency. Despite recent advances in screening programs and the development of innovative therapeutic strategies (e.g. targeted therapy and immunotherapy) have allowed to ameliorate the management of cancer patients, melanoma incidence and mortality rates are constantly increasing worldwide highlighting the need for novel diagnostic and prognostic biomarkers, as well as new potential therapeutic targets. In this regard, a growing number of studies have recently highlighted that the development of cutaneous melanoma is not only associated with gene mutations but also with epigenetic alterations, which may induce the dysregulation of oncogenes and tumor suppressor genes, as well as the activation of different signaling pathways involved in cancer initiation and progression. Among the epigenetic alterations, DNA methylation is the most characterized playing a critical role in the regulation of cancer-related genes. As widely reported in the literature, promoter hypomethylation is strictly associated to activation of oncogenes. Similarly, intragenic DNA methylation seems to be actively involved in transcriptional regulatory processes; however, its functional role has not been completely elucidated yet. Of note, several studies reported that tumor microenvironment-related genes are epigenetically regulated by DNA methylation, including the *Gelatinase-Associated Lipocalin* (*NGAL*) and its receptor *Solute Carrier Family 22 Member 17* (*SLC22A17*) that are involved in iron trafficking mediating either the iron influx or efflux through the cell membrane.

On these bases, the present study aimed to investigate the role of DNA methylation in the regulation of *SLC22A17* gene expression in cutaneous melanoma, as well as the involvement of *NGAL/SLC22A17* axis in iron homeostasis and ferroptosis.

To this purpose, bioinformatic analyses were conducted by using The Cancer Genome Atlas (TCGA) and Gene Expression Omnibus (GEO) datasets to evaluate the *SLC22A17* expression and DNA methylation profiling in cutaneous melanoma and identify putative methylation hotspots as diagnostic and prognostic biomarkers. In addition, *in vitro* functional studies were conducted on different melanoma cell lines to assess the correlation between DNA methylation and expression of *SLC22A17* by 5-azacytidine (5-Aza) treatment, whereas ammonium iron (III)

citrate, 1S,3R-RSL 3, and Erastin treatments allowed to explore the role of *NGAL/SLC22A17* axis in iron trafficking and ferroptosis. In particular, the effect of ferroptosis activators was assessed in A375 cells transfected with *NGAL* and *SLC22A17* variants 1, 2, and 3. Validation study was also conducted analyzing the methylation levels of the *in silico* identified cg17199325 hotspot in FFPE melanoma and nevi samples by the custom Methylation-Sensitive Restriction Enzyme-droplet digital PCR (MSRE-ddPCR) assay to evaluate its clinical relevance as epigenetic biomarker for cutaneous melanoma.

The computational analyses showed a significant downregulation of *SLC22A17* in melanoma patients compared to healthy controls, suggesting that *SLC22A17* could act as a tumor suppressor gene. Moreover, a strong positive correlation was observed between *SLC22A17* gene/variants expression and intragenic DNA methylation. The bioinformatic results were further confirmed by the *in vitro* study on 5-Aza treated melanoma cells, which demonstrated that *SLC22A17* expression is strictly regulated by the DNA methylation status of both promoter and body regions. Interestingly, the MSRE-ddPCR analysis revealed that the DNA methylation levels of the *in silico* identified cg17199325 hotspot were higher in FFPE melanoma samples compared to nevi and related to disease progression. Finally, the A375 cells overexpressing *SLC22A17* variant 3 ($A375^{Empty/SLC22A17Var3}$) acquired resistance to iron overload and 1S,3R-RSL 3 treatment. However, the baseline sensitivity was restored by the concomitant overexpression of *NGAL* ($A375^{NGAL/SLC22A17Var3}$), indicating that *NGAL/SLC22A17* axis could play a critical role in ferroptosis of melanoma cells.

Overall, the results of this study indicated that the cg17199325 hotspot could represent a promising diagnostic biomarker of cutaneous melanoma, highlighting the regulatory role of DNA methylation on the *SLC22A17* gene expression. However, the results obtained so far need to be clinically validated in a larger cohort of melanoma patients. In addition, the involvement of *SLC22A17* variant 3 in ferroptosis resistance could pave the way to the development of novel effective strategies for the treatment of melanoma patients.

TABLE OF CONTENTS

1. INTRODUCTION

Cutaneous melanoma is one of the most common skin cancers, which is characterized by the malignant transformation of melanocytes. Of note, melanoma incidence rates have rapidly increased worldwide over the last decades, especially among fair-skinned populations of European ancestry. Moreover, it represents an important leading cause of cancer death due to its high metastatic potential and aggressiveness. However, early screening and diagnosis are generally associated with good prognosis (Lopes J et al., 2022; Rashid S et al., 2023). Therefore, awareness of the risk factors together with increased surveillance are essential to prevent metastasis and reduce mortality rate.

As widely reported in the literature, melanocyte neoplastic transformation is triggered by both modifiable and non-modifiable risk factors. Exposure to ultraviolet (UV) radiation, fair skin, nevus count, ethnicity, age, genetic predisposition, lifestyle, and suppressed immune system are well established risk factors (Leonardi GC et al., 2018). In particular, chronic and intermittent exposure to UV rays is associated to the development of approximately 70% of melanoma cases. Indeed, several studies reported that UV rays may induce oxidative stress-related DNA damage, stimulating the production of reactive oxygen species (ROS) and DNA photoproducts (Sample A and He YY., 2018). In this context, melanin plays a controversial role. Although it protects skin cells against UV-induced damage, increased melanin synthesis may lead to the overproduction of intracellular ROS, playing a pivotal role in the pathogenesis of cutaneous melanoma (Jenkins NC and Grossman D., 2013; Obrador E et al., 2019; Strashilov S and Yordanov A., 2021).

Besides UV radiation, the accumulation of genomic alterations represents another important risk factor related to melanoma initiation and progression. Notably, both germline and somatic mutations may lead to the overactivation of different signaling transduction pathways and loss of regulatory processes controlling cell cycle, proliferation, differentiation, senescence, and apoptosis (Paluncic J et al., 2016; Motwani J and Eccles MR., 2021).

Besides the established gene mutations, a growing body of studies highlighted that epigenetics is also involved in the development of several cancer types, including

melanoma (Sarkar D et al, 2015; Giunta EF et al., 2021; Karami Fath M et al., 2022). Among the epigenetic regulatory mechanisms, DNA methylation represents the most well-studied, whose aberration may induce silencing of tumor suppressor genes or activation of oncogenes (Micevic G et al, 2017). Recently, it has been reported that DNA methylation status also plays a critical role in the modulation of Tumor Microenvironment (TME). In particular, accumulating evidence showed that aberrant DNA methylation significantly affects the expression levels of TME-related genes involved in the regulation of cell cycle, cell growth, proliferation, and migration, as well as differentiation, apoptosis, and molecules trafficking (Xie Z et al., 2023; Yang J et al., 2023). Therefore, investigating the role of DNA methylation in the regulation of such genes could provide novel diagnostic and prognostic biomarkers, as well as potential drug targets for the treatment of cutaneous melanoma.

1.1 Clinicopathological features of cutaneous melanoma

Cutaneous melanoma is a malignant form of skin cancer arising from melanocytes, which are melanin-producing dendritic cells mainly localized in the basal epidermis but also found in hair follicles, uvea, mucosal surfaces, and meninges (Long GV et al., 2023). The melanocytes are responsible for the production of the melanin pigment through the hydroxylation of the amino acid tyrosine catalyzed by tyrosinase, which occurs inside specific organelles called melanosomes (Ostrowski SM and Fisher DE., 2021). Once synthesized, melanin is transported from melanocytes' dendrites to neighboring keratinocytes. The synthesis and release of melanin are induced by the melanocyte-stimulating hormone (MSH) that is produced by skin keratinocytes in response to UV radiation exposure (Leonardi GC et al., 2018). Indeed, melanin determines the skin, hair, and iris pigmentation and acts as a redox UV-absorbing agent, thus preventing DNA damage of epidermal cells. In addition, melanin shows antioxidant properties acting as an indirect scavenger of ROS induced by UV radiation (Solano F., 2020).

Cutaneous melanoma represents the most lethal type of cancer among skin tumors due to its aggressiveness and high metastasis rate. Historically, cutaneous melanoma has been classified into four subtypes based on the clinical and histologic

manifestations: superficial spreading melanoma (SSM), nodular melanoma (NM), lentigo maligna melanoma (LMM), and acral lentiginous melanoma (ALM) (El Sharouni MA et al., 2020). SSM is the most common subtype of melanoma accounting for more than 70% of all lesions and is often diagnosed in middle-aged people (Ostrowski SM and Fisher DE., 2021). SSM can develop on any site of the body, especially affecting the body regions exposed to intense and intermittent sunlight (e.g. trunk and extremities). Lesions are often asymmetrical and present irregular or unclear borders, diverse shades of brown/black, and increased dimensions. After an initial phase of radial growth, which is slow and prolonged, the tumor enters a vertical growth phase causing dermal invasion, nodule development, and ultimately bleeding and ulceration (Trindade FM et al., 2021). NM subtype mainly develops on the trunk, head, and neck but may also occur in other body regions. NM accounts for ~ 10-15% of all melanoma cases and is associated with poorer prognosis and a higher fatality rate compared to the other subtypes. Indeed, NM is generally characterized by a symmetric nodule that only shows a vertical growth phase and spreads quickly. Therefore, this melanoma subtype is often diagnosed at an advanced stage (Dessinioti C et al., 2021). LMM represents a less common form of melanoma (7-15% of all cases) and generally affects the head, neck, and hands in elderly people after years of sun exposure. The main features of this subtype include large dimensions, irregular margins, and lesions generally black or brown (Connolly KL et al., 2015). Finally, ALM represents only 2-3% of melanomas in Caucasians, while it is more frequently diagnosed in Asian and African subjects accounting for 35% of cases. ALM mainly affects elderly people, in which usually appears as a pigmented macule on the palms, soles, and under the nail bed (Goydos JS and Shoen SL., 2016).

1.2 Worldwide epidemiological data of cutaneous melanoma

Nowadays, cutaneous melanoma represents a global public health issue. Overall, it is the fifth most frequent tumor in men (5% of all cancer cases) and the seventh in women (4% of all cancer cases) (Sung H et al., 2021). The incidence has risen drastically in fair-skinned populations since the 1930s probably due to changes in tanning attitudes and increased exposure to UV radiation (Martin JM et al., 2009).

Despite the rise in incidence, the melanoma mortality rate has remained almost unchanged (Hartman RI and Lin JY., 2019). Indeed, the global incidence rate of cutaneous melanoma was 1.6% of all new cancer cases in 2018, with a mortality rate of 0.6% (Bray F et al., 2018). However, according to the GLOBOCAN database, there was only an increase in incidence (1.7%) in 2020, while there was a stabilization in the mortality rate. Worldwide, 324,635 new cases of melanoma and 57,043 deaths of melanoma occurred in 2020 for both sexes (Sung H et al., 2021). In particular, the vast majority of diagnosed cases in 2020 were patients older than 50 years old (79.7%) and males, since 174,000 cases were registered in males and 151,000 cases in females (Arnold M et al., 2022). Of note, the incidence rate is significantly affected by several factors, including geographic area, ethnicity, socioeconomic conditions, sex, and age of patients. Notably, among all the melanoma cases registered in 2020, the largest number occurred in Europe (46.4%), followed by North America (32.4%) (Arnold M et al., 2022). Conversely, melanoma incidence is low in African and Asian countries (2.1% and 7.3% of all cases, respectively), indicating that pigmented skin of non-Caucasian population is more protected compared to fair skin phototypes (Fajuyigbe D and Young AR., 2016). Interestingly, melanoma is the fifth most frequent tumor in the United States, where the incidence rate has continued to rise since 1975 growing over 300% (Saginala K et al., 2021).

Similarly, this malignant neoplasm represents one of the most common cancer in Italy, with a total of 14,900 new cases (8,100 men vs 6,700 women) and 2,065 deaths (1,193 men vs 872 women) occurred in 2020. Notably, the epidemiological data in Italy showed a similar trend to that recorded globally; indeed, the incidence rate of cutaneous melanoma increased both in men and women between 2008 and 2016, whereas the mortality rate remained stable with a total of 49,312 deaths recorded from 1982 to 2016. In addition, five-year survival rate is higher in women than in men (89% and 85%, respectively) with a total of 89,800 women living in Italy after a diagnosis of cutaneous melanoma compared to 80,100 men, indicating that the melanoma mortality rate in Italy is higher in elderly men (Briatico G et al., 2022).

1.3 Melanoma-associated risk factors

Although the exact causes of cutaneous melanoma have not been fully elucidated yet, several risk factors have been associated with the occurrence of this malignant tumor (Jitian Mihulecea CR and Rotaru M., 2023). Of note, the identified critical factors promoting melanoma development can be classified into three groups (genetic, epigenetic, and environmental), further divided into modifiable (UV radiation, lifestyle, and nutritional factors) and non-modifiable ones (phototype, genetic predisposition and heredity, atypical nevi, and immunodeficiency) (Figure 1) (Serman N et al., 2022).

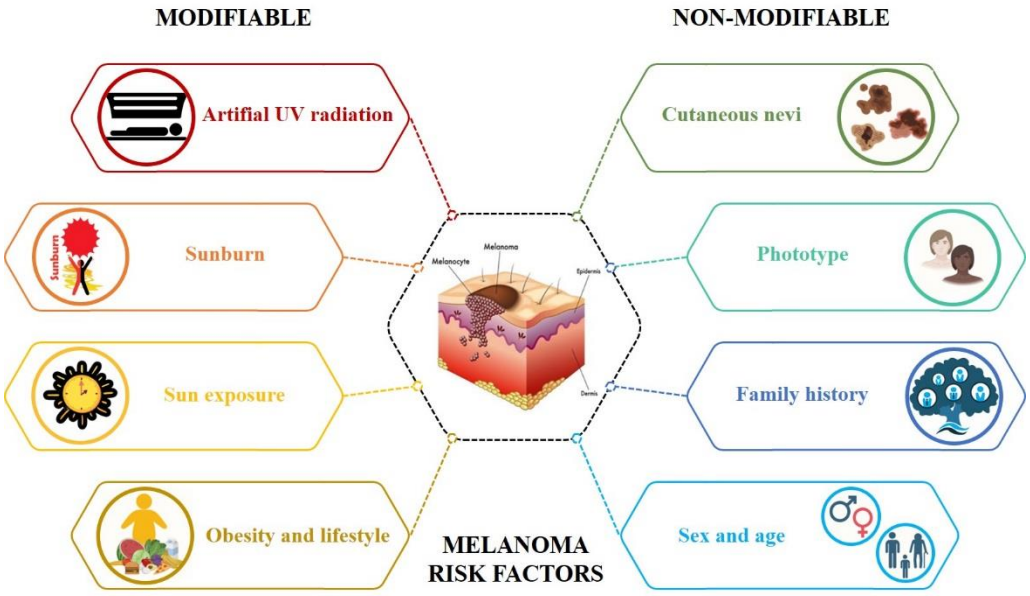

Figure 1. Main modifiable and non-modifiable risk factors related to melanoma

1.3.1 Modifiable risk factors

As widely reported in the literature, solar UV exposure represents one of the most important modifiable risk factors for cutaneous melanoma. Of note, UV radiation may be classified into three main types according to its wavelength: UVA (315-400 nm), UVB (280-315 nm), and UVC (<280 nm). Among these, UVA and UVB are the most dangerous and may induce carcinogenic skin damage, while UVC radiation is not dangerous since UVC is unable to penetrate earth's atmosphere (Sample A and He YY., 2018; Conforti C and Zalaudek I., 2021). Specifically, UVA

(95% of solar UV radiation) may penetrate deep into the dermis and cause indirect DNA damage, stimulating ROS production and increasing oxidative stress, which lead to DNA double strand breaks (DSBs) and interstrand crosslinks (ICLs) (Karran P and Brem R., 2016). Conversely, UVB (5-10% of solar UV radiation) is more genotoxic than UVA radiation and induces direct DNA damage through the formation of cyclobutane pyrimidine dimers and 6−4 photoproducts due to the cycloaddition of the C5–C6 double bonds and the addition of a covalent bond between C6-C4 of adjacent pyrimidines, respectively (Sample A and He YY., 2018). Under physiological conditions, ROS-induced toxic effects and DNA photoproducts are recognized and repaired; however, any alteration of these pathways may significantly increase the risk of cutaneous melanoma (Karran P and Brem R., 2016; Khan AQ et al., 2018)

Although previous evidence reported that chronic solar UV exposure was strictly associated to melanoma development, an increasing number of recent studies highlighted that intermittent solar UV exposure may be more damaging to exposed cells, inducing the accumulation of genetic mutations (Pinault L and Fioletov V., 2017; Arisi M et al., 2018). Notably, repeated sunburns due to intermittent sun UV exposure during childhood significantly raise the risk of skin cancer, while tanning seems to play a protective role against genotoxic effects induced by UV radiation (Behrens CL et al., 2013; Wu S et al., 2016).

Besides solar UV radiation, artificial sources of UV rays also play a critical role in melanoma development due to the higher emission of UVA compared to natural exposure (Zhang M et al., 2012). Of note, World Health Organization (WHO) has recently classified tanning beds as potentially carcinogenic since their widespread use among young people led to an increase of melanoma cases in the last few years (Dessinioti C and Stratigos AJ., 2022). In this field, primary prevention strategies should be enhanced to reduce the exposure to these risk factors, especially among younger individuals. For instance, the use of protective creams with high sun protection factor (SPF), hats, and sunglasses represent a valuable strategy to limit sunburns. Similarly, avoid sun UV exposure during midday hours and the use of tanning beds may significantly contribute to reduce the risk of cutaneous melanoma (Lagacé F et al., 2023; McKenzie C et al., 2023).

Other well-defined modifiable risk factors are represented by lifestyle and dietary habits. Of note, numerous studies reported that a diet rich in fruits, vegetables, whole grains, and legumes significantly reduces melanoma risk since these foods are characterized by a high content of antioxidants, vitamins, minerals, fibers, and phytochemicals (Yang K et al., 2018; Malagoli C et al., 2019). In this regard, Mediterranean diet may be considered a typical example of balanced diet with beneficial effects on health status. Notably, several studies highlighted that a regular intake of fatty fish, an important source of omega-3 fatty acids, as well as olive oil, may contribute to skin health (Noel SE et al., 2014; Mahamat-Saleh Y et al., 2020). Conversely, daily lifestyle based on tobacco smoking, heavy alcohol consumption, poor physical activity, diets high in red meats and refined carbohydrates is associated with an increased risk of skin cancers (Sawada Y and Nakamura M., 2021). Although both obesity and high body mass index (BMI) are important cancer-associated risk factors, their role in cutaneous melanoma development has not been fully elucidated yet. Interestingly, previous studies showed that overweight/obese people (> 50 years old) are exposed to a higher risk of melanoma compared to healthy weight individuals (Dobbins M et al., 2013; De Giorgi V et al., 2017). More recently, it has been reported that obesity and high BMI are positively associated with clinical outcomes of melanoma patients, termed as "obesity paradox". Specifically, the overall survival (OS) of obese patients was 2-fold higher than melanoma patients with normal BMI (Hayes AJ and Larkin J., 2018; Smith LK et al., 2020). Therefore, additional studies should be undertaken to provide a better understanding of the interplay between obesity and cutaneous melanoma.

1.3.2 Non-modifiable risk factors

Skin pigmentation is a major non-modifiable risk factors for cutaneous melanoma. In this regard, Fitzpatrick Scale was developed in 1972 to classify phototypes based on skin color and tendency to burn or tan following solar UV exposure, as well as hair and eye color (Gupta V and Sharma VK., 2019). Specifically, this classification system includes six different skin phototypes of which I-IV skin types refer to people with fair skin, whereas V and VI subtypes for people with dark skin (Table 1).

Table 1. Skin phototypes according to Fitzpatrick classification

Type	Characteristics	Sunburn potential
I	Pale/freckled skin, red/blond hair, blue/green/grey eyes	Always burns, never tans
II	Fair skin, blond/brown hair, all eye colors	Burns easily, sometimes tans
III	Light brown skin and hair, brown/grey eyes	Tans easily, sometimes burns
IV	Olive skin, dark brown hair, brown eyes	Tans easily, rarely burns
V	Medium brown skin, dark brown/black hair, brown eyes	Tans easily, rarely burns
VI	Dark skin, black hair, dark brown eyes	Tans easily, never burns

Of note, subjects belonging to phototypes I and II with fair skin, red/blond hair, blue/green eyes, and freckles are more exposed to genotoxic effects caused by sun UV radiation and risk of skin cancers compared to phototypes V and VI (Grigore M et al., 2018). Indeed, differences in skin pigmentation and response to UV radiation are strictly related to melanin pigment and its relative composition (eumelanin/pheomelanin ratio). Specifically, fair skin phototypes are characterized by high pheomelanin content, which is phototoxic and unable to adequately protect against UV rays. Conversely, eumelanin pigment of dark skin phototypes (types V and VI) shows antioxidants properties, protecting skin from UV damage and reducing ROS levels (Maresca V et al., 2015; Ito S et al., 2018).

Besides skin phototype, the number and anatomical location of melanocytic nevi are predictive factors of melanoma risk (Alendar T and Kittler H., 2018; Jayasinghe D et al., 2022). Notably, recent studies highlighted that subjects with more than 100 melanocytic nevi are exposed to a 6-fold increased risk of melanoma compared to people with less than 15 nevi (Rastrelli M et al., 2014; Bhatt M et al., 2016). Although the presence of melanocytic nevi on skin surface may be considered a pivotal risk factor, it is important to note that only 20%-40% of melanomas derive from preexisting nevi, while the remaining 60%-80% of cases may originate *de novo* (Saida T., 2019).

Similarly, dysplastic nevi with ill-defined borders, uneven color, and larger than 7 mm are associated to a high risk of melanoma (Shreberk-Hassidim R et al., 2023). In particular, dysplastic nevi are mainly localized on anatomical regions not exposed to sunshine (e.g. scalp, buttocks, and breasts) and may be considered as a

continuum between common nevi and melanoma (Goldstein AM and Tucker MA., 2013). In this field, since dysplastic nevi could represent precancerous lesions evolving into melanoma, screening campaigns are important to monitor any changes in skin lesions over time, as well as to identify new suspected lesions (Weyers W., 2018; Becevic M et al., 2021).

Among non-modifiable risk factors, genetic predisposition may also play a pivotal role in melanoma pathogenesis. Of note, individuals having a first-degree relative with melanoma are exposed to a 2-fold increased risk compared with those without a family history (Read J et al., 2016; Soura E et al., 2016). In this regard, several germline mutations have been associated to melanoma development over the years, especially mutations affecting *Cyclin-Dependent Kinase Inhibitor 2A* (*CDKN2A*), *Melanocortin 1 Receptor* (*MC1R*), and *Cyclin-Dependent Kinase 4* (*CDK4*) (Law MH et al., 2012; Toussi A et al., 2020). Moreover, germline mutations may also occur in DNA repair genes, including *Microphthalmia-associated Inducing Transcription Factor* (*MITF*), *Telomerase Reverse Transcriptase* (*TERT*), and *BRCA1 associated protein-1* (*BAP1*) (De Simone P et al., 2017; Stolarova L et al., 2020). As recently reported, individuals with a family history of melanoma inheriting such germline mutations are exposed to 70% increased lifetime risk of skin cancers (Wei EX et al., 2019).

Similarly, melanoma risk is enhanced in subjects with a previous diagnosis of Familial Atypical Multiple Mole Melanoma (FAMMM) syndrome, an autosomal dominant genodermatosis characterized by multiple melanocytic nevi on skin surface with variable size and color. Notably, 50%-80% of FAMMM patients develop melanoma before 40 years old, especially those with more than 50 dysplastic nevi (Lynch HT and Shaw TG., 2016). In addition, Li-Fraumeni syndrome represents another autosomal dominant syndrome strictly related to an increased risk of developing melanoma (Sandru F et al., 2022).

Human Immunodeficiency Virus (HIV) infection has been also described as a potential risk factor for cutaneous melanoma. In particular, recent studies reported that HIV-positive patients had a 2-fold increased risk of skin cancers compared to uninfected subjects, especially elderly people chronically exposed to UVB radiation (Olsen CM et al., 2014; Marra A et al., 2017). Although the incidence rate of

melanoma among HIV-positive patients seems to be associated with impaired immune response, further studies are mandatory to better clarify the potential relationship between HIV infection and skin cancer risk (Facciolà A et al., 2020).
Other non-modifiable risk factors are associated to melanoma, including age, sex, and ethnicity. Of note, recent evidence showed that males are more likely to be affected by skin cancer than females (2.5-fold increased risk of melanoma) (Collier V et al., 2021); however, sex disparity in cancer risk changes by age. In particular, women aged between 18-50 years old and men over 60 are at higher risk for cutaneous melanoma compared to the opposite-sex groups (Schwartz MR et al., 2019). In addition, it has been reported that fair-skinned Caucasian individuals are more exposed to melanoma risk compared to African and Asian subjects (Ward-Peterson M et al., 2016).

1.4 Classification and management of cutaneous melanoma

The current classification of cutaneous melanoma refers to the American Joint Committee on Cancer (AJCC) system, which is periodically updated to reflect advances in understanding of disease. The AJCC staging system is based on the following TNM scoring parameters: primary tumor size and extent (T), lymph node involvement (N), and presence of metastases (M). The combination of these parameters allows to distinguish cutaneous melanoma into different groups. Specifically, stages I and II include melanomas localized to epidermis (< 1 mm and 1-4 mm thick, respectively), stage III refers to melanoma cases with lymph node involvement, while stage IV patients are characterized by distant metastases to other organs, including brain, lungs, liver, bones, and gut (Figure 2) (Garbe C et al., 2022).

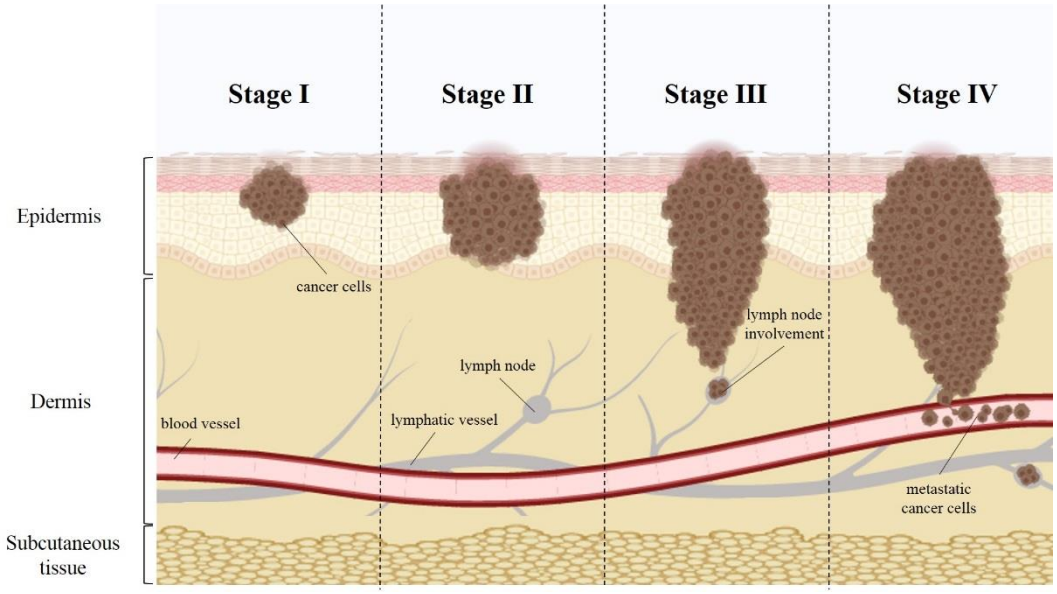

Figure 2. Schematic representation of cutaneous melanoma staging

Of note, the staging of cutaneous melanoma is also based on other important parameters, such as Clark's level and Breslow thickness. Briefly, Clark's level, a classification system developed by Wallace H. Clark Jr. in 1969, refers to the epidermal invasion to evaluate melanoma severity and aggressiveness. Notably, the Clark scale consists of five invasion levels, of which the highest levels represent negative prognostic factors for melanoma patients (Table 2) (Clark WH Jr et al., 1969).

Table 2. Clark's classification system

Level	Histological features
I	Lesion is limited to the epidermis (Melanoma *in situ*)
II	Cancer cells invade the papillary dermis
III	Tumor invades the junction of the papillary and reticular dermis
IV	Cancer cells penetrate the reticular dermis
V	Melanoma extends beyond the dermis into the subcutaneous tissue

Breslow's index, introduced by the pathologist Alexander Breslow in 1970, represents another critical parameter to assess the thickness of cancer lesions. In

particular, tissue biopsy analysis is based on the measurement of the vertical distance between the epidermis surface and the deepest point of cancer cell invasion. This classification method is composed of four different stages typically expressed in millimeters (Table 3) (Breslow A., 1970).

Table 3. Breslow's classification system and related survival percentage of melanoma patients

Level	Breslow's depth	5-year survival
I	≤ 0.75 mm (equivalent to Clark level II)	80% - 90%
II	0.76 mm – 1.50 mm (equivalent to Clark level III)	70% - 80%
III	1.51 mm – 4 mm (equivalent to Clark level IV)	60% - 70%
IV	≥ 4 mm (equivalent to Clark level V)	≤ 50%

Interestingly, melanoma patients with larger Breslow thickness are associated with a high risk of metastasis and poor prognosis due to the infiltration of subcutaneous tissue and vessels (Table 3) (Rashed H et al., 2017). In addition to Clark's level and Breslow's depth index, other important parameters for melanoma staging are ulceration, presence of mitotic figures, vascular invasion, and tumour-infiltrating lymphocytes (TILs) (Scolyer RA et al., 2020).

1.4.1 Available strategies for the diagnosis of cutaneous melanoma

Cutaneous melanoma is frequently diagnosed at advanced stages due to lack of early symptoms and clinical signs during its development. In this field, the early detection of precancerous lesions, as well as the identification of new cancer-related biomarkers, could significantly enhance the prognosis of melanoma patients and, consequently, reduce the mortality rate.

Currently, the available guidelines for diagnosis of cutaneous melanoma are based on different non-invasive or minimally invasive approaches, including skin self-exam and clinical examination performed by a dermatologist. Since dysplastic nevi and early melanomas are mainly localized on the epidermis surface, skin examination of the suspected lesions may be performed using non-invasive methods. In this regard, the so-called "ABCDE" criteria were introduced since 1985

to evaluate typical morphological signs of suspicious lesions. Specifically, the acronym “ABCDE” is based on the evaluation of lesion’s macroscopic features, such as asymmetry (A), border irregularity (B), color variation (C), diameter > 6 mm (D), and evolution rate of lesion (E) (Duarte AF et al., 2021). Besides “ABCDE” criteria, “EGF” acronym represents an important parameter for the detection of aggressive nodular melanoma. In particular, “E” (Elevated) refers to the raised appearance of nodule-like lesion on cutaneous surface, “F” (Firm) indicates the fibrous consistency of lesion to the touch, while “G” (Growth) refers to the rapid and progressive growth of lesion (García-Lozano JA et al., 2019). Of note, Glasgow 7-point checklist (7PCL) is another method to distinguish a benign pigmented skin lesion from early melanoma assigning a score based on the presence or absence of specific criteria. Briefly, 7PCL is composed of seven criteria, of which three main parameters focusing changes in size, shape, and color, and four additional criteria referred to diameter > 7 mm, inflammation, crusting or bleeding, and sensory changes (Walter FM et al., 2013). However, 7PLC is not widely used due to its complexity compared to the aforementioned criteria.

Although the reported criteria play a critical role in primary prevention, the gold standard strategy for diagnosis of cutaneous melanoma is represented by dermatological examination. In this field, dermoscopy, also known as dermatoscopy or epiluminescence microscopy, is a non-invasive diagnostic technique used by trained dermatologists to identify potential skin lesions. Notably, dermoscopy involves use of a handheld device (i.e. polarized and non-polarized dermatoscopes), which provides a magnified and illuminated view of skin's surface (Holmes GA et al., 2018). This non-invasive method allows detecting morphological alterations and skin lesion features, including pigment networks, streaks, irregular dots/globules, and vascular patterns. In addition, digital dermoscopy represents a valuable strategy for monitoring changes of existing lesions over time (Thomas L and Puig S., 2017). Notably, baseline snapshot of nevi may be collected and compared to regular dermoscopic examinations to detect any signs of malignant transformation. Dermoscopy shows both high sensitivity and sensitivity for the early detection of cancerous lesions and significantly reduces the number of false-negative diagnoses in melanoma screening (Davis S et al., 2020).

Other non-invasive techniques for the early diagnosis of melanoma are Total Body Photography (TBP), Reflectance Confocal Microscopy (RCM), and Optical Coherence Tomography (OCT). In particular, TBP is a high-resolution imaging technique used to obtain a detailed visual record of the patient's skin surface. TBP is a valuable tool for monitoring skin lesions and significantly improves the diagnostic accuracy of melanoma, especially in high-risk individuals (Hornung A et al., 2021). Similarly, RCM is an advanced imaging technique able to provide real-time and high-resolution images of the skin at the cellular level. RCM is more sensitive and specific than conventional dermoscopy, showing a great potential for the assessment of lesions difficult to diagnose (Dinnes J et al., 2018). Finally, OCT is a laser-based imaging methodology that may be employed to retrieve cross-sectional 2-D and 3-D images of the skin, allowing to define lesion depth and borders. However, OCT is not typically used as primary strategy for melanoma diagnosis due to its low sensitivity in detecting early cases (Rajabi-Estarabadi A et al., 2019).

The reported non-invasive methodologies represent valuable diagnostic strategies; however, the accurate diagnosis of cutaneous melanoma is mainly based on the analysis of biopsy specimens to evaluate the histological features of melanocytic cells and establish their malignant potential. In this regard, complete excisional biopsy is the gold standard method for defining the clinical stage since it resects the lesion beyond its margins (1-2 mm) (Pavlidis ET and Pavlidis TE., 2022). Other biopsy techniques include incisional, punch, and shave biopsy. In particular, incisional biopsy allows removing a small part of suspected lesion and is generally indicated for large lesions (> 2 cm in diameter) localized on the face. Conversely, punch biopsy is performed using a circular cutting tool to retrieve a small portion of lesion, while shave biopsy (superficial or deep scallop) allows to obtain a thin layer of suspected lesion by shaving (Ahmadi O et al., 2021; Greenwood JD et al., 2022). However, punch and shave biopsy are less commonly used and may potentially due to partial sampling and underestimation of the lesion that may lead to misdiagnosis (Shellenberger RA et al., 2020). Interestingly, Sentinel Lymph Node (SLN) biopsy is another diagnostic procedure to detect if cancer cells have spread to nearby lymph nodes. Briefly, SLN biopsy is based a radioactive tracer to

identify and remove the SLNs that have received drainage from the primary tumor (Dogan NU et al., 2019).

Currently, different cancer-related biomarkers are used in clinical practice for the early diagnosis of cutaneous melanoma, as well as to predict patient prognosis and guide treatment decisions. Specifically, serum S100 calcium-binding protein B (S100B) and lactate dehydrogenase (LDH) levels are promising biomarkers for melanoma relapse (Gassenmaier M et al., 2021; Janka EA et al., 2021). In addition, gene mutation detection and gene expression profiling provide key information regarding tailor treatment plans and clinical outcomes of melanoma patients (Yang K et al., 2020; Naik PP., 2021). Interestingly, a number of recent studies focused on circulating tumor DNA (ctDNA) and DNA methylation hotspots to evaluate their potential as diagnostic and prognostic biomarkers; however, further studies are mandatory to validate their application in clinical practice for the early diagnosis of cutaneous melanoma (Aleotti V et al., 2021; Tivey A et al., 2022).

1.4.2 Therapeutic approaches for the treatment of cutaneous melanoma

Treatment and management of cutaneous melanoma may vary depending on patient's health status and age, stage, extent of the disease, genetic mutations, and potential side effects associated with treatment options. Currently, surgery represents the first-line treatment strategy for stage I melanomas by wide local excision to remove lesion beyond its margins (1-2 mm of normal skin) (Burke EE and Sondak VK., 2018). Of note, surgical excision of early-stage melanomas significantly reduces the recurrence risk, enhancing 5-years OS rate of cancer patients (Conic RZ et al., 2018). However, surgery is ineffective for advanced and metastatic melanomas due to the extension of the tumor bulk that is difficult to remove completely (Testori AAE et al., 2019). Therefore, advanced melanoma patients generally undergo other therapeutic approaches, including chemotherapy, targeted therapy, immunotherapy, or radiotherapy.

Until the last decade, chemotherapy represented the only therapeutic strategy for treatment of advanced melanoma. Notably, the cell cycle alkylating agents dacarbazine and temozolomide were the most used chemotherapy drugs for malignant metastatic melanoma due to their cytotoxic effects on cancer cells (Luke

JJ and Schwartz GK., 2013). However, it has been widely demonstrated that melanoma is not highly responsive to standard chemotherapy (response rate < 20%). Currently, chemotherapy is generally used as palliative care for melanoma cases with no effective treatment options (Wilson MA and Schuchter LM., 2016).

Over the years, standard chemotherapy has been substituted by targeted therapy, especially for treatment of melanoma patients harboring *BRAF* and *MEK* mutations. Several recent studies highlighted that targeted therapy drugs are effective to block molecular pathways driving cancer cells growth and proliferation. Moreover, it has been reported that targeted therapy-related side effects are more manageable than chemotherapy (Kee D and McArthur G., 2014; Wong DJ and Ribas A., 2016). Approved targeted therapy drugs for cutaneous melanoma are represented by BRAF inhibitors and MEK inhibitors. Specifically, BRAF inhibitors include Vemurafenib, Dabrafenib, and Encorafenib and are used for the treatment of cancer patients with *BRAF*-mutant melanoma, whereas the most common MEK inhibitors are Cobimetinib, Trametinib, and Binimetinib (Grimaldi AM et al., 2017; Proietti I et al., 2020). Interestingly, combination therapies based on BRAF and MEK inhibitors (Vemurafenib + Cobimetinib and Dabrafenib + Trametinib) significantly improved clinical outcomes and quality life of melanoma patients. Similarly, Encorafenib + Binimetinib combined therapy also showed higher effectiveness and lower toxicity than monotherapy (Eroglu Z and Ribas A., 2016; Subbiah V et al., 2020). Furthermore, recent studies focused on *PIK3CA*-mutant melanoma to explore potential effectiveness of combination therapies based on BRAF/MEK inhibitors and PI3K inhibitors in reducing treatment resistance (Aasen SN et al., 2019; Candido S et al., 2022a).

Recently, immunotherapy has completely revolutionized treatment and management of advanced melanoma patients. In particular, immunotherapy drugs are designed to stimulate immune response against cancer cells, targeting specific molecules or pathways involved in immune activity inhibition (Ralli M et al., 2020). Of note, immune checkpoint inhibitors (ICIs) are the most used to bind and block inhibitory checkpoint receptors expressed by both cancerous cells and immune cells. The approved ICIs for treatment of cutaneous melanoma include anti-Programmed Cell Death Protein 1 (PD-1) and anti-Cytotoxic T-Lymphocyte-

associated Antigen 4 (CTLA-4) monoclonal antibodies (Seidel JA et al., 2018). Ipilimumab represents the first Food and Drug Administration (FDA)-approved CTLA-4 blocking antibody for treatment of melanoma, while Nivolumab and Pembrolizumab are the most used anti-PD-1 monoclonal antibodies (Jain S and Clark JI., 2015; Ivashko IN and Kolesar JM., 2016). Interestingly, recent studies reported that combined anti-PD-1 and anti-CTLA-4 checkpoint blockade was more effective than monotherapy for treatment of metastatic melanoma patients, resulting in a significant increase of OS rate (> 55%) (Willsmore ZN et al., 2021; Wong JSL et al., 2021).

Vaccine therapy is another type of immunotherapy aiming to stimulate immune response against cancer cells. At this regard, Slingluff and colleagues reported that 6-Melanoma Helper Peptide (6-MHP), a peptide-based vaccine designed to induce the helper T cell responses to melanoma antigens, induced immune response in a large percentage of melanoma patients, enhancing their progression free interval (PFI) (Slingluff CL Jr et al., 2013). Therefore, multi-peptide vaccines findings encourage further studies to validate their application combined with other available therapies.

Radiotherapy, also known as radiation therapy (RT), may be considered a valuable treatment option for cutaneous melanoma. Specifically, RT uses high-energy X-rays or photons to damage and kill cancer cells. RT is generally employed as adjuvant therapy after surgery to reduce recurrence risk. Moreover, RT may be also used as palliative care for advanced melanoma patients with brain and bone metastases (Dabestani PJ et al., 2021). Interestingly, the combination of RT and ICIs showed promising results, improving clinical outcome of cancer patients (Tagliaferri L et al., 2022). However, large and well-designed clinical trials should be undertaken to confirm such evidence.

Finally, photodynamic therapy (PDT) is a minimally invasive therapeutic strategy for superficial spreading melanoma and precancerous lesions. Briefly, PDT is a topic treatment based on a photosensitizing agent activated by laser light. Followed the absorption of photosensitizing agent by cancer cells, the treated area is exposed to a wavelength of light activating photosensitizer to produce ROS and destroy

cancer cells. However, PDT may require multiple sessions depending on the extent of melanoma (Baldea I et al., 2018; Naidoo C et al., 2018).

1.5 Signaling pathways and genetic alterations involved in melanoma development

Over the years, several studies highlighted that neoplastic transformation of melanocytes is due to progressive accumulation of genetic alterations, which lead to aberrant gene expression and activation of different molecular pathways associated with melanoma initiation and development. Of note, both germline and somatic mutations play a critical role in tumorigenesis, inducing the up-regulation of oncogenes or down-regulation of tumor suppressor genes and, consequently, alteration of signaling pathways involved in cell proliferation and apoptosis regulation, especially the Mitogen-Activated Protein Kinase (MAPK) and Phosphoinositide 3 Kinase / Protein Kinase B / Mammalian Target of Rapamycin (PI3K/Akt/mTOR) pathways (Amaral T et al., 2017; Chamcheu JC et al., 2019).

1.5.1 MAPK and PI3K/AKT/mTOR pathways

The MAPK and PI3K/Akt/mTOR pathways are essential signaling pathways in cutaneous melanoma oncogenesis, whose constitutive activation leads to abnormal proliferation of pre-malignant melanocytes (Leonardi GC et al., 2018). The MAPK pathway is one of the most well-characterized signal transduction pathways regulating different of biological processes. Briefly, the MAPKs cascade (Ras/Raf/MEK/ERK) is activated by extracellular ligands, including Epidermal Growth Factor (EGF), which bind to their receptors (e.g. EGF receptor) and induce the tyrosine kinase activity of the cytoplasmic domain, resulting in receptor dimerization and transphosphorylation on tyrosine residues. Then, the activated receptor recruits Growth factor receptor-bound protein 2 (Grb2), which in turn binds guanine nucleotide exchange factors (GEFs) (e.g. Son of Sevenless, SOS) by Sequence homology 2 (SH2) (Braicu C et al., 2019; Ullah R et al., 2022). Ras activation is induced by GEFs, mediating the conversion of inactive Ras-Guanosine diphosphate (GDP) to active Ras-Guanosine triphosphate (GTP). Consequently, activated Ras serves as a molecular switch by recruiting Raf serine/threonine

kinases (e.g. Raf-1, A-Raf, and B-Raf), whose phosphorylation activates the signaling cascade of downstream proteins, such as MEK1/2 and Extracellular signal-regulated kinase 1/2 (ERK1/2) (Savoia P et al., 2019). Finally, activated ERK translocates into the nucleus to phosphorylate various nuclear transcription factors (TFs) and other targets, resulting in the up-regulation or down-regulation of specific genes involved in the regulation of cell growth and proliferation, differentiation, migration, survival, apoptosis, and other cellular processes (Figure 3) (Guo YJ et al., 2020).

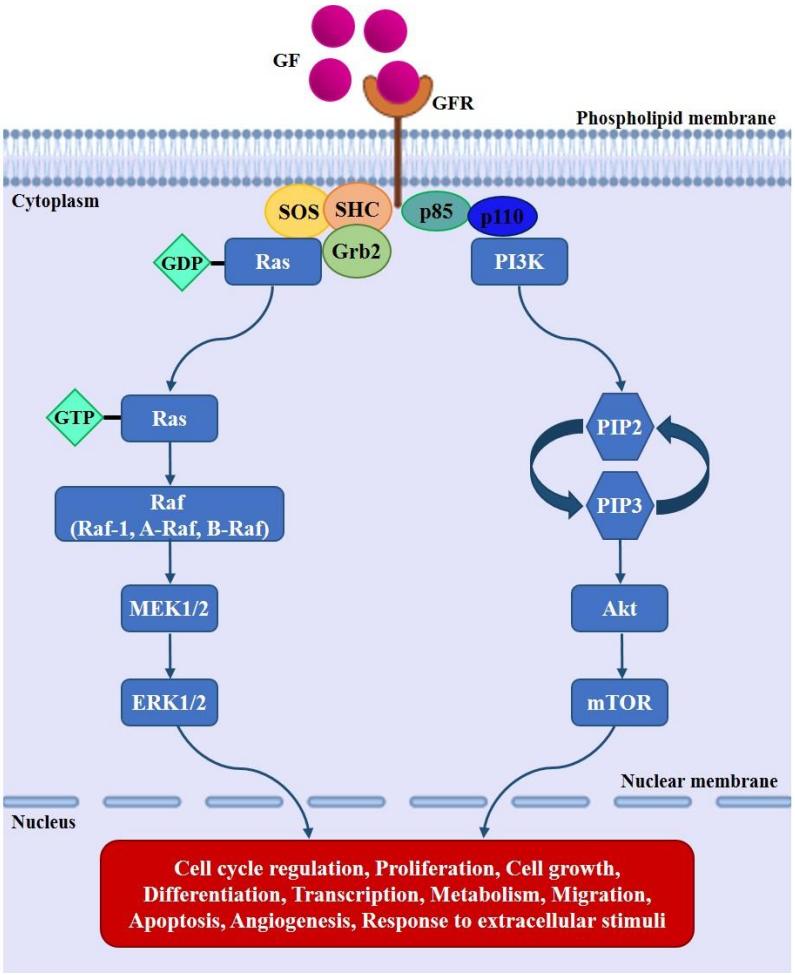

Figure 3. The MAPK and PI3K/Akt/mTOR signaling transduction pathways

Under physiological conditions, the MAPK pathway is regulated through a negative feedback phosphorylation by ERK1/2 to produce the correct biological response (Lake D et al., 2016). However, its dysregulation may lead to uncontrolled cell

growth and development of different cancer types, including melanoma. Of note, *BRAF* and *N-Ras* activating mutations are the most common genetic alterations affecting melanoma patients (50%-70% and 15%-30% of melanoma cases, respectively), which lead to the constitutive activation of the MAPK pathway driving cancer cell proliferation and survival (Wellbrock C and Arozarena I., 2016). In this regard, targeted therapy based on BRAF/MEK inhibitors allowed obtaining striking clinical response in melanoma patients harboring these genetic mutations (Yaeger R and Corcoran RB., 2019).

The PI3K/Akt/mTOR pathway, also known as PI3K/Akt pathway, represents another important signaling pathway involved in the regulation of different biological functions in response to extracellular stimuli (Ersahin T et al., 2015). Under physiological conditions, Receptor Tyrosine Kinases (RTKs) are activated by extracellular signals (e.g. growth factors, cytokines, and hormones), whose activity induces the conversion of Phosphatidylinositol [4,5]-bisphosphate (PIP2) into Phosphatidylinositol [3,4,5]-trisphosphate (PIP3) by PI3K (Fruman DA et al., 2017). PI3K is a lipid kinase enzyme composed of two regulatory subunits (p85 and p55) and a catalytic subunit (p110). Of note, PI3Ks may be divided into three classes based on their structure and substrate. Among these, class I PI3K contains different catalytic subunits (e.g. p110α produced from Phosphatidylinositol 3-kinase, PI3KCA) involved lipid phosphorylation by converting PIP2 into PIP3, a key secondary messenger for the activation of different signaling proteins, such as Akt and Phosphoinositide-dependent kinase-1 (PDK1) (Yang J et al., 2019). Notably, phosphorylated Akt activates the serine/threonine kinase mTOR, which acts in two functionally distinct complexes (mTORC1/2) regulating various cellular processes. Specifically, mTORC1 is a central regulator of cell growth, proliferation, autophagy inhibition, and protein synthesis, while mTORC2 primarily regulates cell survival, cytoskeletal organization, and glucose metabolism (Figure 3) (Karagianni F et al., 2022). The PI3K/Akt pathway is tightly regulated by the tumor suppressor gene *Phosphatase and Tensin Homolog* (*PTEN*), which prevents inappropriate signaling by dephosphorylating PIP3 to PIP2 (Haddadi N et al., 2018). Dysregulation and constitutive activation of the PI3K/Akt pathway may be induced by several genetic mutations, including deletion mutations with *PTEN* loss

of function, *PI3KCA* activating mutations (e.g. H1047R, E542K, and E545K), as well as mutations affecting *Akt* (Cho JH et al., 2015; Cabrita R et al., 2020; Candido S., 2022a). In this regard, PI3K inhibitors have been recently developed to target this pathway with promising results by decreasing cancer cell proliferation. However, further studies are needed to explore the potential benefits of such therapeutic approach (Lo Russo PM., 2016).

Overall, the evaluation of molecular alterations characterizing melanoma patients is important to define the correct classification of cutaneous melanoma and establish patient-specific treatment strategy.

1.5.2 Somatic and germline mutations

Over the years, several genetic mutations have been associated to increased risk of cutaneous melanoma. Of note, somatic mutations are generally due to UV radiation exposure, which induces DNA damages by ROS production. Specifically, UVA and UVB rays may lead to the formation of 8-oxo-7,8-dihydro-2'-deoxyguanosine (8-oxodGuo), causing G → T transversion mutations during DNA replication (Loras A et al., 2022). Other mutational hotspots associated to UV rays may be induced by the formation of pyrimidine dimers and 6-4 photoproducts, as well as the methylation of cytosine residues, which lead to DNA fragmentation. Somatic mutations generally affect *Tumor Protenin 53* (*TP53*), a tumor suppressor gene involved in the regulation of cellular homeostasis, apoptosis, and DNA repair processes (Sample A and He YY., 2018). UV-induced somatic mutations may also affect other genes involved in the regulation of cellular processes, including *BRAF*, *N-Ras*, *Neurofibromin 1* (*NF1*), *KIT Proto-Oncogene - Receptor Tyrosine Kinase (c-KIT), Melanocyte Inducing Transcription Factor* (*MITF*), and *Telomerase Reverse Transcriptase* (*TERT*) (Day CP et al., 2017; Khan AQ et al., 2018; Loras A et al., 2022).

The *BRAF* gene encodes for a cytoplasmatic serine/threonine kinase protein (766 amino acids) composed of two regulatory domains and a catalytic domain, which play a critical role in the MAPK signaling transduction pathway. Of note, activated BRAF induces the phosphorylation of downstream proteins MEK1/2 and ERK1/2, activating the MAPK signaling cascade and, consequently, enhancing the

expression levels of genes involved in the regulation of cell growth and proliferation (Alqathama A., 2020). *BRAF* mutations cause the constitutive activation of the MAPK pathway, leading to the abnormal proliferation of pre-malignant melanocytes. Interestingly, *BRAF* mutations have been detected in 50%-70% of melanomas, of which the most common missense mutation BRAFV600E (90% of *BRAF* mutations). Specifically, the BRAFV600E mutation is due to substitution of the amino acid valine for glutamic acid in codon 600 of exon 15 (nucleotide 1799 T > A; codon GTG > GAG) (Candido S et al., 2014; Ottaviano M et al., 2021). Besides BRAFV600E, another common activating mutation (5%-10% of *BRAF* mutations) is BRAFV600K, in which the amino acid valine is replaced by lysine (GTG > AAG). Other less frequent mutations (< 5% of *BRAF* mutations) are characterized by substitution of the amino acid valine for arginine (GTG > AGG) or aspartic acid (GTG > GAT), known as BRAFV600R and BRAFV600D, respectively (Kong BY et al., 2016). Although *BRAF* mutations have been detected in a large percentage of melanoma cases and other cancer types (e.g. colorectal, ovarian, thyroid, and lung cancers), *BRAF* activating mutations alone are insufficient for tumorigenesis since other driver and passenger mutations are necessary for malignant phenotype and cancer development (Castellani G et al., 2023).

NRAS is another frequently mutated gene in cutaneous melanoma patients. Specifically, *NRAS* is a member of the RAS gene family encoding for a monomeric GTPase protein involved in different signaling transduction pathways, including the MAPK and PI3K/Akt pathways (Randic T et al., 2021). Interestingly, *NRAS* mutations have been detected in 15%-30% of all melanoma cases, of which the most frequent mutations occur at codon 61; other less frequent mutations may be found at codon 12 and 13 (Muñoz-Couselo E et al., 2017). These mutations generally lead to the constitutive activation of the NRAS protein due to the loss of its GTPase activity, resulting in the activation of the MAPK and PI3K/Akt signaling pathways and, consequently, aberrant cell growth and proliferation. As widely reported in the literature, UV radiation exposure represents an important risk factor for both *BRAF* and *NRAS* activating mutations (Leonardi GC et al., 2018). In this regard, previous studies reported that the *NRAS* and *BRAF* mutations were mutually

exclusive in melanoma patients; however, it has been recently demonstrated that both mutations may be simultaneously detected in the same melanoma specimens (Chiappetta C et al., 2015; Uguen A et al., 2016).

Although *NF1* mutations are mainly related to the development of neurofibromatosis type 1, *NF1* inhibiting mutations have been also detected in 12%-18% of melanomas (Philpott C et al., 2017). Notably, the *NF1* tumor suppressor gene encodes for neurofibromin, a GTPase-activating protein (GAP) that plays a critical role in regulating cell growth and proliferation. Briefly, neurofibromin negatively regulates Ras activation pathways, enhancing the hydrolysis of the active Ras-GTP form to the inactive Ras-GDP form (Bergoug M et al., 2020). Inhibitory mutations affecting the *NF1* gene are nonsense, missense, and frameshift mutations, which lead to the production of a truncated and nonfunctional neurofibromin protein. Recent studies showed that *NF1* loss of function mutations significantly increased drug resistance to BRAF inhibitors *in vitro* and *in vivo* (Manzano JL et al., 2016; Zhong J et al., 2022). Interestingly, it has been also reported that non-overlapping genetic mutations in *NF1*, *BRAF*, and *NRAS* are detected in at least 80% of metastatic melanoma patients (Panning A et al., 2023).

c-Kit is another gene found to be highly mutated in different melanoma subtypes, especially ALM, mucosal melanoma, and melanoma arising on sun-damaged skin. The protein product of the proto-oncogene *c-Kit* belongs to the RTKs family, whose activation is mediated by its ligand Stem Cell Factor (SCF). The SCF/c-Kit interaction leads to the activation of signaling transduction pathways involved into cell growth, differentiation, migration, and survival (Pham DDM et al., 2020). Under physiological conditions, the activation of c-Kit signaling pathway occurs during embryogenesis; however, *c-Kit* somatic mutations induce signaling pathway reactivation, promoting tumor invasion, metastases, and loss of the apoptotic process. Of note, recent studies also demonstrated that c-Kit protein levels are up-regulated in a large percentage of advanced melanoma patients (Ponti G et al., 2017; Meng D and Carvajal RD., 2019; Delyon J et al., 2020).

Other sun-induced somatic mutations have been associated to the development of cutaneous melanoma, including those affecting the *TERT* and *c-Met* genes. *TERT*

encodes a rate-limiting catalytic subunit of telomerase, which plays a pivotal role in maintaining chromosome ends by adding telomeric DNA repeats (TTAGGG repeats) (Nagore E et al., 2019). Under physiological conditions, telomerase silencing in somatic cells leads to senescence and apoptosis, while genetic mutations induce its aberrant expression promoting cell immortalization and cancer progression. Indeed, *TERT* promoter mutations have been detected in 65% of primary and metastatic melanoma cases (Hugdahl E et al., 2018). Similarly, sun-induced somatic mutations affecting the oncogene *c-Met* lead to the constitutive activation of the c-Met RTK, inducing aberrant cell proliferation and migration. However, *c-Met* activating mutations are relatively rare in cutaneous melanoma patients (Czyz M., 2018; Zhou Y et al., 2019).

Besides the reported somatic mutations, several germline mutations have been associated to melanoma development, including germline mutations affecting the *CDKN2A* and *CDK4* genes (Aoude LG et al., 2020; Stolarova L et al., 2020). Specifically, *CDKN2*A encodes for the INK4/p16 and ART/p14 proteins, which induce cell cycle arrest inhibiting phosphorylation of the Retinoblastoma (Rb) protein by CDK4/CDK6 complex and ubiquitination of p53 by Mouse double minute 2 homolog (MDM2), respectively. *CDKN2A* inhibiting mutations have been detected in a large percentage of FAMMM and in 40% of melanomas (Chan SH et al., 2021). Although most mutations affecting the *CDKN2A* gene are germline mutations, it is important to underlie that *CDKN2A* mutations may be also accumulated during the lifetime by somatic cells (Ming Z et al., 2020). *CDK4* is another cell cycle regulator gene encoding for the homonymous protein CDK4 that form a cyclin-CDK complex with its functional homologue CDK6 to promote cell cycle transition from G1 to S phase (Guo L et al., 2020). Of note, several studies reported that *CDK4* germline mutations enhancing the CDK4/CDK6 complex activity, coupled with *CDKN2A* loss of function mutations, are related to 50% increased risk of melanoma development (Kollmann K et al., 2019; Sargen MR et al., 2020).

Other germline mutations may affect genes involved in DNA repair mechanisms, such as *BAP1*, *MC1R*, and *MITF*. In particular, the *BAP1* tumor suppressor gene encodes for an enzyme belonging to the deubiquitinase superfamily that regulates

several biological processes, including DNA replication and repair, cell death, and metabolism (Carbone M et al., 2020). Of note, *BAP1* inhibiting mutations cause the increase of BRCA1 ubiquitination, leading to ineffective DNA repair and progressive accumulation of genetic mutations. *BAP1* germline mutations are frequently detected in uveal melanoma patients (47% of all cases), while somatic mutations occur in only 5% of sporadic primary melanomas (Kumar R et al., 2015; Uner OE et al., 2021). *MC1R* plays a critical role in determining skin and hair color by regulating melanin production. In this regard, recent studies reported that *MC1R* gene variants are associated to increased risk of cutaneous melanoma (Tagliabue E et al., 2018; Manganelli M et al., 2021). Similarly, the *MITF* gene is involved in melanocyte development, differentiation, and melanin production. As reported in the literature, both germline and somatic mutations induce *MITF* overexpression and, consequently, increased melanin production and cell proliferation, contributing to the pathogenesis of melanoma (Hartman ML and Czyz M., 2015; Gelmi MC et al., 2022).

1.6 Alteration of epigenetic regulatory mechanisms in cancer pathogenesis

The term epigenetics, from the Greek "ἐπί" (above) and "γεννητικός" (relative to family inheritance), was first introduced in 1942 by embryologist Conrad H. Waddington to define a new field of genetics that studies the causal interactions between genes and their cellular products leading to phenotype production (Deichmann U., 2016). Currently, epigenetics is defined as a branch of biology that investigates the stable changes in gene expression or cellular phenotype with no alterations in DNA sequence. In particular, epigenetic modifications play a crucial role in embryonic development by inducing cell differentiation and regulating gene expression levels (Tronick E and Hunter RG., 2016).

Over the years, different epigenetic modifications have been described, including DNA methylation, histone modifications, and non-coding RNAs (ncRNAs) (Berger SL et al., 2009; Skvortsova K et al., 2018). Briefly, DNA methylation consists of the transfer of a methyl group (-CH_3) to the DNA strand itself, generally to the carbon-5 position of the cytosine base within the cytosine-guanine (CpG) dinucleotide, forming 5-methylcytosine (5mC) (Angeloni A and Bogdanovic O.,

2021). As widely reported in the literature, DNA methylation play a pivotal role in the regulation of gene expression, determining genomic imprinting and recruiting gene expression-associated proteins or silencing genes in a tissue-specific manner via the inhibition of TFs binding to DNA sequence (Ehrlich M and Lacey M., 2013; Moore LD et al., 2013). Histone modifications represent another important epigenetic regulatory mechanism, which significantly contribute to chromatin condensation or decondensation influencing gene transcription (Klemm SL et al., 2019). Interestingly, the N-terminal amino acid residues of histone proteins may undergo a variety of covalent modifications (e.g. methylation, acetylation, citrullination, phosphorylation, ubiquitination, SUMOylation, crotonylation, and ADP-ribosylation) that are mediated by specific enzymes (Zhang Y et al., 2021). Similarly, gene expression levels and chromatin remodeling may be also modulated by ncRNAs, a class of RNA molecules that are transcribed from DNA but do not serve as templates for protein synthesis (Patty BJ and Hainer SJ., 2020). Specifically, ncRNAs include different RNA molecules depending on their length, including small interfering RNAs (siRNAs, 20-25 nt), long ncRNAs (lncRNAs, 200-10,000 nt), circular RNAs (circRNAs, 200-1,000 nt), small nuclear RNAs (snRNAs, 100-300 nt), small nucleolar RNAs (snoRNAs, 60-300 nt), and micro RNAs (miRNAs, 18-24 nt) (Statello L et al., 2021). In particular, microRNAs have recently attracted growing interest as potential cancer biomarkers and pharmacological targets since miRNAs are able to affect gene expression either promoting the complete degradation of target mRNAs or inhibiting protein translation (Morales S et al., 2017; Ali Syeda Z et al., 2020).

These potentially reversible modifications, also known as “epimutations”, may occur during the lifestyle due to the exposure to various environmental factors (e.g. diet, pollution, and stress). Moreover, epimutations can be transmitted from one generation to the next via cell division. Notably, when epigenetic marks affecting germ cells (ova and spermatozoa) are inherited by offspring, epimutations may have a long-lasting impact on gene expression and phenotype (Lacal I and Ventura R., 2018; Xavier MJ et al., 2019). In this regard, several studies highlighted that alteration of epigenetic regulatory mechanisms is strictly associated with several pathological conditions. Of note, epigenetic alterations have recently emerged as

key contributors of aberrant gene expression by enhancing cell sensitivity to DNA damage, cell cycle progression, as well as transcription or silencing of cancer-related genes (Ilango S et al., 2020; Recillas-Targa F., 2022; Davalos V and Esteller M., 2023). Among the reported epimutations, DNA methylation is the most well-studied epigenetic regulatory mechanism, whose alteration is related to increased risk of different tumor types, including cutaneous melanoma (Lakshminarasimhan R and Liang G., 2016; Skvortsova K et al., 2018).

1.6.1 DNA methylation and its functional role in tumorigenesis

DNA methylation is one of the most well-characterized epigenetic processes in physiological and pathological conditions. Of note, DNA methylation is required in mammalian early embryonic development to regulate parental allele-specific expression of imprinted genes, in which occurs at Imprinting control regions (ICRs) harboring differentially methylated regions (DMRs) (Elhamamsy AR et al., 2017). Moreover, X-chromosome inactivation (XCI) is associated with specific DNA methylation patterns (Sharp AJ et al., 2011). DNA methylation is also essential to guarantee preservation of genome stability and integrity by inhibiting transposable elements activation, as well as the maintenance of DNA replication timing precision (Du Q et al., 2021). Conversely, aberrant DNA methylation represents an epigenetic hallmark associated with tumor initiation and progression, leading to reduced gene expression of tumor suppressor genes and activation of oncogenes (Saghafinia S et al., 2018; Chen C et al., 2022).

Mechanistically, DNA methylation is due to the transfer of $-CH_3$ group to DNA sequence by using S-adenosyl-L-methionine (SAM) as donor provided by the methionine cycle (Jones PA., 2012). The reversible addition or removal of $-CH_3$ groups is catalyzed by specific enzymatic families, defined as “writers” and “erasers”. Interestingly, DNA methyltransferases (DNMTs) are a large group of proteins involved in *de novo* methylation and maintenance, whereas Ten-eleven translocation (TET) dioxygenases have a primary role in DNA demethylation (Guibert S and Weber M., 2013). Specifically, DNMT3 family (DNMT3A, DNMT3B, DNMT3C, and DNMT3L) is involved in *de novo* methylation during embryonic processes. In particular, DNMT3A and DNMT3B, both highly

expressed in embryonic stem cells, are the canonical DNMTs that catalyze the establishment of methylation marks on genomic DNA. DNMT3L has no catalytic function and is just an accessory protein that facilitates the methyltransferase activity of DNMT3A/B, DNMT3C has been only identified in rodents as a tandem copy of DNMT3B, while the maintenance of methylation status during DNA replication is regulated by DNMT1, which preferentially catalyzes the methylation of the hemimethylated DNA (Lyko F., 2017; Chen Z and Zhang Y., 2020). Conversely, DNA demethylation is regulated by TET family proteins (TET1, TET2, and TET3), which catalyze the sequential oxidation of 5mC into 5-hydroxymethylcytosine (5hmC), 5-formylcytosine (5fC), and 5-carboxylcytosine (5caC). In addition, passive DNA demethylation may be related to loss of function of DNMT1 during DNA replication (Wu X and Zhang Y., 2017; Ross SE and Bogdanovic O., 2019).

Although DNA methylation generally involves the C5 of cytosine within the palindromic CpG dinucleotides to form 5mC, it may also occur at N4 of cytosine, N7 of guanine, and N6 of adenine (Smith ZD and Meissner A., 2013). The CpG dinucleotides are short interspersed DNA sequences (~ 200-1000 bp), known as CpG islands, whose guanine and cytosine (GC) content is > 50%. CpG islands are not homogenously distributed throughout the genome and may be found at significantly higher densities in gene-rich compared to gene-poor areas (Han L et al., 2008; Deaton AM and Bird A., 2011). Specifically, CpG islands are typically located within and close to transcription start sites (TSS) of the promoter region (1,000 bp upstream of the TSS to 300 bp downstream of the TSS). Moreover, CpG islands may be also found in non-promoter regions, such as intragenic CpG islands, which are located between 300 bp downstream of TSS and 300 bp upstream of transcription termination site (TTS), 3'-end CpG islands (300 bp upstream of TTS to 300 bp downstream of TTS), and intergenic CpG islands (300 bp downstream of TTS to 1,000 bp upstream of TSS) (Maunakea AK et al., 2010; Rivera CM and Ren B., 2013). Under physiological conditions, CpG islands methylation status depends on specific-related gene, cell type, and environmental conditions (Angeloni A and Bogdanovic O., 2021).

As widely reported in the literature, aberrant DNA methylation represents one of the most important epigenetic alterations occurring during tumorigenesis, which may affect gene expression of tumor suppressor genes and oncogenes. Of note, the addiction of -CH_3 groups at promoter region results in gene silencing of tumor suppressor genes due to the inhibition of TFs binding to DNA motifs (Esteller M., 2007; Yamashita K et al., 2018; Bouras E et al., 2019). Moreover, Methyl CpG-binding domain proteins (MBPs) also play a critical role in the alteration of gene expression by recognizing and recruiting 5mC, which lead to condensed and closed chromatin reducing access to TFs and inhibiting transcription (Parry L and Clarke AR., 2011; Fournier A et al., 2012; Du Q et al., 2015). Conversely, hypomethylation of the promoter region may induce activation of proto-oncogenes (Figure 4) (Sizemore ST et al., 2014; Du X et al., 2019; Fu Y et al., 2021).

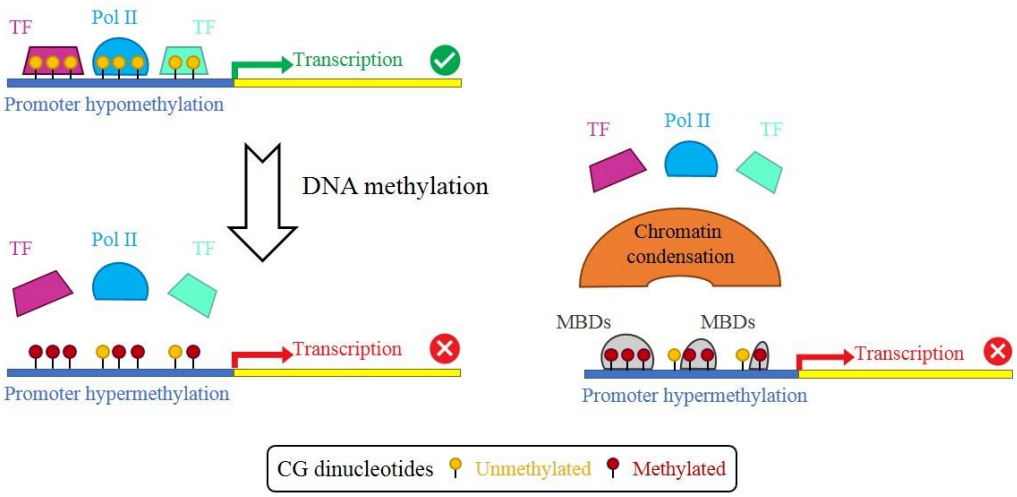

Figure 4. Promoter DNA methylation and regulation of gene expression

Although the involvement of promoter DNA methylation in gene expression regulation has been widely demonstrated over the years, the functional significance of intragenic DNA methylation has not been completely elucidated yet. In this field, a growing body of recent studies highlighted that intragenic DNA methylation could be actively involved in transcriptional regulatory processes (Hunt BG et al., 2013; Mendizabal I et al., 2017; Cain JA et al., 2022). Of note, the methylation levels of intragenic CpG islands are higher than promoter CpGs during embryonic and adult development, suggesting their role in tissue-specific reprogramming (Auclair G et

al., 2014). In particular, the methylation status of intragenic CpG islands positively affects gene expression, acting as enhancer and influencing transcriptional elongation and alternative splicing. Furthermore, gene body methylation may act as a repressor of transcription initiation from alternative transcription start sites (Figure 5) (Shenker N and Flanagan JM., 2012; Jeziorska DM et al., 2017; Neri F et al., 2017).

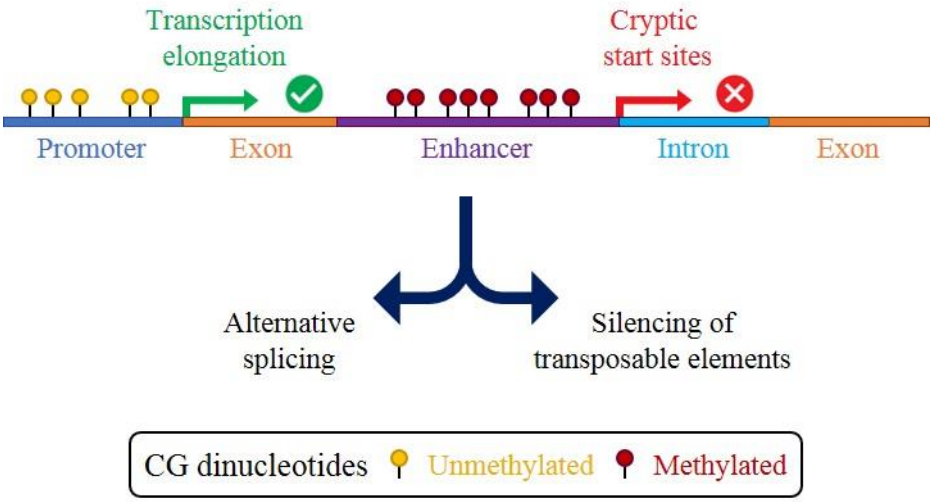

Figure 5. Intragenic DNA methylation and regulation of gene expression

Moreover, it has been reported that body methylation levels are strictly associated to replication timing. Specifically, early replicating genes showed high methylation levels within the body region, confirming the positive correlation between intragenic methylation status and transcriptional regulation (Kulis M et al., 2013). Collectively, these epigenetic hallmarks represent an attractive starting point for new tumor-related biomarkers, as well as potential targets for personalized therapies, whose application in clinical practice could enhance both the early diagnosis and management of cancer patients.

1.6.2 Aberrant DNA methylation in cutaneous melanoma

As previously reported, aberrant DNA methylation represents a specific hallmark of cancer, which results in up- or down-regulation of several genes that regulate cell growth and proliferation, DNA repair, apoptosis, transcription, and other cellular

processes (Jankowska AM et al., 2015; Pan Y et al., 2018). Interestingly, several recent studies also demonstrated the relationship between DNA methylation status and TME, a dynamic and complex microenvironment composed of tumor cells, immune cells (e.g. macrophages, T cells, B cells, and natural killer cells), and non-immune cells (e.g. fibroblasts, stromal cells, and endothelial cells) that plays a pivotal role in promoting tumor invasion and metastasis. Notably, accumulating evidence showed that aberrant DNA methylation may affect behavior of fibroblasts, as well as stromal and immune cells, promoting tumor phenotype and TME remodeling (Zhang MW et al., 2017; Xie Z et al., 2023; Yang J et al., 2023).

In this field, a growing body of studies investigated the role of DNA methylation in cutaneous melanoma development to identify new DNA methylation hotspots as potential diagnostic/prognostic biomarkers and therapeutic targets. For instance, Falzone and colleagues focused on the *MMP9* gene, whose overexpression is related to extracellular matrix degradation, tumor invasiveness, and metastasis. Specifically, the authors demonstrated that *MMP9* expression levels were positively correlated with the methylation status of the CpG2 island in different melanoma cell lines, highlighting that hypermethylation of *MMP9* intragenic region could play a critical role in melanoma development and progression (Falzone L et al., 2016). Interestingly, Jørgensen *et al.* investigated *in vitro* the modulation of DNA methylation as potential treatment option for malignant melanoma. Specifically, the authors noted that inhibition of DNA methylation through 5-aza-2'-deoxycytidine (5-aza-dC) enhanced the expression levels of *Human Leukocyte Antigen* (*HLA*)-*G*, an immune checkpoint molecule with therapeutic potential, indicating that targeting DNA methylation by DNMT inhibitors could enhance immunotherapy response of melanoma patients (Jørgensen N et al., 2020). Recently, Hoffmann *et al.* evaluated the correlation between DNA methylation status and gene expression of *Programmed Lell Death 1 Ligand 2* (*PD-L2*), an immune checkpoint receptor ligand involved in immune response regulation. Notably, the researchers found that *PD-L2* expression was negatively regulated by promoter methylation status both in cancer cell lines and melanoma patients, suggesting that *PD-L2* promoter hypomethylation and mRNA overexpression may predict a better PFI and prolonged OS in melanoma patients receiving anti-PD-1 immunotherapy

(Hoffmann F et al., 2020). Similarly, Niebel and colleagues demonstrated that DNA methylation is implicated in the regulation of *T cell immunoreceptor with Ig and ITIM domains* (*TIGIT*) gene expression, a "second generation" immune checkpoint under investigation as potential therapeutic target for cutaneous melanoma. Notably, the authors highlighted that *TIGIT* methylation status could serve as predictive biomarker in melanoma patients undergoing immunotherapy (Niebel D et al., 2022).

Although several studies explored impact of aberrant DNA methylation patterns on expression of key regulatory genes, the precise relationship between hyper- and hypo-methylation of the promoter/body regions and gene expression levels have not been completely elucidated yet and further studies are mandatory to better clarify the functional role of DNA methylation in tumorigenesis. In this field, high-throughput technologies, including Next Generation Sequencing (NGS) and microarray, has drastically enhanced the knowledge of DNA methylation status in cancer patients, providing novel insights regarding the functional role of aberrant DNA methylation. In particular, these technologies allowed the generation of large-scale data to define the whole methylome and are often publicly available for *in silico* studies aimed to identify novel DNA methylation hotspots as potential cancer biomarkers and therapeutic targets. Moreover, DNA methylation markers could provide valuable information for clinicians in assessing the disease severity and tailoring personalized treatment strategies (Barros-Silva D et al., 2018; Nikolouzakis TK et al., 2020; Merkel A and Esteller M., 2022).

1.7 Role of tumor microenvironment in cancer development and progression

The term "tumor microenvironment" (TME) refers to the complex and dynamic ecosystem surrounding a tumor with a critical role in its development and progression. Indeed, cancer cells establish myriad heterotypic interactions with non-cancerous cells and factors within TME to generate a tumor-supportive environment (Xiao Y and Yu D., 2021; De Visser KE and Joyce JA., 2023). Besides tumor cells, TME consists of a wide range of non-cancerous cells, depending on the specific tissue and tumor type. In this regard, TME hallmark features are immune cells, endothelial and stromal cells, cancer associated fibroblast (CAFs), pericytes

and other cell types (e.g., adipocytes and neurons), as well as non-cellular components, including the extracellular matrix (ECM) and released products (e.g. growth factors and extracellular vesicles), blood and lymphatic vessels (Figure 6) (Anderson NM and Simon MC., 2020).

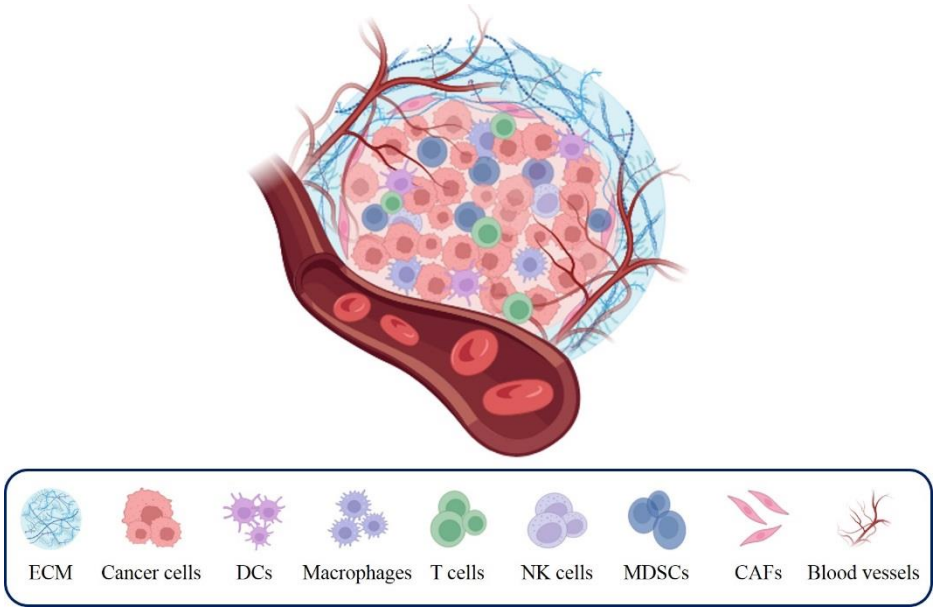

Figure 6. Cellular and extracellular components of TME

Immune cells represent one of the principal components of TME. Notably, there are two types of immune cells within TME: tumor-antagonizing and tumor-promoting immune cells (Lei X et al., 2020). Tumor-antagonizing immune cells include $CD8^+$ cytotoxic T cells, effector $CD4^+$ T cells, natural killer (NK) cells, dendritic cells (DCs), inflammatory M1 macrophages and N1-polarized neutrophils. At early stages of tumorigenesis, tumor-antagonizing immune cells are involved in cell-mediated targeting and killing of malignant cells; however, cancer cells may escape from immune surveillance through various mechanisms, including upregulation of immune checkpoint molecules, tumor-antigen loss, secretion of immunosuppressive cytokines and chemokines, as well as the release of regulatory T cells (Tregs) and Myeloid-Derived Suppressor Cells (MDSCs) (Dong Y et al., 2021). Notably, Tregs and MDSCs are the main tumor-promoting immune cells of TME, which tend to promote T-cell dysfunction and tumor development. The balance between these immune cell populations and their activity within TME is a

dynamic process that may change during cancer development and treatment, affecting clinical outcome of cancer patients (Qayoom H et al., 2023).

Another component of TME is represented by the endothelial cells, which foster tumor initiation and progression via angiogenesis. As tumor increases in size, cancer cells release several pro-angiogenic factors, including Platelet-Derived Growth Factor (PDGF), Vascular Endothelial Growth Factor (VEGF), and angiopoietins, which induce an angiogenic switch in endothelial cells. The formation of new blood vessels allows satisfying oxygen, macromolecules, and nutrient demands of malignant cells to sustain tumor growth (Sobierajska K et al., 2020; Al-Ostoot FH et al., 2021). Interestingly, the newly formed blood vessels show unique structural and functional features compared to normal vasculature. Indeed, blood vessels of tumor vasculature are generally immature, irregular, tortuous, dilated, and leaky (Ebeling S et al., 2023; Wang Q et al., 2023). Beyond angiogenesis, emerging literature data suggest that tumor endothelial cells are key regulators of immune functions within TME. Specifically, endothelial cells may induce tumor immunosuppression by reducing the recruitment of immune cells in TME and downregulating cancer cells antigen presentation (Nagl L et al., 2020; Fang J et al.,2023).

As widely reported in the literature, CAFs are the most dominant components in tumor stroma. Notably, CAFs derive from the recruitment and activation of different cell types, including resident fibroblasts, tumor-infiltrating mesenchymal stem cells (MSCs), and even differentiated epithelial cells undergoing the Epithelial-to-Mesenchymal Transition (EMT). Once activated, CAFs contribute to the remodeling of TME and sustain tumor development through several mechanisms (Liu T et al., 2019; Wright K et al., 2023). In particular, CAFs may secrete pro-angiogenic and immunosuppressive factors to inhibit immune cells activity. Moreover, CAFs are implicated in promoting cancer cell proliferation and survival, as well as resistance to cancer therapies (Lavie D et al., 2022). Interestingly, a growing body of studies recently reported that CAFs are involved in ECM remodeling. Specifically, CAFs may cause excessive ECM proteins deposition, including collagen and fibronectin, as well as the activation and overexpression of Matrix Metalloproteinases (MMPs) that play a critical role in

ECM degradation (Belhabib I et al., 2021; Yuan Z et al., 2023). ECM is a complex network of macromolecules composed of proteoglycans, glycoproteins, and various growth factors that form a physical scaffold for cellular components (Eble JA and Niland S., 2019). During tumorigenesis, ECM composition and density alterations are due to high levels of ECM proteins and collagen deposits, which result in increased ECM stiffness and degradation. Altered ECM, in turn, induces various physical signals that are mechanically transmitted to tumor cells, enhancing tumor invasiveness and metastatic dissemination (Huang J et al., 2021; Yuan Z et al., 2023).

Over the years, numerous studies have highlighted the pivotal role of TME in many cancer features, including cancer cell growth and proliferation, tumor invasiveness and immune escape, metastasis, and drug resistance. In this field, various molecules may be involved in the modulation of TME during tumorigenesis. For instance, it has been recently reported that the Neutrophil Gelatinase-Associated Lipocalin (NGAL) and Matrix Metallopeptidase-9 (MMP-9) significantly contribute to establishment and remodeling of TME, favoring tumor invasiveness and metastasis. Specifically, NGAL, also known as Lipocalin 2 (LCN2), forms a complex with MMP-9 (NGAL/MMP-9 complex) that increases MMP-9 stability and gelatinolytic activity, leading to ECM degradation and cancer cell invasion (Candido S et al., 2016; Huang H., 2018; Crescenzi E et al., 2021). Moreover, MMP-9 showed immunosuppressive effects by modulating the expression levels of inflammatory cytokines and chemokines and antagonizing T cell–mediated anti-tumor responses (Juric V et al., 2018). Interestingly, NGAL is also involved in iron trafficking by regulating either the uptake of extracellular iron or removal of intracellular iron, with different effects depending on TME context. In particular, the iron homeostasis is mediated by the interaction between NGAL and NGAL receptor (NGALR), better known as Solute Carrier Family 22 member 17 (SLC22A17) (Xiao X et al., 2017; Crescenzi E et al., 2023).

1.7.1 SLC22A17

The SLC superfamily represents a large group of over 450 membrane transport proteins organized into more than 65 families, which play a critical role in the

molecular trafficking of organic ions and biomolecules by either passive facilitative or secondary active transport mechanisms (Zhang Y et al., 2019; Pizzagalli MD et al., 2021). Interestingly, recent studies reported that SLCs may be involved in tumorigenesis by acting as oncogenes or tumor suppressor genes, depending on cancer type. Notably, the overexpression of tumor promoting SLCs seems to be associated with cancer immune escape, EMT, drug resistance, and angiogenesis. Conversely, downregulation of tumor suppressor SLCs may enhance cancer cell growth and proliferation (Rashid K et al., 2021). In addition, SLCs have been described to support cancer cell metabolism, which is characterized by high glucose consumption and subsequent lactate production even in the presence of oxygen (Warburg effect) (Song W et al., 2020).

In this field, recent evidence highlighted that dysregulation of the *SLC22A17* gene (previous name 24p3R) is implicated in development, progression, and drug resistance of several tumor types (Liu F et al., 2018; Wei J et al., 2020; Candido S et al., 2022b; Lavoro A et al., 2023). As previously reported, *SLC22A17* mediates iron homeostasis via the interaction with NGAL, resulting in *NGAL/SLC22A17* complex internalization by receptor-mediated endocytosis, while complex recycling is involved in iron efflux. Interestingly, different *SLC22A17* variants may be implicated in iron trafficking regulation. In particular, *SLC22A17* variants 1 and 2 have been described as bilateral iron transporters mediating both extracellular iron uptake and removal of intracellular iron, while *SLC22A17* variant 3 could exclusively mediate iron influx (Candido S et al., 2016; Xiao X et al., 2017). Notably, the *SLC22A17* variant 3 is characterized by an internal deletion of 125 nucleotides and producing a 207 amino acid protein with four putative membrane-spanning domains. This alternative spliced variant is mainly co-localized with NGAL protein at the cell membrane, playing a pivotal role in intracellular iron delivery. Interestingly, Fang and colleagues reported that *SLC22A17* variant 3 expression is strictly associated with esophageal cancer development, indicating that its overexpression could promote malignancy (Fang WK et al., 2007).

In this regard, many studies reported that *NGAL/SLC22A17* targeting induces intracellular iron overload and significantly increases the vulnerability of cancer cells to ferroptosis inducers (Liu J et al., 2021; Yao F et al., 2021). Similarly,

Chaudhary and colleagues investigated the relationship between ferroptosis and *NGAL/SLC22A17* complex, highlighting that NGAL contributes to reduce iron-induced oxidative stress by decreasing iron intracellular concentration in colorectal cancer cells (Chaudhary N et al., 2021). Recently, our research group conducted a multi-cancer *in silico* study on the *LCN2/SLC22A17/MMP-9* axis to evaluate the role of DNA methylation in TME remodeling. Interestingly, we reported that the expression levels of *LCN2* and *MMP-9* were upregulated in most tumor types, whereas the *SLC22A17* gene was downregulated (66.7% of tumors), suggesting that *SLC22A17* could have a tumor suppressor potential. Moreover, we demonstrated that the *LCN2*, *SLC22A17*, and *MMP-9* expression levels were negatively correlated with promoter DNA methylation status, whereas intragenic hypermethylation was strictly related to *SLC22A17* and *MMP-9* overexpression (Candido S et al., 2022b). Although *NGAL* and *MMP9* role in the modulation of TME has been widely investigated, the exact involvement of *SLC22A17* in cancer development has not been completely elucidated yet. Therefore, further studies are mandatory to clarify the relationship between *SLC22A17* and iron metabolism, whose imbalance either promotes tumor growth or induces oxidative stress–mediated ferroptosis. Moreover, the identification of underlying genetic and epigenetic regulatory mechanisms could provide novel epigenetic cancer hallmarks with diagnostic and prognostic values and suitable for epi-drug targeting.

1.8 Ferroptosis as a potential treatment option for cutaneous melanoma

Ferroptosis is defined as a non-apoptotic cell death process due to the iron-dependent accumulation of lipid peroxides, which ultimately leads to cell damage and death (Yan HF et al., 2021). Compared to other programmed cell death forms (e.g. apoptosis, necrosis, pyroptosis, and autophagy), cells undergoing ferroptosis show no swelling of the cytoplasm and organelles, nor rupture of the cell membrane. Moreover, ferroptotic cells are not characterized by alterations in nuclear size, chromatin condensation, or the formation of apoptotic vesicles, which are the typical hallmarks of apoptosis (Li J et al., 2020). Conversely, distinctive features observed in ferroptotic cells are represented by morphological changes in

mitochondria, including smaller mitochondria, increased mitochondrial bilayer density, and loss of mitochondrial cristae (Battaglia AM et al., 2020).

Functionally, ferroptosis is regulated by different pathways. Of note, iron metabolism (e.g. iron uptake, storage, utilization, and efflux) is an essential part of driving intracellular lipid peroxidation and ferroptosis. In particular, iron accumulation may lead to the formation of highly reactive hydroxyl free radicals (HO^-) and subsequent ROS production through the well-known Fenton reaction, in which free Fe^{2+} ions react with hydrogen peroxide (H_2O_2) to form Fe^{3+} ions and hydroxyl radicals, leading to DNA oxidative damage and ferroptosis (Chen X et al., 2020; Rochette L et al., 2022). Moreover, iron trafficking (iron influx and efflux) is also mediated by NGAL/SLC22A17 complex, whose dysregulation may lead to intracellular iron accumulation, sensitizing cells to ferroptosis (Chaudhary N et al., 2021; Yao F et al., 2021).

Besides iron metabolism, the cystine/glutamate antiporter (System Xc^-), glutathione (GSH), and glutathione peroxidase 4 (GPX4) (System Xc^-/GSH/GPX4 axis) are other key regulators of ferroptosis. Specifically, the System Xc^- is a chloride-dependent and sodium-independent antiporter of cystine and glutamate, consisting of catalytic subunit xCT/Solute Carrier Family 7 Member 11 (SLC7A11), a transmembrane transporter with an essential role in maintaining oxidative homeostasis. Similarly, GSH and GPX4 are closely related in protecting cells against oxidative stress. Notably, GSH plays a pivotal role as a co-factor for GPX4, which converts GSH into oxidized glutathione (GSSG) to reduce lipid hydroperoxides and protect cells from oxidative damage. Conversely, the inhibition of the System Xc^-/GSH/GPX4 axis may induce the accumulation of lipid peroxides and drives the cells toward ferroptotic cell death (Li FJ et al., 2022; Zhang XD et al., 2023).

Interestingly, ferroptosis inducers have attracted growing interest as a novel therapeutic approach for cancer treatment (Chen Z et al., 2023). Notably, Erastin showed great potential for cancer therapy, inducing ferroptosis in cancer cells via inhibition of System Xc^- (Shibata Y et al., 2019; Zhao Y et al., 2020). Similarly, it has been reported that 1S, 3R-RSL 3 (RSL-3)-based treatment could represent a valuable anticancer option to induce ferroptosis via GPX4 inhibition with

promising results in several tumor types (Sui X et al., 2018; Li S et al., 2021). Moreover, perturbation of iron metabolism by supplying exogenous iron with ammonium iron (III) citrate significantly reduced cancer cell proliferation and invasion by triggering ferroptosis process (Wu W et al., 2021; Yuan Y et al., 2021). In this context, recent studies also investigated the pharmacological induction of ferroptosis in cutaneous melanoma as a potential therapeutic target.

For instance, Luo and colleagues focused on miRNA-mediated ferroptosis in melanoma, investigating the role of miRNA-137. Of note, the authors demonstrated that the knockdown of miRNA-137 significantly enhanced the expression levels of *Solute Carrier Family 1 member 5* (*SLC1A5*) glutamine transporter, sensitizing melanoma cells to Erastin- and RSL-3-induced ferroptosis (Luo M et al., 2018). Recently, miRNA-130b-3p and miRNA-21-3p have been also identified as key regulators of ferroptosis, suggesting that miRNAs targeting could represent a valuable strategy to induce ferroptosis and increase the efficacy of immunotherapy for melanoma treatment (Liao Y et al., 2021; Guo W et al., 2022). Interestingly, Leu *et al*. investigated the molecular mechanisms of ferroptosis sensitivity in cutaneous melanoma, highlighting that inhibition of *V-Erb-B2 Avian Erythroblastic Leukemia Viral Oncogene Homologue 3* (*ErbB3*) increased the efficacy of ferroptosis inducers (Leu JI et al., 2022). Similarly, Wang and colleagues found that *Calcium/calmodulin-dependent protein kinase kinase 2* (*CAMKK2*) was another negative regulator of ferroptosis in melanoma by regulating the AMP-activated protein kinase/Nuclear factor erythroid 2–related factor 2 (AMPK/NRF2) pathway. Specifically, the researchers reported that *CAMKK2* targeting could enhance ferroptosis sensitivity and, consequentially, improve response to anti-PD-1 immunotherapy in melanoma patients (Wang S et al., 2022).

Collectively, the reported studies highlight that ferroptosis-based nanodrug targeting strategies may represent a valuable treatment option to suppress melanoma progression; however, further investigations are mandatory to elucidate the relationship between ferroptosis and melanoma.

2. AIM OF THE STUDY

The development of novel therapeutic strategies, such as targeted therapy and immunotherapy, has significantly improved the management of melanoma patients. However, current epidemiological data indicate that incidence and mortality rates are still increasing worldwide due to the lack of clinical symptoms at early stages of disease. Indeed, melanoma diagnosis is often formulated at advanced stage when cancer cells have already infiltrated the subcutaneous layer, reducing treatment options and survival rate of cancer patients. Therefore, the identification of new cancer-related biomarkers, as well as potential pharmacological targets, is mandatory to enhance the early diagnosis and clinical outcome of melanoma patients. In this field, previous studies demonstrated that the TME-related genes *NGAL* and its membrane receptor *SLC22A17*, both involved in iron trafficking, are modulated by DNA methylation status, representing an attractive starting point for novel epigenetic biomarkers and promising therapeutic targets.

Based on these premises, the present study aimed to evaluate the role of DNA methylation in the regulation of *SLC22A17* expression in cutaneous melanoma to identify novel methylation hotspots as potential cancer biomarkers. Moreover, the involvement of *SLC22A17* in iron homeostasis and ferroptosis of melanoma cells was also explored. To this purpose, *in silico* study was first performed to analyze the *SLC22A17* gene/variants expression and DNA methylation profile in melanoma by using The Cancer Genome Atlas (TCGA) and Gene Expression Omnibus (GEO) datasets. Secondly, *in vitro* studies were conducted on different melanoma cell lines to validate bioinformatic results, which highlighted a significant correlation between *SLC22A17* expression and DNA methylation levels. Moreover, DNA methylation levels of the *SLC22A17* downstream promoter hotspot (cg17199325) were also analyzed in a case series of FFPE melanoma and nevi samples by the custom MSRE-ddPCR assay to evaluate the translational relevance of the *in silico* and *in vitro* results. Finally, the role of *SLC22A17* in ferroptosis was also investigated by a functional study on A375 cells as melanoma cell model.

Overall, the results of the present study could pave the way for novel diagnostic/prognostic biomarkers, as well as potential pharmacological targets for effective therapeutic strategies in cutaneous melanoma treatment.

3. MATERIALS AND METHODS

3.1 Omics data collection from public repositories

The differential analyses of *SLC22A17* expression and DNA methylation status between melanoma samples and normal tissues (nevus) were performed by consulting the GEO public database (https://www.ncbi.nlm.nih.gov/geo/). Specifically, the GSE112509 dataset was used to retrieve expression data (Illumina HiSeq 2000) of 57 primary melanoma samples and 23 melanocytic nevi, while the GSE120878 dataset was analyzed to obtain DNA methylation levels (Illumina Infinium HumanMethylation450 BeadChip array) of 89 primary invasive melanomas and 73 nevi.

The UCSC Xena Functional Genomics Explorer platform was consulted to perform *SLC22A17* gene/variants expression and DNA methylation profile using the cohort TCGA Pan-Cancer (PANCAN) melanoma (SKCM) (N = 470) (https://xenabrowser.net/). Briefly, gene expression RNAseq - TOIL RSEM fpkm and transcript expression RNAseq - TOIL RSEM fpkm datasets were used to retrieve expression data, while DNA methylation levels of CG probesets were obtained from DNA methylation (Methylation450K) dataset. Moreover, UCSC Xena tool was used to retrieve OS and PFI data from the TCGA PANCAN SKCM cohort.

3.2 Cell cultures

To validate the results obtained from bioinformatics analyses and confirm the correlation between DNA methylation and *SLC22A17* gene/variants expression, the methylation status of three DNA methylation hotspots belonging to the upstream/downstream promoter and body regions, as well as *SLC22A17* gene/variants expression levels, were evaluated on seven melanoma cell lines available at the cell biobank of the Laboratory of Experimental Oncology of the University of Catania. Notably, A375, A2058, M14, SK-MEL-23, SK-MEL-28, and WM115 melanoma cell lines were cultured in RPMI 1640 medium (Cat. No. 10-040 - Corning® Life Sciences), while MeWo cell line was cultured in EMEM medium (Cat. No. 15-010 - Corning® Life Sciences). Both culture media were

supplemented with 10% Fetal Bovine Serum (FBS), 2 mM L-glutamine, 100 IU penicillin, and 100 μg/mL streptomycin (Cat. No. 35-079, Cat. No. 25-005, Cat. No. 30-001 - Corning® Life Sciences). Each cell line was seeded in 100 mm cell-culture dishes (Qiagen, Hilden, Germany) at the density of 1 x 10^6 cells in 10 mL of complete culture medium and grown until 80% confluency in a humidified incubator at 37°C and 5% CO_2. Cell pellets were then collected by scraping cell cultures in cold Phosphate-Buffered Saline (PBS) (Cat. No. 21-040 - Corning® Life Sciences) and frozen at -80 °C until the subsequent phase of genomic DNA and total RNA extraction.

3.3 Collection of FFPE melanoma and nevi samples

The analysis of the *SLC22A17* methylation hotspot (cg17199325), belonging to the downstream promoter region, was performed on a cohort of 32 melanoma patients (median age 60.5; range 32 - 88) and 15 healthy controls (median age 37; range 18 - 55). The patients and controls were enrolled at the National Cancer Institute "Fondazione G. Pascale" (Naples, Italy) and had similar ethnic backgrounds. Specifically, ten Formalin-Fixed Paraffin-Embedded (FFPE) sections of 5-8 μm were collected for each sample by using standard procedures. The study was conducted by the guidelines of the Declaration of Helsinki and approved by the Institutional Review Board of the National Cancer Institute "Fondazione G. Pascale" (Naples, Italy).

The socio-demographic and clinical-pathological features of the subjects enrolled in the study are reported in Table 4.

Table 4. Socio-demographic and clinical characteristics of melanoma patients and healthy controls

	Melanoma		Nevi	
	N.	**(%)**	***N.***	**(%)**
Samples	32	(68.1%)	15	(31.9%)
Age (years)				
< 45	6	(18.8%)	10	(66.7%)
45 – 60	10	(31.2%)	5	(33.3%)
> 60	16	(50%)	0	(0%)
Gender				
Male	19	(59.4%)	5	(33.3%)
Female	13	(40.6%)	10	(66.7%)
Stage				
pT0	0	(0%)		
pT1	2	(6.3%)		
pT2	4	(12.5%)		
pT3	10	(31.2%)		
pT4	15	(46.9%)		
Missing	1	(3.1%)		
Breslow (mm)				
0 - 2	5	(15.6%)		
2 - 4	11	(34.4%)		
> 4	14	(43.7%)		
Missing	2	(6.3%)		
Clark level				
I	0	(0%)		
II	1	(3.1%)		
III	1	(3.1%)		
IV	24	(75%)		
V	3	(9.4%)		
Missing	3	(9.4%)		
BRAF Status				
Wild type	5	(15.6%)		
Mutated	11	(34.4%)		
Missing	16	(50%)		
Number of Mitosis				
0 - 1	5	(15.6%)		
2 - 4	12	(37.5%)		

5 - 10	10	(31.2%)
> 10	2	(6.3%)
Missing	3	(9.4%)
TILs		
Absent	3	(9.4%)
No Brisk	15	(46.9%)
Brisk	10	(31.2%)
Missing	4	(12.5%)
Vascular Invasion		
Negative	23	(71.9%)
Positive	5	(15.6%)
Missing	4	(12.5%)
Ulceration		
Negative	11	(34.4%)
Positive	20	(62.5%)
Missing	1	(3.1%)

3.4 Genomic DNA and total RNA extraction

Genomic DNA was extracted from melanoma cell lines by using the PureLink™ Genomic Mini Kit (Cat. No. K1820-01 - Invitrogen, Thermo Fisher Scientific™, Waltham, MA, United States) according to the manufacturer's instructions. Specifically, cell pellets were resuspended in 200 µL PBS (Cat. No. 21-040 - Corning® Life Sciences) and transferred to a sterile tube containing 20 µL Proteinase K provided with the extraction kit. Then, 20 µL RNase A were added to the sample, and the reaction mix was briefly vortexed and incubated at room temperature (RT) for 2 min. Following the incubation, 200 µL PureLink™ Genomic Lysis/Binding Buffer were added to the sample, and the digestion mix was incubated at 55°C for 10 min to promote protein digestion. Then, 200 µL BioUltra Ethanol for molecular biology ≥ 99.8% (Cat. No. 51976 - Sigma Aldrich) were added to the sample, and the digestion mix was briefly vortexed to obtain a homogeneous solution. The lysate (~ 640 µL) was transferred to the PureLink™ Spin Column provided with the kit and centrifuged at 10,000 x g at RT for 1 min. Then, 500 µL of Wash Buffer 1 were added to the column, and the sample was centrifuged at maximum speed for 1 min at RT to wash the genomic DNA blocked by the silica membrane. The wash step was repeated by using 500 µL of Wash

Buffer 2. Finally, genomic DNA was eluted by adding 50 µL PureLink™ Genomic Elution Buffer, and the sample was centrifuged at maximum speed for 1 min at RT. The extracted genomic DNA was stored at -20°C until further analyses.

Total RNA was extracted from each melanoma cell line using the TRIzol™ Reagent (Cat. No. 15596018 - Invitrogen, Thermo Fischer Scientific™, Waltham, MA, United States) according to the manufacturer's protocol. Briefly, 1 mL TRIzol™ Reagent was added to cell pellet, and the sample was incubated at RT for 5 min to obtain nucleoproteins complex dissociation. Then, 200 µL of chloroform (Cat. No. 3955301 - SERVA Electrophoresis GmbH) were added to the sample, and the reaction mix was incubated for 2 min at RT. Following the incubation, the sample was centrifuged for 15 min at 12,000 x g at 4°C, and the aqueous phase containing RNA was recovered and transferred to a new tube. Then, 500 µL of isopropanol were added to the aqueous phase and the sample was incubated for 10 min at RT before centrifugation at 12,000 x g at 4°C for 10 min. after removing the supernatant, cell pellet was resuspended in 1 mL of 75% ethanol before a second centrifugation at 7,500 x g at 4°C for 5 min. Finally, the RNA pellet was resuspended by adding 30 µL of DNase/RNase-free distilled water (Cat. No. 10977-035 - Invitrogen, Thermo Fischer Scientific™, Waltham, MA, United States) and the obtained total RNA was stored at -80 until the downstream analyses.

Genomic DNA from FFPE tissues was extracted using the QIAamp DNA FFPE Tissue Kit (Cat. No. 56404 - Qiagen, Hilden, Germany) according to the manufacturer's protocol. Specifically, 1 mL xylene was added into a microcentrifuge tube containing eight FFPE sections (5–10 µm thick) and the sample was centrifuged at maximum speed for 2 min at RT. After removing the supernatant, cell pellet was resuspended with 1 mL of BioUltra Ethanol for molecular biology ≥ 99.8% (Cat. No. 51976 - Sigma Aldrich) to remove residual xylene, and the sample was centrifuged. Then, the supernatant was removed, and the opened tube was incubated at RT for 10 min until ethanol has completely evaporated. Following the incubation, 180 µl Buffer ATL and 20 µl proteinase K were added to the tube, and the sample was incubated at 56°C for 1 h and 90°C for 1 h. Following the incubation, 200 µl Buffer AL and 200 µl BioUltra Ethanol for molecular biology ≥ 99.8% (Cat. No. 51976 - Sigma Aldrich) were added to the

reaction mix, and the sample was vortexed to obtain a homogeneous solution. The lysate was transferred to the QIAamp MinElute column provided with the kit and centrifuged at 6,000 x g at RT for 1 min. Then, 500 µL of Buffer AW1 were added to the column, and the sample was centrifuged at 6,000 x g for 1 min at RT to wash the genomic DNA blocked by the silica membrane. The wash step was repeated by using 500 µL of Buffer AW 2. Following an additional centrifuge to remove residual ethanol, genomic DNA was eluted by adding 50 µL Buffer ATE to the center of the membrane, and the sample was centrifuged at maximum speed at RM for 1 min. Finally, the extracted genomic DNA was stored at -20°C until further analyses.
Nanodrop-1000 (Thermo Fischer Scientific™) was used to assess the amount and quality of genomic DNA and total RNA extracted from melanoma cell lines, as well as genomic DNA derived from melanoma and nevi FFPE samples.

3.5 Bisulfite conversion and Sanger sequencing

The DNA methylation profiling of melanoma cell lines was performed by bisulfite conversion followed by PCR amplification and Sanger sequencing. In particular, the EpiTect Plus DNA Bisulfite Kit (Cat. No. 59124 - Qiagen, Hilden, Germany) was used to perform bisulfite conversion of genomic DNA obtained from each melanoma cell line. Briefly, bisulfite reaction was prepared by mixing 1,200 ng of genomic DNA, 85 µL of Bisulfite mix, 35 µL DNA protect buffer, and RNase-free water up to a final volume of 140 µL. The bisulfite reaction mix was incubated according to the following thermal cycler conditions: 95°C for 5 min, 60°C for 25 min, 95°C for 5 min, 60°C for 85 min, 95°C for 5 min, and finally 60°C for 175 min. Then, the amplification of bisulfite-converted DNA samples was executed preparing a reaction mix containing 100 ng of bisulfite-converted DNA, 10 µL of 2X ddPCR Supermix for Probes (No dUTP) (Cat. No. 1863024 - Bio-Rad Laboratories Inc, Hercules, CA, United States), 10 µM (final concentration) of forward and reverse primers for each target, and H_20 molecular biology grade up to a final volume of 20 µL.
The Bisulfite Primer Seeker (https://www.zymoresearch.eu/) was used to design bisulfite primers. PCR thermal conditions and primer sequences are reported in Table 5.

Table 5. Primer sequences and amplification conditions used for the amplification of *SLC22A17* targets starting from bisulfite-converted DNA

Primer ID	Sequence	Ampl. conditions
Prom1 Fw	5'-TTAGGGTTTAGGGGAGGGAG-3'	95°C for 10 min, followed by 40 cycles of 94°C for 30 s, 55°C for 1 min, and finally 98°C for 10 min
Prom1 Rev	5'-CTACCTAAACTAACTACTATCCTTCAA-3'	
Prom2 Fw	5'-GTGATTTTTATAGTGTTGTYGATTTT-3'	
Prom2 Rev	5'-CTACAAAACTACAAAACRAAATCTCTTC-3'	
Prom3 Fw	5'-GTGAGTATAGGAAGGTTATTATAGTTTT-3'	
Prom3 Rev	5'-TAACTAAAAACAACCTCCCAATAC-3'	
Prom4 Fw	5'-ATATTAGATTTTATTGGGGATGTGAGAA-3'	
Prom4 Rev	5'-AAAACTATAATAACCTTCCTATACTCAC-3'	
Body1 Fw	5'-GGATTTTTAGGGTTTTGAGATTTTTTTA-3'	
Body1 Rev	5'-AATCAATAATAAAAATAACCAAAATCAA-3'	
Body2 Fw	5'-TTTGTTTAGGTTTTTTTGAAGAATTTAG-3'	
Body2 Rev	5'-TACTATCAAAAAAATAACACCTTATTCC-3'	
Body3 Fw	5'-GGGTTAGGTTAGTAGTTGGAAT-3'	
Body3 Rev	5'-ACRAATAACATAAACAATAAAACTATAAAA-3'	
3'UTR1 Fw	5'-TTTTYGGTAGTAGTATAATGTTGAGAAT-3'	
3'UTR1 Rev	5'-AACCTAAACCTAATCATAACTCTAAAAA-3'	
3'UTR2 Fw	5'-GTTATAGYGGGTAGGGGGTG-3'	
3'UTR2 Rev	5'-ATTCTCAACATTATACTACTACCRAA-3'	

PCR products were cleanup using the PureLink PCR Purification Kit (Cat. No. K310001 - Invitrogen, Thermo Fisher Scientific™, Waltham, MA, United States) according to the manufacturer's protocol. Specifically, 80 µL of Binding Buffer were added to the PCR product (20 µL), and the sample was transferred to the PureLink® Spin Column provided with the kit and centrifuged at 10,000 x g for 1 min at RT. After removing the flow through, 650 µL of Wash Buffer were added to the column, and the sample was centrifuged at 10,000 x g for 1 min at RT. Then, 50 µL of Elution Buffer were added to the center of column to eluting DNA, and the sample was centrifuged at maximum speed for 1 min. The amount and quality of purified PCR products were assessed by Nanodrop-1000 (Thermo Fischer Scientific™). Finally, the purified PCR products were sequenced with the Mix2Seq Kit (Eurofins Genomics Germany GmbH, Ebersberg, Germany) according to the manufacturer's procedure. Chromas Lite software (version 2.6.6) was used to perform the analysis of DNA sequences.

3.6 Standard Methylation-sensitive restriction enzyme assay

To evaluate the DNA methylation levels of the *SLC22A17* methylation hotspots, Standard Methylation-sensitive restriction enzyme (MSRE) assay was performed for DNA samples derived from each melanoma cell line. In particular, three different reaction tubes were prepared by mixing 200 ng of genomic DNA, 1X CutSmart Buffer (Cat. No. B7204), and 20 UI of HpaII enzyme (Cat. No. R0171S) for tube 1 [Mix HpaII], 20 UI of MspI enzyme (Cat. No. R0106S) for tube 2 [Mix MspI], no enzyme for tube 3 [Mix (-)], and H_20 molecular biology grade up to a final volume of 10 µL (all the reagents were purchased from New England Biolabs, Germany). Then, the reaction tubes were incubated at 37°C for 1 h and stopped with Proteinase K (final concentration 1 mg/mL) (Cat. No. EO0491 - Invitrogen, Thermo Fisher Scientific™, Waltham, MA, United States), incubating the samples at 55°C for 30 min and 95°C for 10 min. Of note, the MspI enzyme was used in standard MSRE to test digestion efficiency. Following the MSRE digestion, 1 µL of each digested sample (20 ng/µL) was used for the downstream MSRE-qPCR amplification.

3.7 MSRE-qPCR and RT-qPCR

SYBR green-based real time PCR was performed with the Applied Biosystem 7500 Real-Time PCR System to assess the DNA methylation levels of three *SLC22A17* methylation hotspots mapped in the upstream promoter (chr14:23,821,982-23,822,182 - GRCh37/hg19), downstream promoter (chr14:23,821,211-23,821,359 - GRCh37/hg19), and body (chr14:23,816,960-23,817,116 - GRCh37/hg19) regions. Specifically, the amplification of MSRE-digested DNA samples obtained from melanoma cell lines was performed by preparing a reaction mix containing 10 µL of Luminaris Color HiGreen qPCR Master Mix - high ROX (Cat. No. K0361 - Invitrogen, Thermo Fischer Scientific™, Waltham, MA, United States), 10 µM (final concentration) of forward e reverse primers for each target, 1 µL of MSRE-digested DNA (20 ng/µL) and H_20 molecular biology grade up to a final volume of 20 µL. Of note, DNA methylation percentage was computed by using the formula: $100 \times 2^{-(\text{Ct of undigested sample} - \text{Ct of HpaII digested sample})}$. PCR thermal conditions

and primer sequences are reported in Table 6. All the experiments were performed in triplicate.

Table 6. Primer sequences and thermal conditions used for MSRE-qPCR amplification

Primer ID	Sequence	Ampl. conditions
MSRE UpP Fw	5'-AAGGATGCGCTGTCCTCTG-3'	50°C for 2 min and 95°C for 10 min, followed by 40 cycles of 95°C for 10 s, 60°C for 30 s, and 72°C for 30 s
MSRE UpP Rev	5'-AGAGCGGGATCTCTTCGAGC-3'	
MSRE DownP Fw	5'-GAGGCAATGGTTGAAGTCCG-3'	
MSRE DownP Rev	5'-CTAATGCCTCTGGCTGGGAG-3'	
MSRE Body Fw	5'-AGCAACGAACAGAGCCTGAA-3'	
MSRE Body Rev	5'-ATCCTGGGCTTCACCAAGTG-3'	

To evaluate the *SLC22A17* all variants and variants 1, 2, and 3 expression levels in melanoma cell lines, reverse transcription was carried out using SuperScript IV Reverse Transcriptase (Cat. No. 18090010 - Invitrogen, Thermo Fisher Scientific™, Waltham, MA, United States). Briefly, the reaction mix was prepared by mixing 1,500 ng of total cellular RNA, 1 µL of random examers (100 µM final concentration), 1 µL of Deoxynucleotide Triphosphates (dNTPs) (100µM final concentration), and DEPC-treated water up to a final volume of 14 µL. The samples were incubated at 65°C for 5 min and on ice for 1 min. Following the incubation, 6 µL of RT reaction, containing 4 µL of 5x SSIV Buffer, 1 µL of DTT (100mM final concentration), and 1 µL of SuperScript IV Reverse Transcriptase (200 UI/µl), were added to each sample. Finally, the samples were incubated at 23°C for 10 min, 55°C for 10 min, and 80°C for 10 min. The amplification of obtained cDNA was performed with the Applied Biosystem 7500 Real-Time PCR System by preparing an amplification mix containing 10 µL of Luminaris Color HiGreen qPCR Master Mix - high ROX (Cat. No. K0361 - Invitrogen, Thermo Fischer Scientific™, Waltham, MA, United States), 10 µM (final concentration) of forward e reverse primers for each target, 1 µL of cDNA (25 ng/µL) and H_20 molecular biology grade up to a final volume of 20 µL. The ΔΔCt relative quantification method was performed to assess the expression of *SLC22A17* all variants and variants 1, 2, and 3 using *Glyceraldehyde-3-Phosphate Dehydrogenase* (*GAPDH*) signal value as

control reference. Primers and amplification conditions are reported in Table 7. All the experiments were performed in triplicate.

Table 7. Primer sequences and thermal conditions used for RT-qPCR amplification

Primer ID	Sequence	Ampl. conditions
All Var Fw	5'-TGGTTTGTTCCTGGAGTCCG-3'	50°C for 2 min and 95°C for 10 min, followed by 40 cycles of 95°C for 10 s, 60°C for 30 s, and 72°C for 30 s
All Var Rev	5'-GCATGGGCAATGAAGTTGGT-3'	
Var1 Fw	5'-GGTCACCGTGGACCGATTT-3'	
Var1 Rev	5'-TTGGGGTTCCCTTGTTGAGC-3'	
Var2 Fw	5'-ATTGGCGATTCCTACAGCGA-3'	
Var2 Rev	5'-AGCCTCGTTCAGATAATCCCAC-3'	
Var3 Fw	5'-GGTGTCTACCTGATGCCGAAT-3'	
Var3 Rev	5'-CGGTTTCGCTCAGCCAGGAT-3'	
GAPDH Fw	5'-AGAAGGCTGGGGCTCATTTG-3'	
GAPDH Rev	5'-AGGGGCCATCCACAGTCTTC-3'	

3.8 Methylation-sensitive restriction enzyme - droplet digital PCR assay

The analysis of the *in silico* identified *SLC22A17* methylation hotspot (cg17199325) was performed on FFPE melanoma and nevi samples by using the custom Methylation-sensitive restriction enzyme – droplet digital PCR (MSRE-ddPCR) assay, previously developed by our research group.

Of note, the MSRE-ddPCR assay consists of one-tube reactions in which methylation-sensitive restriction enzymes (e.g. HpaII) directly digest DNA targets in the ddPCR reaction mix. Moreover, a synthetic DNA methylation control (methCTRL) is used to assess digestion efficiency of the restriction enzymes. Specifically, methCTRL is an artificially demethylated exogenous DNA fragment generated by PCR amplification of a sequence of the fluorescent protein Clover (210 bp), which contains 1 CCGG restriction site. To generate methCTRL, 10 ng of pcDNA3.1-*CLOVER* plasmid (Plasmid #40259 - Addgene) was amplified using the Phusion High-Fidelity DNA Polymerase kit (Cat. No. F-530XL - Thermo Fisher Scientific™, Waltham, MA, United States) according to the manufacturer's protocol. PCR thermal conditions and primer sequences are reported in Table 8. The PCR product was subsequently treated with 1 µL DpnI (Cat. No. FD1703 - Thermo Fisher Scientific™, Waltham, MA, United States) at 37°C for 15 min and then the

enzyme was inactivated at 80°C for 20 min. Finally, the PCR product was purified using the PureLink PCR Purification Kit (Cat. No. K310001 - Thermo Fisher Scientific™, Waltham, MA, United States) and quantified with Nanodrop-1000 (Thermo Fischer Scientific™). Since the methCTRL is completely degraded by the HpaII enzyme, the detection of the copies/µL following ddPCR amplification represents a direct measurement of digestion efficiency.

Table 8. Primer sequences and thermal conditions used for the generation of methCTRL

Primer ID	Sequence	Ampl. conditions
T7 Fw	5'-TAATACGACTCACTATAGGG-3'	98°C for 20 s, followed by 35 cycles of 98°C for 1 s, 72°C for 15 s, and finally 72°C for 1 min
EGFP-N bis Rev	5'-CTTGCCGTTGGTGGCATCGC-3'	

To perform MSRE-ddPCR assay, two different amplification mixes were prepared for each sample, one containing HpaII and the other with no enzyme as undigested control. Briefly, each amplification mix (final volume 22 µL) was prepared by mixing 11 µL of 2X ddPCR Supermix for Probes (No dUTP) (Cat. No. 1863024 - Bio-Rad Laboratories Inc, Hercules, CA, United States), 900 nM (final concentration) of forward and reverse primers and 450 nM (final concentration) of FAM/HEX probes for *SLC22A17* target and methCTRL. Probe and primer sequences, as well as amplification conditions, are reported in Table 9. Up to 20 ng of DNA sample and 10^{-6} ng of methCTRL (final volume 5 µL) were added to each MSRE-ddPCR mix along with 10 UI of HpaII restriction enzyme (Cat. No. R0171S - New England Biolabs, Germany) in the HpaII mix, while DNase/RNase free H_2O was added to the undigested control mix to reach a final volume of 22 µL. Amplification mixes were then incubated at 37°C for 30 min before droplet generation.

Table 9. Primer and probe sequences and amplification conditions for MSRE-ddPCR amplification

Primer ID	Sequence	Ampl. conditions
MSRE DownP Fw	5'-GAGGCAATGGTTGAAGTCCG-3'	95°C for 10 min, followed by 40 cycles of 94°C for 30 s, 55°C for 1 min, and finally 98°C for 10 min (ramp rate 2°C/s)
MSRE DownP Rev	5'-CTAATGCCTCTGGCTGGGAG-3'	
MSRE DownP probe	[FAM]5'-GCCGCTGCACGAGGGGTCGG-3'[BHQ1]	
methCTRL Fw	5'-CACTATAGGGAGACCCAAG-3'	
methCTRL Rev	5'-AACTTGTGGCCGTTTAC-3'	
methCTRL probe	[HEX]5'-CTGTTCACCGGGGTGG-3'[BHQ1]	

Following the enzymatic digestion, droplet generation was performed by loading 20 µL of each ddPCR amplification mix in DG8 Cartridges along with 70 µL of Droplet Generation Oil (Cat. No. 1863005 - Bio-Rad Laboratories, Inc., USA) within the sample and oil wells, respectively. Then, the cartridge was covered with Gasket (Cat. No. 1863009 - Bio-Rad Laboratories, Inc., USA) and transferred into Droplet Generator QX100 (Bio-Rad Laboratories Inc, Hercules, CA, United States) for droplet generation according to the manufacturer's instructions. The droplet mixture was recovered from the cartridge and transferred into a 96-well plate (Cat. No. 12001925 - Bio-Rad Laboratories, Inc., USA) to perform PCR amplification by the C1000 Touch Thermal Cycler (Bio-Rad Laboratories Inc, Hercules, CA, United States). Finally, the QX200 Droplet Reader (Bio-Rad Laboratories, Inc., USA) was used for droplet quantification. Absolute quantification (copies/µL) was retrieved by using QuantaSoft software (version 1.7.4 - QuantaSoft, Prague, Czechia). The fluorescence amplitude of droplets was also considered to evaluate efficiency of the amplification reaction.

The DNA methylation percentage of the *SLC22A17* target was retrieved by considering the ratio between ddPCR absolute quantification of the *SLC22A17* DNA methylation in HpaII mix and the undigested control mix (CTRL mix) for each sample by the following formula:

$$\%\ \text{of methylation} = \left(\frac{\text{HpaII mix}}{\text{CTRL mix}}\right)^{\text{target}} \times \left(1 - \left(\frac{\text{HpaII mix}}{\text{CTRL mix}}\right)^{\text{MethCTRL}}\right) \times 100$$

Of note, to overcome the bias in DNA methylation percentage estimation due to the inhibition of the enzymatic digestion, data normalization was performed by using an enzymatic digestion coefficient computed by reciprocal ratio between the methCTRL absolute quantification in HpaII and the CTRL mix.

3.9 A375 cell transfection and retroviral transduction

To evaluate the role of the *NGAL/SLC22A17* complex in iron trafficking and ferroptosis, A375 melanoma cell line was used to induce overexpression of *NGAL* and *SLC22A17* variants 1, 2, and 3 (Figure 7).

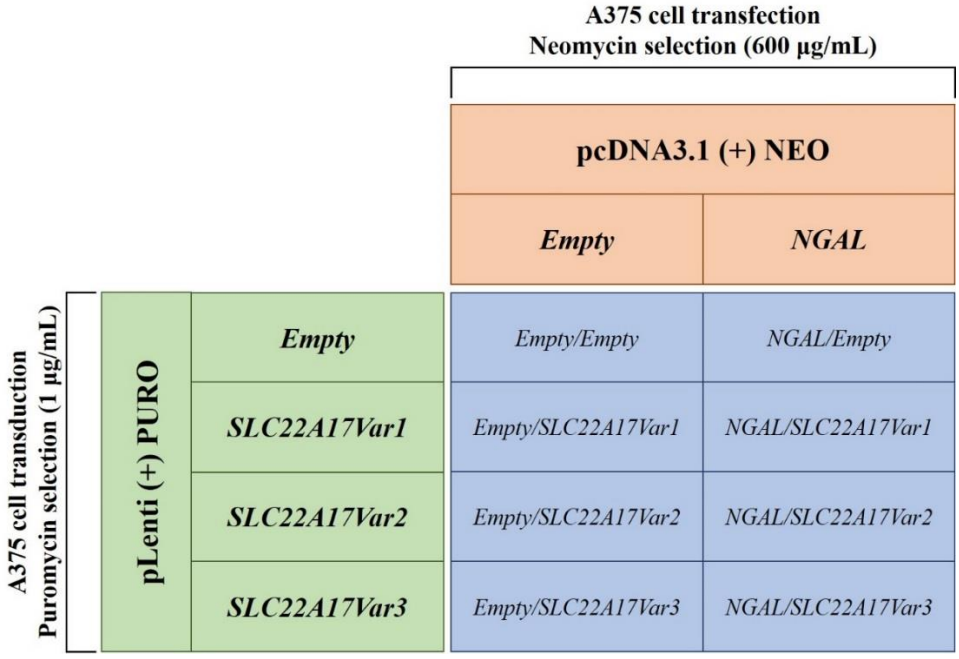

Figure 7. Schematic representation of A375 cell transfection and transduction

Regarding cell transfection, pcDNA3.1 (+) NEO containing *NGAL* wild type construct and relative empty vector backbones were kindly provided by Prof. James A. McCubrey of the East Carolina University (North Carolina, USA). Briefly, A375 cells were first seeded in 6-well plate at the density of 2.4 x 10^5 cells per well in 2 mL of complete RPMI-1640 medium and incubated at 37°C and 5% CO_2 for 24h. The next day, the transfection mix containing 4.5 µL Attractene transfection reagent (Cat. No. 301004 - Qiagen, Hilden, Germany), 1,200 ng of plasmid DNA (pcDNA3.1-*Empty*, pcDNA3.1-*NGAL* wild type, and pcDNA3.1-*CLOVER*) and

100 µL Opti-MEM™ Reduced Serum Medium (Cat. No. 31985-062 - Invitrogen, Thermo Fisher Scientific™, Waltham, MA, United States) was incubated at RT for 15 min and then added to each well after replacing the culture medium (2 mL). The pcDNA3.1 (+) NEO - *CLOVER* (Plasmid #40259 - Addgene), also available in our lab, was used to evaluate transfection efficiency by fluorescence detection. Following 24h of incubation, clonal selection was performed by using Neomycin (Geneticin - G418) (Cat. No. 10131-035 - Invitrogen, Thermo Fisher Scientific™, Waltham, MA, United States) at final concentration of 600 µg/mL.

The retroviral transduction was performed by using retroviral transfer plasmid pLenti (+) PURO (Plasmid #39481 - Addgene) to clone the coding sequence (CDS) of *SLC22A17* variants 1, 2, and 3 (NCBI Reference Sequence: NM_020372.4, NM_016609.7, and NM_001289050.1, respectively). The CDS of *SLC22A17* variants 1, 2, and 3 were obtained by PCR using first strand cDNA isolated from Human Pulmonary Fibroblast (HPF) cell line, also available in our lab. In particular, PCR amplification was first performed to obtain fragment 1 (813 bp for *SLC22A17* variants 1 and 2, 688 bp for *SLC22A17* variant 3) and fragment 2 (907 bp for *SLC22A17* variant 1, 853 bp for variants 2 and 3). Specifically, PCR amplification of fragments 1 and 2 was executed by Phusion™ Plus DNA Polymerase kit (Cat. No. F630l - Invitrogen, Thermo Fisher Scientific™, Waltham, MA, United States) preparing the following amplification mix: 0.2 µL Phusion plus master mix, 4 µL 5X Buffer, 0.4 µL dNTPs (10 µM final concentration), 1 µL forward and reverse primers (10 µM final concentration) for each fragment, 50 ng DNA, and H_20 molecular biology grade up to final volume of 20 µL. PCR thermal conditions and primer sequences are reported in Table 10.

PCR products were separated by agarose gel electrophoresis and isolated using GeneJET Gel Extraction Kit (Cat. No. K0691 - Invitrogen, Thermo Fisher Scientific™, Waltham, MA, United States) according to manufacturer's protocol. Briefly, gel slices containing DNA fragments were excised using a razor blade and transferred into 2 mL tube. Then, 1:1 volume of Binding buffer was added to each tube, and the gel mixtures were incubated at 60°C for 10 min. Following the incubation, the solubilized gel solution was transferred to the GeneJET purification column provided with the kit and centrifuged at 12,000 x g for 1 min. After

removing the flow through, 700 µL of Wash Buffer were added to the column, and the sample was centrifuged. Finally, 50 µL of Elution Buffer were added to the center of column to eluting DNA, and the sample was centrifuged at maximum speed for 1 min. The amount and quality of purified fragment 1 and 2 were assessed by Nanodrop-1000 (Thermo Fischer Scientific™).

Table 10. Primer sequences and amplification conditions used for *SLC22A17* variants amplification

Primer ID	Sequence	Ampl. conditions
Fragment 1 Fw	5'-GGTGCTCTTCGTGGCTCTG-3'	98°C for 30 s, followed by 35 cycles of 94°C for 10 s, 60°C for 10 s, 72°C for 40 s, and finally 75°C for 5 min
Fragment 1 Rev	5'-CGGTTTCGCTCAGCCAGGAT-3'	
Fragment 2 Fw	5'-ATCCTGGCTGAGCGAAACCG-3'	
Fragment 2 Rev	5'-CCCGATCTTCTTGCCACCTT-3'	
Assembly Fw	5'-GTAGGAATTCATGGCCTCGGACCCCATCTT-3'	
Assembly Rev	5'-GTAGGAATTCTCAGAGGGCAGGGTTGGGGGT-3'	

The purified DNA fragments 1 and 2 were then used to perform Assembly PCR and obtain the CDS of *SLC22A17* variants 1, 2 and 3 (1720 bp, 1666 bp, and 1541 bp, respectively). As above reported, PCR amplification was performed by Phusion™ Plus DNA Polymerase kit (Cat. No. F630l - Invitrogen, Thermo Fisher Scientific™, Waltham, MA, United States) using 1 ng for each purified DNA fragment (see Table 10 for primer sequences and thermal conditions). Finally, PCR products were separated by agarose gel electrophoresis and isolated using the GeneJET Gel Extraction Kit (Cat. No. K0691 - Invitrogen, Thermo Fisher Scientific™, Waltham, MA, United States) according to manufacturer's protocol.

The obtained CDS of the *SLC22A17* variants 1, 2, and 3 were cloned via EcoRI (Cat. No. ER0271 - Invitrogen, Thermo Fisher Scientific™, Waltham, MA, United States) in transfer plasmid pLenti (+) PURO (Plasmid #39481 - Addgene). To this purpose, ligation reaction mix was prepared as follows: 1U T4 DNA Ligase (Cat. No. EL0011 - Invitrogen, Thermo Fisher Scientific™, Waltham, MA, United States), 2 µL 10x T4 DNA Ligase Buffer, 50 ng transfer plasmid DNA pLenti (+) PURO, insert DNA (3:1 molar ratio over vector), and DNase/RNase-free H_2O up to final volume of 20 µL. Following the incubation at 22°C for 10 min, 5 µL of ligation mix was used for transformation of chemically competent cells by One

Shot™ Stbl3™ Chemically Competent *E. coli* kit (Cat. No. C737303 - Invitrogen, Thermo Fisher Scientific™, Waltham, MA, United States).

The PureLink™ HiPure Plasmid Filter Maxiprep Kit (Cat. No. K210016 - Invitrogen, Thermo Fisher Scientific™, Waltham, MA, United States) was then used to isolate plasmid DNA from bacterial culture. Specifically, the Stbl3-based overnight culture was first centrifuged at 4,000 x g for 10 min. After medium removing, 10 mL of Resuspension Buffer and 10 mL of Lysis Buffer were added to cell pellet. Following the incubation at RT for 5 min, 10 mL of Precipitation Buffer were added to the mixture and the sample was centrifuged. The supernatant was transferred into the equilibrated HiPure Filter Maxi Column provided with the kit, leaving the lysate to filter through the column by gravity flow. After column wash, 15 mL Elution Buffer were added to the column to recover the purified DNA. Then, 10.5 mL isopropanol were added to the eluate, and the sample was centrifuged at 12,000 x g for 30 min at 4°C. After supernatant removing, 5 mL 70% ethanol were added to pellet, and the tube was centrifuged for 5 min. Finally, 200 µL of TE Buffer were added to the air-dry pellet, and the obtained plasmid DNA was stored at -20°C. Insert orientation and sequence were verified by PCR and Sanger sequencing, respectively.

Retroviral particles were obtained by using the packaging HEK 293T cells, available in our lab. Briefly, HEK 293T cells were first seeded in 6-well plate at the density of 5 x 10^5 cells per well in 2 mL of complete DMEM medium (Cat. No. 10-017-CV) supplemented with 10% FBS (Cat. No. 35-079), 2 mM L-glutamine (Cat. No. 25-005), 100 IU penicillin - 100 µg/ml streptomycin (Cat. No. 30-001) (all purchased from Corning® Life Sciences) and grown at 37°C and 5% CO_2. The next day, HEK 293T cells were transduced with the pLenti-*Empty*, pLenti-*SLC22A17Var1*, pLenti-*SLC22A17Var2*, pLenti-*SLC22A17Var3*, and pLenti-*CLOVER* retroviral vectors using Attractene transfection reagent (Cat. No. 301004 - Qiagen, Hilden, Germany) according to the manufacturer's protocol. Specifically, lentiviral packaging mix was prepared as follows: 2.19 µL pRRE, 1 µL pREV, 1.44 µL pVSVg, plasmid DNA for each transfer vector, 4.5 µL Attractene, and 100 µL Opti-MEM™ Reduced Serum Medium (Cat. No. 31985-062 – Invitrogen, Thermo Fisher Scientific™, Waltham, MA, United States). The transfer plasmid pLenti-

CLOVER, already available in our lab, was also used to test transduction efficiency. The next day, the culture medium was replaced, and HEK 293T cells were maintained in a humified incubator (37°C and 5% CO_2) for 24h. Then, the conditioned medium was filtered through a 0.45 μm filter and an equal volume of complete RPMI-1640 medium, supplemented with polybrene solution (4 μg/mL final concentration), was added to each filtered supernatant. Finally, lentiviral mixture (4 mL) was added to previously transfected A375 cells growing overnight in 6-well plate, and spinfection was performed by centrifugation at 12,000 x g for 60 min. The next day, the culture medium was replaced, and the transducted A375 cells were selected by using Puromycin Dihydrochloride (Cat. No. A1113803 - Invitrogen, Thermo Fisher Scientific™, Waltham, MA, United States) at final concentration of 1 μg/mL.

3.10 Cell viability assay and cell treatments

The 3-(4,5-Dimethylthiazol-2-yl)-2,5-Diphenyltetrazolium Bromide (MTT) assay was performed to establish the IC_{50} dose of 5-Azacytidine (5-Aza) (Cat. No. A2385 - Sigma-Aldrich) for the treatment of A375, WM115, SK-MEL-23, and SK-MEL-28 cells, as well as to evaluate the IC_{50} doses of 1S,3R-RSL 3 (Cat. No. SML2234 – Sigma Aldrich), Erastin (Cat. No. E7781 - Sigma Aldrich), and ammonium iron (III) citrate (Cat. No. A11199 - Invitrogen, Thermo Fisher Scientific™, Waltham, MA, United States) in A375 transfected cells. Notably, all the reported melanoma cell lines were seeded in 96-well plates at the density of 2 x 10^3 cells per well in 100 μL of complete medium, except for WM115 (3 x 10^3 per well), prior to the treatment with serial dilutions of 5-Aza (100 - 10 - 1 - 0.1 - 0.01 - 0.001 μM), 1S,3R-RSL 3 (100 - 10 - 1 - 0.1 - 0.01 - 0.001 μM), Erastin (10 - 1 - 0.1 - 0.01 - 0.001 - 0.0001 μM), and ammonium iron (III) citrate (Fe3+) (100 - 10 - 1 - 0.1 - 0.01 - 0.001 mM). DMSO (Cat. No. D8418 – Sigma Aldrich) was used as vehicle control for all the treatments, except for ammonium iron (III) citrate that was resuspended in complete RPMI-1640 medium. After 72h of treatment, the culture medium was removed and 100 μL of MTT solution (Cat. No. 158990010 - Thermo Fisher Scientific™, Waltham, MA, United States) (MTT + RPMI-1640 *ratio* 1:10) were added to each well, incubating the plate at 37°C and 5% CO_2 for 3h. Following the

incubation, the MTT solution was removed and 100 µL DMSO (Cat. No. D8418 – Sigma Aldrich) were added to each well for the dissolution of formazan crystals. Finally, the absorbance of each well was measured at 620 nm by using the Tecan Sunrise^{TM} microplate reader to retrieve the optical density (OD) values of each well. All the experiments were performed in triplicate.

The A375, WM115, SK-MEL-23, and SK-MEL-28 cell lines were treated with 5-Aza (Cat. No. A2385 - Sigma-Aldrich) according to the previously computed IC_{50} dose (0.75 µM for A375 and WM115, 1.9 µM for SL-MEL-23, and 3.5 µM for SK-MEL-28) to evaluate the effect of DNA demethylation on *SLC22A17* all variants and variants 1, 2, and 3 expression. Briefly, each melanoma cell line was seeded in standard 100 mm cell-culture dishes (Qiagen, Hilden, Germany) at the density of 1 x 10^6 cells in 10 mL of complete medium and treated with the relative IC_{50} dose of 5-Aza for five consecutive days. Following the treatment, the medium culture was replaced, allowing the cells to grow for 24h/48h. Then, the adherent cells were collected by scraping, and cell pellets were obtained by centrifugation and frozen at -80 °C until downstream analyses. All the experiments were performed in triplicate. Of note, the M14, A2058, and MeWo cell lines were excluded from the 5-Aza functional study due to low baseline methylation levels of the selected DNA methylation hotspots.

3.11 Statistical analyses

For the *in silico* study, the differential analyses of the *SLC22A17* expression and DNA methylation levels were performed by Mann-Whitney test for comparing two groups, while the comparison analyses of more than two groups were executed through Kruskal-Wallis test and Dunn's multiple comparisons test (GraphPad Prism - version 8.0.2, GraphPad Software, San Diego, CA, USA). The difference between the comparison groups was reported as Fold Change (FC) computed according to the formula: $\pm 2^{|median\ 1 - median\ 2|}$. Correlation analysis between the *SLC22A17* gene/variants expression and CG probesets DNA methylation levels (TCGA PANCAN SKCM) was performed by GraphPad Prism (version 8.0.2) using Pearson's correlation test. OS and PFI analyses of both *SLC22A17* gene/variants expression and CG probesets methylation levels (TCGA PANCAN SKCM) were

performed by Kaplan Meier analysis (GraphPad Prism - version 8.0.2). Chi square and *p*-value were estimated through Log-rank (Mantel-Cox) test and the median survival time was calculated for each Kaplan Meier curve.

Regarding *in vitro* experiments, statistical analyses of the *SLC22A17* all variants/variants 1, 2, and 3 expression levels were performed by two tailed T-test for two groups comparison, whereas One-way ANOVA test and Tukey's multiple comparisons test were used to compare more than two groups. Differential analysis of *SLC22A17* DNA methylation levels was conducted by Mann-Whitney test for two comparison groups, while Kruskal-Wallis test and Dunn's multiple comparisons test were used for more than two groups.

Similarly, the statistical analysis of the cg17199325 DNA methylation hotspot in FFPE melanoma and nevi samples was performed by Mann-Whitney test for two groups comparison, while Kruskal-Wallis test and Dunn's multiple comparisons test were used for more than two groups (GraphPad Prism - version 8.0.2). Moreover, the Receiver Operating Characteristic (ROC) analysis was also executed by GraphPad Prism (version 8.0.2, GraphPad Software, San Diego, CA, USA) to evaluate sensitivity and specificity of the diagnostic test.

4. RESULTS

4.1 Bioinformatic analysis of *SLC22A17* gene/variants expression and DNA methylation in melanoma and nevi samples

The differential analysis of *SLC22A17* expression and DNA methylation levels between melanoma and nevi samples was performed using the GSE112509 and GSE120878 datasets, respectively (Figure 8). The obtained results showed that the *SLC22A17* gene (ENSG00000092096.14) was significantly downregulated in melanoma compared to nevi (FC = -2.1, $p < 0.01$) (Figure 8A). Of note, differential analysis of *SLC22A17* methylation status showed that the DNA methylation levels of both up- and down-stream promoter CG probesets were weakly higher in melanoma samples compared to controls (from cg23464698 to cg14920289). However, a statistical significance was observed only for the cg17199325 (Beta difference = 0.08, $p < 0.0001$) due to low DNA methylation levels of the promoter region in both comparing groups (Figure 8B).

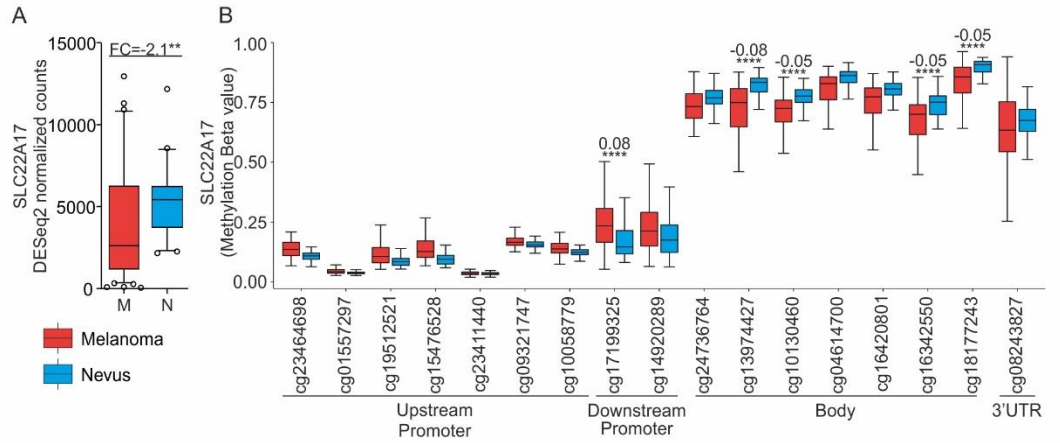

Figure 8. *In silico* analysis of *SLC22A17* expression and DNA methylation status in melanoma and nevi. (A) The differential analysis of *SLC22A17* gene expression (ENSG00000092096.14) between melanoma and nevi samples was performed using the GSE112509 dataset. The difference between the comparison groups was reported as ratio of median values. **(B)** Differential analysis of DNA methylation levels between melanoma and nevi was conducted analyzing the GSE120878 dataset. Beta difference values were calculated as difference between medians of each group. Red and blue boxes indicate melanoma and nevi samples, respectively. *p-value*: ** < 0.01, **** < 0.0001.

An opposite trend was observed for the CG probesets of the body and 3'UTR regions (from cg24736764 to cg08243827), whose DNA methylation levels were

decreased in melanoma compared to nevi samples. Notably, a statistical significance was detected for 4 of 7 CG probesets belonging to the body region (cg13974427, cg10130460, cg16342550, and cg18177243) (Beta difference = from -0.05 to -0.08, $p < 0.0001$) (Figure 8B).

Profiling and correlation analyses of *SLC22A17* gene/variants expression and DNA methylation in melanoma samples were performed using the TCGA Pan-Cancer SKCM cohort (Figure 9). Notably, the ENSG00000092096.14, which included all the coding, non-coding, and retained intron variants, showed the highest expression levels (median $\log_2 = 3.073$), followed by the coding variants ENST00000354772.7 and ENST00000206544.8 (median $\log_2 = 2.4195$ and 0.5859, respectively) (Figure 9A). Regarding DNA methylation status, the profiling analysis revealed that the CG probesets of the upstream promoter region (from cg23464698 to cg10058779) were hypomethylated (median beta value: from 0.01415 to 0.1087), whereas the cg17199325 and cg14920289, belonging to the downstream promoter region, were partially methylated (median beta value: 0.209 and 0.2425, respectively). Conversely, the CG probesets within the body and 3'UTR (from cg24736764 to cg08243827) were all hypermethylated (median beta value > 0.6) (Figure 9B). To better understand the regulatory role of DNA methylation considering the relative position of CG probesets within the *SLC22A17* locus, the expression analysis was also performed by stratifying SKCM patients into five groups according to the methylation levels (Low: ≤ 0.2; Partially: > 0.2 and < 0.6; High: ≥ 0.6) of all the CG probesets pooled in promoter (from cg23464698 to cg14920289) and body (from cg24736764 to cg08243827) subgroups. No SKCM patients were included into promoter-high/body-partially group and body-low subgroups (Figure 9C). Interestingly, the *SLC22A17* expression levels were higher in SKCM patients belonging to the body-high groups compared to body-partially groups. In particular, the highest *SLC22A17* expression levels were detected in SKCM patients of the promoter-low/body-high group (median $\log_2 = 3.338$), while SKCM patients of the promoter-partially/body-partially group showed the lowest expression levels (median $\log_2 = -1.181$), indicating that DNA methylation status of both promoter and body regions had a pivotal role in the regulation of *SLC22A17* expression (Figure 9C).

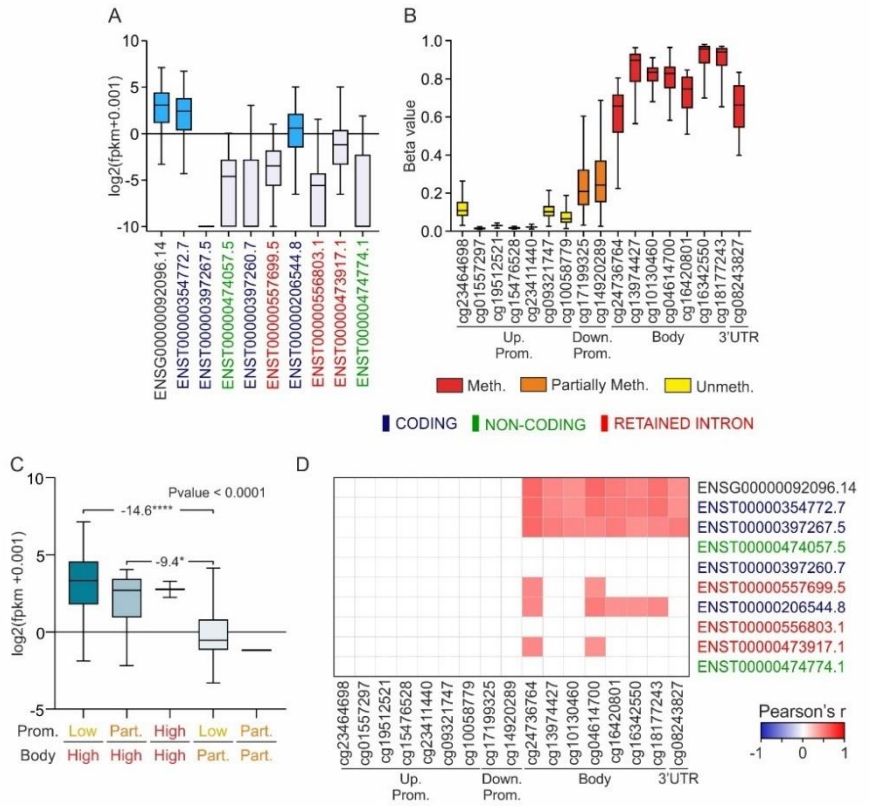

Figure 9. Profiling and correlation analyses of *SLC22A17* gene/variants expression and DNA methylation in melanoma. (A) Box plot analysis of *SLC22A17* gene/variants expression in melanoma samples retrieved from the TCGA Pan-Cancer SKCM cohort was conducted using TOIL RSEM fpkm normalized data. The cyan boxes indicate that the median levels of gene/variants are positive. **(B)** DNA methylation profiling of the *SLC22A17* CG probesets (TCGA Pan-Cancer SKCM cohort) was performed using the Methylation450K dataset. Red, orange, and yellow boxes indicate methylated (Beta value ≥ 0.6), partially methylated (0.6 < Beta value > 0.2), and unmethylated (Beta value ≤ 0.2) CG probesets, respectively. **(C)** The expression analysis of the *SLC22A17* gene (ENSG00000092096.14) was performed by stratifying tumor samples in different groups according to the median values of DNA methylation (Low: ≤ 0.2; Partially: > 0.2 and < 0.6; High: ≥ 0.6) of all promoter CG probesets (from cg23464698 to cg14920289) and the CG probesets belonging to the body region (from cg24736764 to cg08243827). FC and *p-value* are reported for each comparing group (*p-value*: * ≤ 0.05, **** < 0.0001). **(D)** Heatmap of correlation levels between *SLC22A17* gene/variants expression and DNA methylation levels in TCGA Pan-Cancer SKCM. The positive correlation pairs are reported in red (Pearson's r ≥ 0.4, *p-value* ≤ 0.05). The coding variants of *SLC22A17* are labeled in blue, the non-coding variants in green, and red was used for variants with retained introns.

The subsequent correlation analysis highlighted that DNA methylation status of all the CG probesets belonging to the body and 3'UTR regions (from cg24736764 to cg08243827) was positively correlated with the expression levels of ENSG00000092096.14, as well as with the coding variants ENST00000354772.7

and ENST00000397267.5 (Pearson's r > 0.4, $p \leq 0.05$) (Figure 9D). Moreover, the cg24736764 and cg04614700 of the intragenic region also showed a significant positive correlation with the *SLC2A17* variants ENST00000557699.5, ENST00000206544.8, and ENST00000473917.1 (Pearson's r > 0.4, $p \leq 0.05$). No significant correlations were observed between the CG probesets of the up- and down-stream promoter and *SLC22A17* gene/variants expression (Figure 9D).

4.2 OS and PFI analyses of *SLC22A17* gene/variants expression and DNA methylation in TCGA Pan-Cancer SKCM cohort

To evaluate the prognostic significance of *SLC22A17*, Kaplan-Meier analyses were performed by stratifying SKCM samples according to the gene/variants expression and DNA methylation levels (Figures 10 and 11). Of note, OS Kaplan-Meier analyses revealed that SKCM patients with *SLC22A17* (ENSG00000092096.14) expression levels above the median values computed for all patients showed a better OS compared to those with low expression levels (OS time - high expression = 4,000 days; OS time - low expression = 1,780 days) (*Chi square* = 17.13; $p < 0.0001$) (Figure 10A). Similarly, the expression levels of coding variants ENST00000354772.7 and ENST00000206544.8, as well as the retained intron variant ENST00000557699.5, were positively associated to OS of SKCM patients (OS time - high expression ≥ 3,266 days; OS time - low expression ≤ 1,910 days) (*Chi square* ≥ 5.059; $p \leq 0.0245$) (Figures 10B-D).

As regards *SLC22A17* DNA methylation levels, no significant associations were observed for CG probesets belonging to the up-/down-stream promoter and body regions, except for the intragenic cg16342550, whose hypermethylation (Beta value ≥ 0.6) represented a favorable prognostic factor for SKCM patients (OS time - CG probeset hypermethylation = 2,588 days ; OS time - CG probeset hypomethylation = 1,548 days) (*Chi square* = 3.666; $p < 0.05$) (Figure 10E).

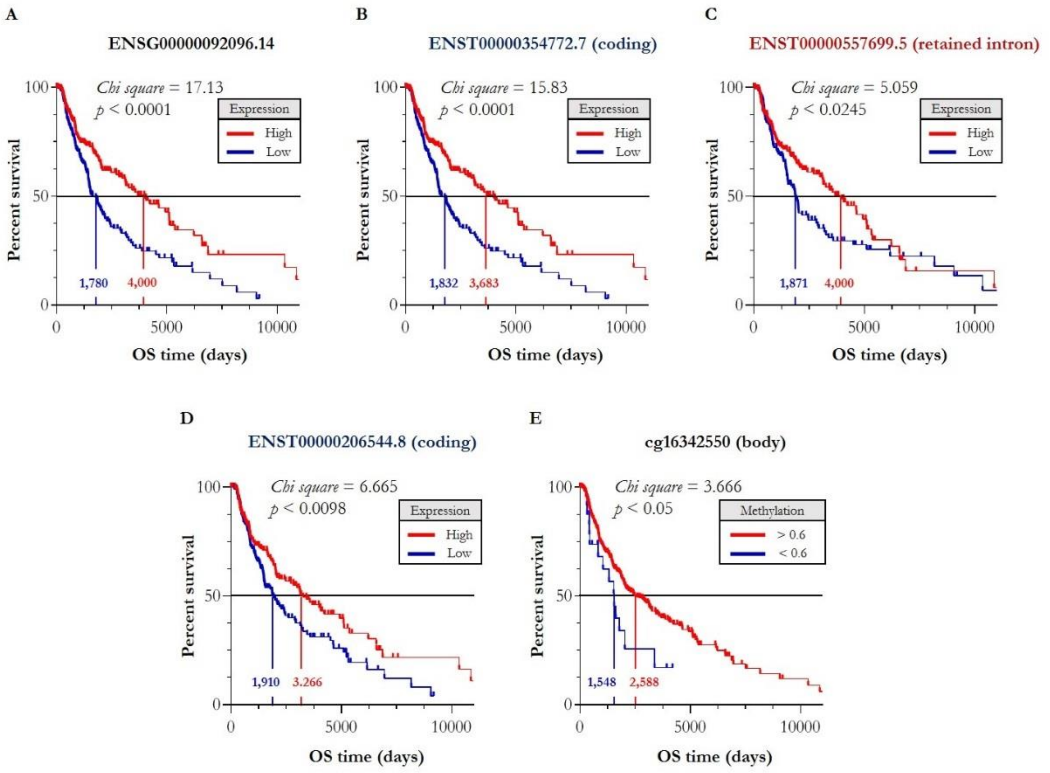

Figure 10. OS Kaplan-Meier analyses of *SLC22A17* expression and DNA methylation levels in melanoma. **(A-D)** The TCGA Pan-Cancer SKCM samples were stratified according to the *SLC22A17* gene/variants expression in high (above median value, red line) and low (below median value, line blue) groups to estimate the difference of OS among the considered groups. **(E)** OS analysis of the SKCM samples stratified in hypermethylated (Beta value ≥ 0.6, red line) and partially/hypo methylated groups (Beta value < 0.6, blue line) according to the methylation levels of the cg16342550 probeset.

Interestingly, a significant positive correlation was found between *SLC22A17* (ENSG00000092096.14) expression levels and PFI of SKCM patients (PFI time - high expression = 1,498 days; PFI time - low expression = 866 days) (*Chi square* = 10.93; $p < 0.0009$) (Figure 11A). Moreover, overexpression of different *SLC22A17* variants (ENST00000354772.7, ENST00000557699.5, ENST00000206544.8, and ENST00000474774.1) showed a strong association with better PFI of SKCM patients (PFI time - high expression ≥ 1,357 days; PFI time - low expression ≤ 986 days) (*Chi square* ≥ 4.413; $p \leq 0.0357$) (Figures 11B-E). Similar to OS analysis, PFI results revealed that just one CG probeset belonging to the body region (cg04614700) represented a favorable prognostic factor for SKCM patients, whose hypermethylation was positively associated with PFI (PFI time - CG probeset

hypermethylation = 1,247 days; PFI time - CG probeset hypomethylation = 757 days) (*Chi square* = 4.205; $p < 0.0403$) (Figure 11F).

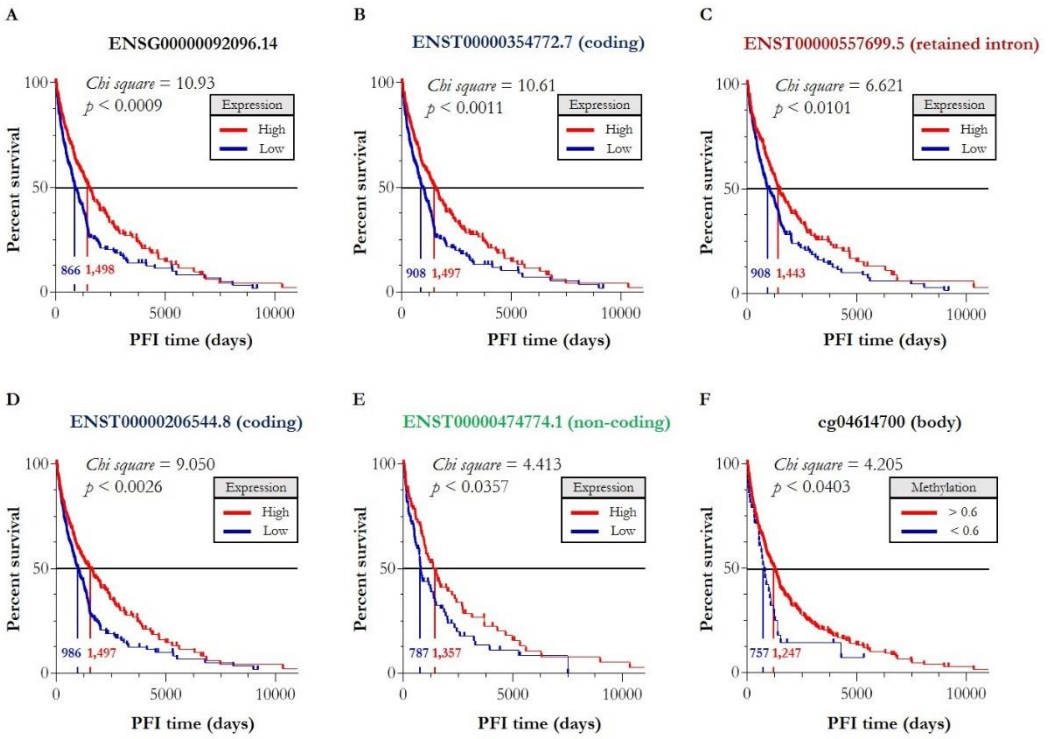

Figure 11. PFI Kaplan-Meier analyses of *SLC22A17* expression and DNA methylation levels in melanoma. **(A-E)** The TCGA Pan-Cancer SKCM samples were stratified according to the *SLC22A17* gene/variants expression in high (above median value, red line) and low (below median value, line blue) groups to estimate the difference of PFI among the considered groups. **(F)** PFI analysis of the SKCM samples stratified in hypermethylated (Beta value ≥ 0.6, red line) and partially/hypo methylated groups (Beta value < 0.6, blue line) according to the methylation levels of the cg04614700 probeset.

4.3 *In vitro* evaluation of *SLC22A17* expression and DNA methylation profile in melanoma cell lines

SLC22A17 expression levels and DNA methylation status were analyzed in seven melanoma cell lines to validate *in silico* results, which highlighted a strong involvement of DNA methylation in the regulation of *SLC22A17* expression. Specifically, A375, A2058, SK-MEL-28, WM115, MeWo, M14, and SK-MEL-23 cell lines were used for the relative quantification of *SLC22A17* all variants and variants 1, 2, and 3 expression by RT-qPCR (Figure 12A). Moreover, three *SLC22A17* methylation hotspots were also analyzed by MSRE-qPCR to evaluate the *SLC22A17* DNA methylation status in the reported melanoma cell lines (Figures

12B-D). The RT-qPCR analysis revealed that WM115 cells showed the highest expression levels of *SLC22A17* all variants/variants 1-3, especially for the variant 3 (Relative expression = All Vars: 7.0; Var1: 5.5; Var2: 6.5; Var3: 7.6).

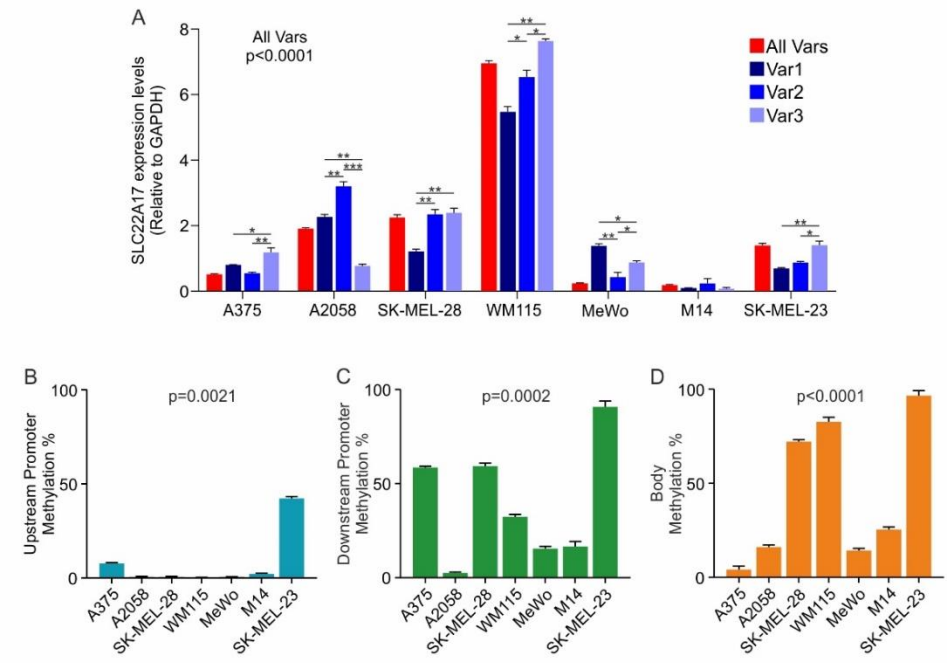

Figure 12. *SLC22A17* all variants/variants 1-3 expression and DNA methylation profiling in melanoma cell lines. (A) The RT-qPCR analysis of *SLC22A17* expression was performed amplifying variants 1,2, and 3, as well as all variants combined together, in seven melanoma cell lines. The differential analysis between *SLC22A17* all variants/variants 1-3 was performed by using One-way ANOVA test and Tukey's multiple comparisons test. *p-value*: * ≤ 0.05, ** < 0.01, *** < 0.001. **(B-D)** The MSRE-qPCR analysis was performed to evaluate DNA methylation levels of three *SLC22A17* hotspots mapped in the upstream promoter (chr14:23,821,982-23,822,182 - GRCh37/hg19), downstream promoter (chr14:23,821,211-23,821,359 - GRCh37/hg19), and body (chr14:23,816,960-23,817,116 - GRCh37/hg19) regions, respectively. Kruskal-Wallis test was performed to compare DNA methylation levels of each *SLC22A17* hotspot among the melanoma cell lines. All the experiments were performed in triplicate.

A similar trend was observed for A375, SK-MEL-28, and SK-MEL-23 cells, in which the expression levels of the *SLC22A17* variant 3 were higher compared to variants 1 and 2 (Relative expression Var3: 1.2, 2.4, and 1.4, respectively) (Figure 12A). Conversely, the expression levels of *SLC22A17* variant 3 were significantly lower compared to *SLC22A17* all variants/variants 1 and 2 in A2058 cells (Relative expression = All Vars: 1.9; Var1: 2.3; Var2: 3.2; Var3: 0.8). Low expression levels

of both *SLC22A17* all variants and wariants 1, 2, and 3 were detected in MeWo and M14 cell lines (Figure 12A). Regarding DNA methylation status, the MSRE-qPCR analysis showed that the *SLC22A17* upstream promoter hotspot was partially methylated only in SK-MEL-23 cells (42.3%), while low/undetectable methylation levels were observed for other melanoma cell lines (≤ 7.9%) (Figure 12B). Of note, the *SLC22A17* downstream promoter hotspot was hypermethylated in SK-MEL-23 (91%), partially methylated in A375, WM115, and SK-MEL-28 (58.8%, 32.6%, and 59.5%, respectively) and hypomethylated in A2058, MeWo, and M14 cells (≤ 16.8%) (Figure 12C). Similarly, high methylation levels of the *SLC22A17* body hotspot were detected in SK-MEL-23, WM115, and SK-MEL-28 (96.9%, 83%, and 72.5%, respectively), whereas low methylation levels were observed in other cell lines (≤ 25.8%) (Figure 12D).

The bisulfite sequencing was also performed for each melanoma cell line to evaluate the relationship between DNA methylation profile and *SLC22A17* expression levels. As reported in the heatmap (Figure 13), higher *SLC2A17* all variants/variants 1, 2, and 3 expression levels detected in WM115 were associated to the upstream promoter hypomethylation (0.7% ± 2.8), as well as downstream promoter and body hypermethylation (66.9% ± 20.4 and 75.4% ± 12.5, respectively).

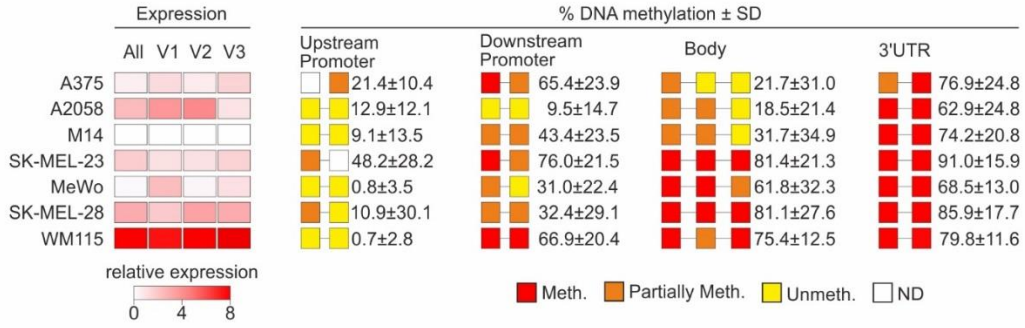

Figure 13. Heatmap of *SLC22A17* gene expression and DNA methylation in melanoma cell lines. On the left panel the *SLC22A17* expression levels of all variants and variants 1, 2, and 3 tested by RT-qPCR. The right panel shows the mean methylation levels ± SD values of the *SLC22A17* promoter (up- and down-stream), body, and 3'UTR regions. DNA methylation analysis was performed by bisulfite conversion followed by PCR amplification and Sanger sequencing. Red, orange, and yellow boxes indicate methylated (Beta value ≥0.6), partially methylated (0.6 < Beta value > 0.2), and unmethylated hotspots (Beta value ≤ 0.2), respectively. SD: standard deviation; ND: not detected.

Similarly, intragenic hypermethylation was also observed for SK-MEL-23 and SK-MEL-28 (body methylation state = 81.4% ± 21.3 and 81.1% ± 27.6, respectively). However, *SLC22A17* expression levels were lower in SK-MEL-23 and SK-MEL-28 compared to WM115 cells probably due to partially methylated state of the upstream promoter in SK-MEL-23 (48.2% ± 28.2) and downstream promoter in SK-MEL-28 (32.4% ± 29.1) (Figure 13). Among other melanoma cell lines, A2058 showed the highest *SLC22A17* all variants/variants 1, 2, and 3 expression levels, followed by A375 cells. In particular, A2058 methylation profile was characterized by low methylation state of the up- and down-stream promoter regions (12.9% ± 12.1 and 9.5% ± 14.7, respectively) and medium/low methylation of body (18.5% ± 21.4), while A375 showed medium/low methylation variance of both up-/down-stream promoter and body regions (21.4% ± 10.4, 65.4% ± 23.9, and 21.7% ± 31.0, respectively) (Figure 13). Finally, the lowest *SLC22A17* expression levels detected in M14 and MeWo cells were associated to hypomethylation of upstream promoter (9.1% ± 13.5 for M14 and 0.8% ± 3.5 for MeWo) and medium/low methylation variance of downstream promoter (43.4% ± 23.5 for M14 and 31.0% ± 22.4 for MeWo) and body regions (31.7% ± 34.9 for M14 and 61.8% ± 32.3 for MeWo). Although the 3'UTR region was hypermethylated (≥ 62.9% ± 24.8) in all melanoma cell lines, no relevant association was observed, indicating that the *SLC22A17* expression levels were mainly regulated by DNA methylation status of promoter and body regions (Figure 13).

4.4 Epigenetic reprogramming of *SLC22A17* expression in melanoma cell lines

SK-MEL-23, WM115, A375, and SK-MEL-28 cell lines were treated with the demethylating agent 5-Aza to further demonstrate the correlation between *SLC22A17* expression and DNA methylation (Figure 14). In particular, SK-MEL-23 were treated at concentration of 1.9 μM, WM115 and A375 at 0.75 μM, and SK-MEL-28 3.5 μM. M14, A2058, and MeWo cells were excluded from 5-Aza functional study due to the low methylation state of up-/down-stream promoter and body hotspots.

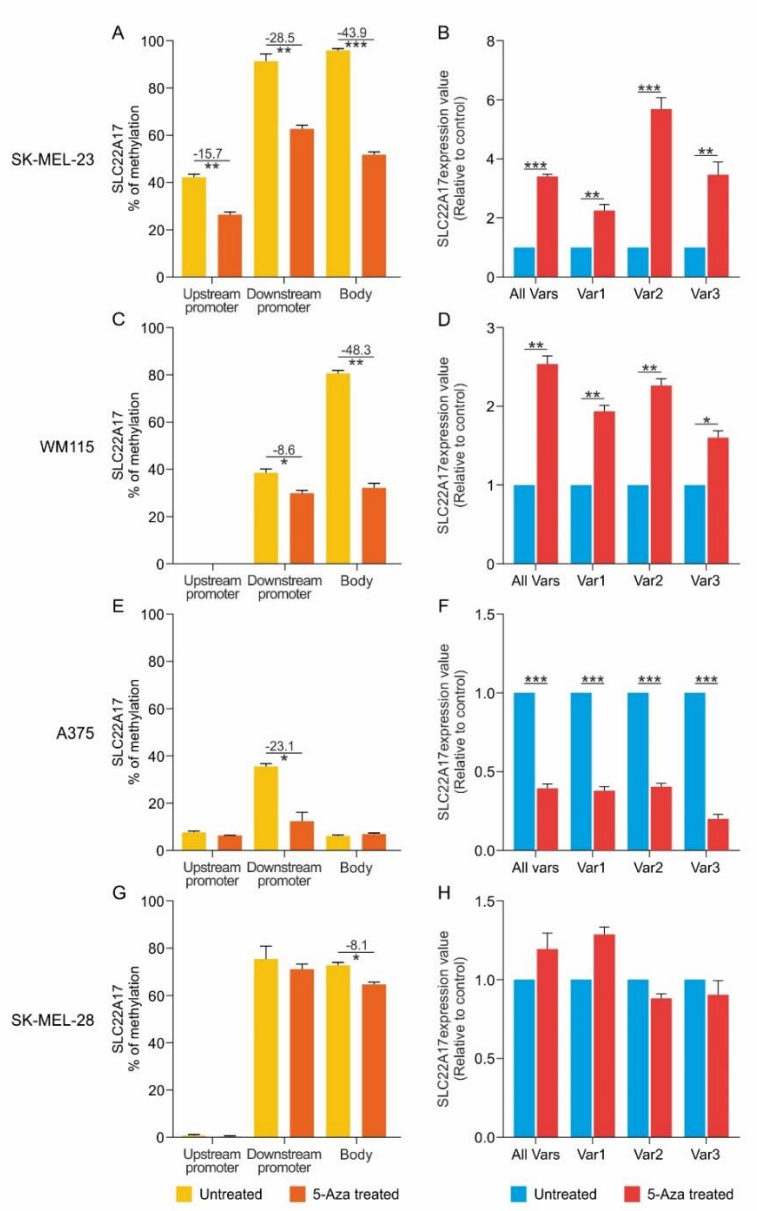

Figure 14. Expression and DNA methylation analyses of *SLC22A17* in 5-Aza treated melanoma cell lines. (A), **(C)**, **(E)**, and **(G)** DNA methylation analysis of the up-/down-stream promoter and body methylation hotspots in 5-Aza treated and untreated melanoma cell lines. The difference of DNA methylation levels between treated and untreated cells is reported as percentage value. **(B)**, **(D)**, **(F)**, and **(H)** *SLC22A17* expression analysis of all variants and variants 1, 2, and 3 in treated and control cells. The statistical significance was assessed by paired two tailed T-test. *p-value*: * ≤ 0.05, ** < 0.01, *** < 0.001. 5-Aza treatment was performed for five days at: 1.9 μM for SK-MEL-23; 0.75 μM for WM115 and A375; 3.5 μM for SK-MEL-28. All the experiments were performed in triplicate.

As expected, DNA methylation levels of all three methylation hotspots were significantly reduced in treated SK-MEL-23 (from 15.7% to 43.9%, $p < 0.01$),

whereas the expression levels of *SLC22A17* all variants and variants 1, 2, and 3 were increased compared to controls (All Vars: FC = 3.4, $p < 0.001$; Var1: FC = 2.3, $p < 0.01$; Var2: FC = 5.7, $p < 0.001$; Var3: FC = 3.5, $p < 0.01$) (Figures 14A and B). Similarly, 5-Aza treatment induced DNA demethylation of downstream promoter and body methylation hotspots in WM115 (upstream promoter: 8.6%, $p \leq 0.05$; body: 48.3%, $p < 0.01$), as well as significant upregulation of *SLC22A17* all variants/variants 1, 2, and 3 in treated compared to untreated WM115 cells (FC range: from 1.6 to 2.5, $p \leq 0.05$) (Figures 14C and D). An opposite trend was observed for A375 cells, in which *SLC22A17* expression levels were significantly downregulated (> 50%, $p < 0.001$) in treated compared to untreated cells probably due to low basal methylation status of all the considered DNA methylation hotspots. Indeed, no methylation variance was observed, except for downstream promoter hotspot (-23.1%) (Figures 14E and F). Moreover, no significant variation was detected neither for DNA methylation hotspots nor for the *SLC22A17* all variants/variants 1, 2, and 3 expression in 5-Aza resistant SK-MEL-28 (Figures 14G and H).

4.5 MSRE-ddPCR analysis of the cg17199325 methylation hotspot in FFPE melanoma and nevi samples

To evaluate the translational relevance of *in silico* and *in vitro* results, DNA methylation levels of the cg17199325 hotspot, belonging to the downstream promoter region, were analyzed in 32 melanoma and 15 nevi FFPE samples (Figure 15).

To this purpose, the custom MSRE-ddPCR assay was performed on FFPE samples demonstrating that DNA methylation levels of the *SLC22A17* hotspot were significantly higher in melanoma compared to nevi samples (median methylation percentage = 33.27% *vs* 20.90%; $p < 0.0001$) (Figure 15A). Moreover, ROC analysis revealed that the cg17199325 hotspot had a good biomarker performance (AUC = 0.85, $p < 0.0001$, cut off = 24.27%), suggesting its potential application as a diagnostic biomarker for cutaneous melanoma (Figure 15B).

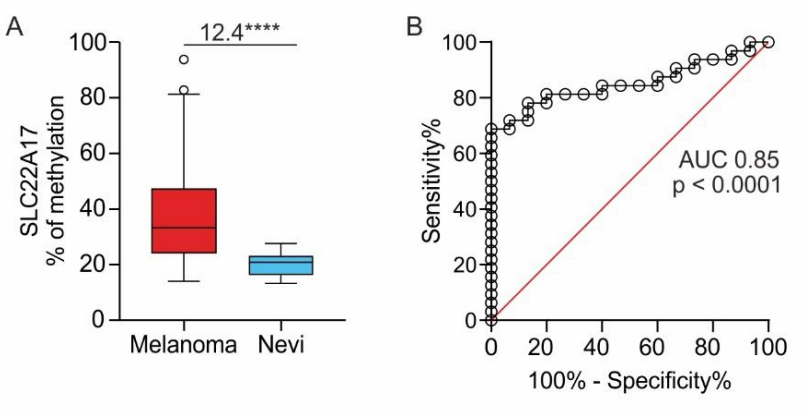

Figure 15. MSRE-ddPCR analysis of the cg17199325 hotspot in FFPE samples of melanoma and benign nevi. (A) DNA methylation levels of the *SLC22A17* downstream promoter hotspot were analyzed in melanoma tissue samples (N = 32) and benign nevi (N = 15) by using the custom MSRE-ddPCR assay. The difference between the comparison groups was evaluated by the Mann-Whitney test. *p-value*: **** < 0.0001. **(B)** Diagnostic test performance was conducted by ROC analysis.

The DNA methylation levels of the cg17199325 hotspot were also evaluated stratifying FFPE melanoma and nevi samples according to the available socio-demographic characteristics (age and gender) but no significant variations were observed among the considered groups (Figures 16A and B).

In addition, FFPE melanoma samples were stratified according to the main clinical-pathological features, including stage, Breslow thickness, *BRAF* status, number of mitosis, TILs, vascular invasion, and ulceration, as well as one-year Disease Free Survival (DFS) and five-year OS (Figures 16C-K).

Interestingly, DNA methylation levels of the *SLC22A17* downstream promoter hotspot were increased in advanced melanoma patients. However, a statistical significance was observed only for ulcerated melanoma (p = 0.009) (Figure 16I). No significance was detected for the other clinical-pathological conditions probably due to reduced number of the analyzed FFPE melanoma samples.

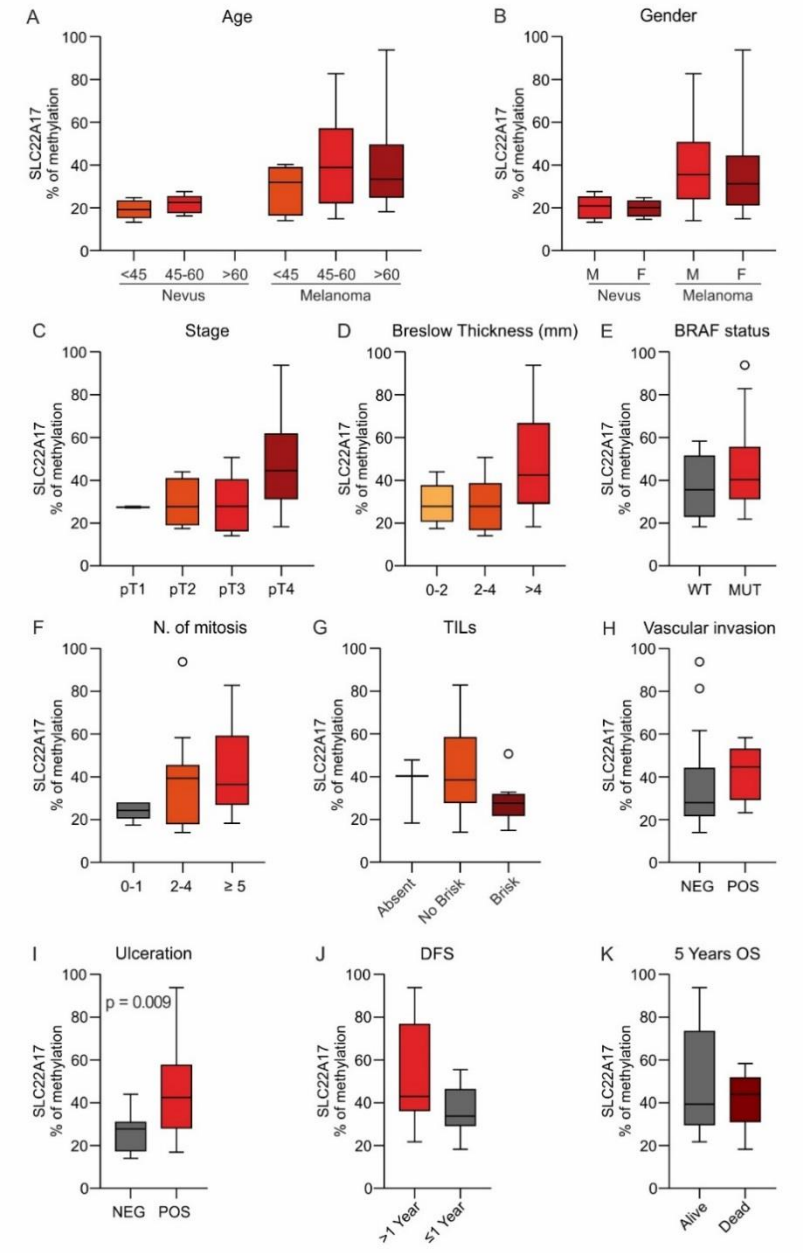

Figure 16. Differential analysis of the *SLC22A17* DNA methylation hotspot in FFPE samples according to demographic and clinical-pathological features. (A-B) DNA methylation levels of the cg17199325 hotspot in FFPE melanoma and nevi samples were stratified according to age and gender. **(C-K)** FFPE melanoma tissues were also stratified according to stage, Breslow thickness (mm), *BRAF* status, number of mitosis, tumor infiltrated leucocytes (TILs), vascular invasion, ulceration, disease free survival (DFS), and five years overall survival (OS). Mann-Whitney test was used for comparing two groups, whereas Kruskal-Wallis test and Dunn's multiple comparisons test were performed for the analyses of more than two groups.

4.6 *NGAL/SLC22A17* axis in ferroptosis regulation of A375 melanoma cell line

A375 cell transfection and transduction were performed to induce *NGAL* and *SLC22A17* variants 1, 2, and 3 overexpression and explore the involvement of *NGAL/SLC22A17* axis in iron trafficking and ferroptosis (Figure 17).

In particular, A375 transfected cells were treated with ferroptosis activators 1S,3R-RSL 3, Erastin, and ammonium iron (III) citrate at different concentrations for three days. Of note, cell viability assay revealed that $A375^{Empty/SLC22A17Var3}$ had a higher resistance to 1S,3R-RSL 3 treatment (IC_{50}: 0.99 ± 0.34 μM) compared to A375 clones with no *SLC22A17* variant 3 overexpression (IC_{50}: 0.04 ± 0.01 μM for $A375^{Empty/Empty}$ and 0.04 ± 0.02 for $A375^{NGAL/Empty}$) ($p \leq 0.05$) (Figure 17A). Moreover, the treatment resistance observed for $A375^{Empty/SLC22A17Var3}$ was significantly reduced by the concomitant overexpression of *NGAL* in $A375^{NGAL/SLC22A17Var3}$ (IC_{50}: 0.02 ± 0.02 μM) ($p \leq 0.05$), restoring baseline sensitivity to RSL-3 (Figure 17A).

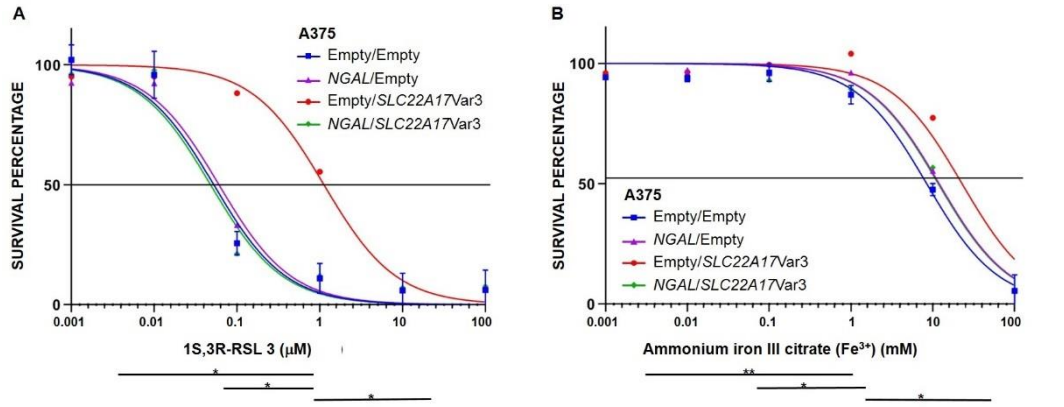

IC_{50} (uM)	*Empty/ Empty*	*NGAL/ Empty*	*Empty/ SLC22A17Var3*	*NGAL/ SLC22A17Var3*
RSL-3	0.04 ± 0.01	0.04 ± 0.02	0.99 ± 0.34	0.02 ± 0.02

IC_{50} (mM)	*Empty/ Empty*	*NGAL/ Empty*	*Empty/ SLC22A17Var3*	*NGAL/ SLC22A17Var3*
Fe^{3+}	8.42 ± 0.05	12.51 ± 0.71	22.74 ± 0.15	11.11 ± 0.81

Figure 17. Ferroptosis activators treatment of $A375^{Empty/Empty}$, $A375^{NGAL/Empty}$, $A375^{Empty/SLC22A17Var3}$, and $A375^{NGAL/SLC22A17Var3}$. Cell viability was evaluated by MTT assay following 72h of treatment with 1S,3R-RSL 3 **(A)** and ammonium iron (III) citrate **(B)** at different concentrations (RSL-3: 100 - 10 - 1 - 0.1 - 0.01 - 0.001 μM) (Fe3+: 100 - 10 - 1 - 0.1 - 0.01 - 0.001 mM). The statistical significance was assessed by paired two tailed T-test. *p-value*: * ≤ 0.05, ** < 0.01. All the experiments were performed in triplicate.

Interestingly, $A375^{Emty/SLC22A17Var3}$ showed increased resistance to ammonium iron (III) citrate treatment (IC_{50}: 22.74 ± 0.15 mM) compared to other cell lines (IC_{50}:

8.42 ± 0.05 mM for A375$^{Empty/Empty}$, 12.51 ± 0.71 mM for A375$^{NGAL/Empty}$, and 11.11 ± 0.81 mM for A375$^{NGAL/SLC22A17Var3}$) ($p \leq 0.05$) (Figure 17B).

Similar to 1S,3R-RSL 3 treatment, the baseline sensitivity to ammonium iron (III) citrate was restored in A375$^{NGAL/SLC22A17Var3}$. Although the A375 clones overexpressing *NGAL* (A375$^{NGAL/Empty}$ and A375$^{NGAL/SLC22A17Var3}$) were slightly resistant to ammonium iron (III) citrate treatment compared to relative control A375$^{Empty/Empty}$, no statistical significance was observed (Figure 17B).

The overexpression of *SLC22A17* variants 1 and 2 (A375$^{Empty/SLC22A17\text{Var2}}$ and A375$^{Empty/SLC22A17\text{Var3}}$) unaffected the resistance to 1S,3R-RSL 3 and ammonium iron (III) citrate treatments compared to the relative control (A375$^{Empty/Empty}$) and A375 clones overexpressing *NGAL* (A375$^{NGAL/Empty}$, A375$^{NGAL/SLC22A17Var2}$, and A375$^{NGAL/SLC22A17Var3}$). Moreover, A375 clones overexpressing *NGAL* and/or *SLC22A17* variants 1, 2, and 3 showed no significant variation of resistance to Erastin treatment compared to A375$^{Empty/Empty}$ (data not shown).

5. DISCUSSION AND CONCLUDING REMARKS

Over the years, several studies demonstrated that both genetic and environmental factors are associated to an increased risk of melanoma development. Notably, chronic and intermittent exposure to UV radiation represents the main modifiable risk factor, leading to accumulation of genetic mutations and neoplastic transformation of melanocytes that acquire a tumor-like phenotype characterized by abnormal cell proliferation and loss of cellular regulatory processes (Bermudez Y., 2014; Emri G et al., 2018; Sun X et al., 2020). Driver and passenger mutations may affect genes involved in several signaling transduction pathways, including the MAPK and PI3K/Akt/mTOR pathways. In particular, alteration of *BRAF* and *NRAS* gene expression leads to the constitutive activation of these signaling pathways, whose dysregulation is related to cutaneous melanoma initiation and progression (Amaral T et al., 2017; Davis EJ et al., 2018; Chamcheu JC et al., 2019).

Besides genetic mutations, epigenetic regulatory mechanisms have been described to be involved in melanoma development. Among epigenetic alterations, DNA methylation is the most well-characterized, which play a pivotal role in the regulation of cancer-related genes. As widely reported in the literature, promoter hypomethylation induces activation of oncogenes, whereas increased DNA methylation levels of the promoter region are associated to tumor suppressor gene silencing (Moarii M et al., 2015; Nishiyama A and Nakanishi M., 2021). Moreover, intragenic DNA methylation seems to be actively involved in multiple gene regulation processes, including alternative promoter usage, cryptic transcription initiation, regulation of short and long ncRNAs, as well as alternative splicing and enhancer activity (Lee SM et al., 2015; Neri F et al., 2017; Wang Q et al., 2022). However, the exact role of intragenic DNA methylation in the regulation of gene expression has not been completely elucidated yet. Interestingly, a growing number of recent studies have also highlighted that aberrant DNA methylation significantly influences TME homeostasis, promoting tumor-like phenotype of stromal and immune cells (Zhang MW et al., 2017; Yang J et al., 2023; Zhong F et al., 2023).

In this field, our research group has previously demonstrated the role of DNA methylation in the modulation of the *NGAL/SLC22A17/MMP-9* network in TCGA tumors, whose dysregulation leads to TME remodeling and cancer progression

(Candido S et al., 2022b). Interestingly, the activation of *NGAL/MMP-9* pathway is strictly related to tumor invasiveness, ECM degradation, and metastatic spreading of cancer cells (Candido S et al., 2016). On the other hand, the *NGAL/SLC22A17* complex seems to play a critical role in ferroptosis, mediating either uptake of extracellular iron or removal of intracellular iron with different effects on tumor cells depending on TME context (Xiao X et al., 2017).

Starting from these observations and our preliminary studies, the present study aimed to deeply explore the epigenetic phenomena affecting *SLC22A17* expression in cutaneous melanoma to identify potential DNA methylation hotspots with diagnostic and prognostic values. In addition, the regulatory role of *SLC22A17* in ferroptosis of melanoma cells was also investigated to provide a starting point for novel therapeutic strategies.

To this purpose, computational analyses were first performed to identify *SLC22A17* expression and DNA methylation profile in melanoma using TCGA and GEO datasets. In particular, differential and correlation analyses were carried out to evaluate the expression levels of each *SLC22A17* variant and the methylation status of relative CG probesets. Moreover, OS and PFI analyses were performed to investigate the diagnostic and prognostic values of *SLC22A17* gene/variants expression and DNA methylation hotspots. The *in silico* results were then validated through *in vitro* functional studies on different melanoma cell lines, which were treated with 5-Aza to investigate the epigenetic phenomena involved in the regulation of *SLC22A17* expression. Moreover, DNA methylation levels of the identified *SLC22A17* hotspot (cg17199325) were analyzed in FFPE melanoma and nevi samples to confirm the translational relevance of the *in silico* and *in vitro* results obtained in the present study. Finally, the role of NGAL/SLC22A17 complex in iron-mediated cell death was also explored by treating A375 transfected cells with ferroptosis inductors.

The bioinformatic analysis showed that *SLC22A17* was significantly downregulated in melanoma compared to nevi samples, suggesting that *SLC22A17* may act as a tumor suppressor gene. This result was consistent with those previously reported in the literature, which demonstrated that *SLC22A17* downregulation was strictly related to initiation, progression, and drug resistance of different tumor

types (Liu F et al., 2018; Wei J et al., 2020; Candido S et al., 2022b; Lavoro A et al., 2023). Interestingly, the expression pattern of *SLC22A17* appeared to be strongly associated with the DNA methylation status of both promoter and body regions. In particular, the expression analysis revealed that SKCM samples showing promoter hypomethylation and body hypermethylation had the highest *SLC22A17* expression levels compared to other groups.

These findings were confirmed by correlation analysis, which highlighted strong positive correlation between *SLC22A17* gene/variants expression and DNA methylation of body CG probesets, indicating that intragenic hypermethylation synergically contributes to *SLC22A17* gene regulation along with promoter methylation. In addition, OS and PFI analyses demonstrated that the overexpression of *SLC22A17* gene (ENSG00000092096.14) and some of its variants (ENST00000354772.7, ENST00000557699.5, ENST00000206544.8, and ENST00000474774.1), as well as the hypermethylation of CG probesets belonging to the intragenic region (cg16342550 and cg04614700), significantly enhanced the survival rate of SKCM patients, indicating that both *SLC22A17* expression and intragenic DNA methylation could represent valuable prognostic biomarkers for cutaneous melanoma.

Then, *in vitro* functional studies were performed to better investigate the role of DNA methylation in the regulation of *SLC22A17* expression. In particular, *SLC22A17* all variants/variants 1, 2, and 3 expression and DNA methylation levels of up-/down-stream promoter and body hotspots were evaluated in seven melanoma cell lines by RT-qPCR and MSRE-qPCR, respectively. The results of *in vitro* analyses revealed that *SLC22A17* expression was strictly associated to hypomethylation of promoter region and intragenic hypermethylation. Of note, 5-Aza treatment of melanoma cells showed that promoter demethylation significantly increased *SLC22A17* all variants/variants 1, 2, and 3 expression levels, especially in SK-MEL-23 and WM115 cell lines. These findings are in agreement with aforementioned *in silico* results, demonstrating that *SLC22A17* expression is strongly regulated by such epigenetic phenomena.

Of note, *in silico* and *in vitro* results were also validated on FFPE melanoma and nevi samples. Notably, the MSRE-ddPCR analysis performed on clinical samples

demonstrated that cg17199325 hotspot, belonging to the *SLC22A17* downstream promoter region, showed higher methylation levels in melanoma compared to benign nevi samples. Notably, the positive correlation observed between the *SLC22A17* DNA methylation hotspot and advanced stages melanoma patients highlighted that the cg17199325 could be considered as a promising diagnostic and prognostic biomarker for cutaneous melanoma.

Finally, functional study was performed on A375 transfected cells to explore the involvement of *NGAL/SLC22A17* axis in iron trafficking and ferroptosis. Interestingly, A375 overexpressing *SLC22A17* variant 3 ($A375^{Empty/SLC22A17Var3}$) acquired resistance to ammonium iron (III) citrate and 1S,3R-RSL 3 treatments compared to A375 overexpressing *SLC22A17* variants 1 and 2 and relative controls. Conversely, baseline sensitivity to ferroptosis activators was restored by the concomitant overexpression of *NGAL* ($A375^{NGAL/SLC22A17Var3}$), indicating that the overexpression of *SLC22A17* variant 3 could play a pivotal role in ferroptosis resistance of melanoma cells.

As previously reported in the literature, dysregulation of *SLC22A17* expression levels could be related to cancer survival and proliferation by affecting the iron metabolism of cancer cells. For instance, it has been reported that aberrant *SLC22A17* expression inhibited iron efflux from tumor cells, resulting in iron-dependent proliferation and resistance to ferroptosis (Devireddy LR et al., 2005; Hvidberg V et al., 2005; Iannetti A et al., 2008). On the other hand, intracellular iron overload induced by *SLC22A17* dysregulation could have detrimental effects on cancer cell survival, inducing oxidative stress and ferroptosis (Lin X et al., 2020; Wu Y et al., 2020). Moreover, recent studies reported that *SLC22A17* expression levels could be predictive of response to ferroptosis activators, representing a potential pharmacological target for novel effective therapeutic strategies against different tumor types (Wei J et al., 2020; Wang X et al., 2021; Zhao S et al., 2021). Based on this evidence, we may suppose that the targeting of *SLC22A17* variant 3 could sensitize melanoma cells to iron-dependent death. In particular, the concomitant overexpression of *NGAL* could exert a pivotal role in reducing drug resistance of melanoma cancer cells. However, further studies are mandatory to

clarify if *SLC22A17* variant 3 overexpression confers ferroptosis resistance in cutaneous melanoma, as well as the role of *NGAL* in ferroptosis induction.

Overall, the present study demonstrates that DNA methylation status of both promoter and intragenic regions significantly affects *SLC22A17* expression levels in cutaneous melanoma. In particular, the cg17199325 methylation hotspot as a potential epigenetic biomarker may pave the way for novel DNA methylation hotspots with diagnostic and prognostic values. Therefore, the MSRE-ddPCR analysis of such DNA methylation hotspots in individuals at risk for cutaneous melanoma or with a previous diagnosis of melanoma could be valuable to predict development risk and prognosis of cancer patients. However, these preliminary results should be further validated in a wider cohort of melanoma patients and healthy controls to obtain a strong clinical relevance. In addition, functional study results highlighting the involvement of *SLC22A17* variant 3 in ferroptosis resistance could represent an attractive starting point for further investigations on *SLC22A17* role in iron-dependent death of melanoma cells aimed to identify potential targets for novel effective therapeutic strategies.

6. REFERENCES

Aasen SN, Parajuli H, Hoang T, Feng Z, Stokke K, Wang J, *et al*. (2019). Effective Treatment of Metastatic Melanoma by Combining MAPK and PI3K Signaling Pathway Inhibitors. *Int J Mol Sci*. 20:4235. doi: 10.3390/ijms20174235.

Ahmadi O, Das M, Hajarizadeh B, Mathy JA. (2021). Impact of Shave Biopsy on Diagnosis and Management of Cutaneous Melanoma: A Systematic Review and Meta-Analysis. *Ann Surg Oncol*. 28:6168-6176. doi: 10.1245/s10434-021-09866-3.

Alendar T, Kittler H. (2018). Morphologic characteristics of nevi associated with melanoma: a clinical, dermatoscopic and histopathologic analysis. *Dermatol Pract Concept*. 8:104-108. doi: 10.5826/dpc.0802a07.

Aleotti V, Catoni C, Poggiana C, Rosato A, Facchinetti A, Scaini MC. (2021). Methylation Markers in Cutaneous Melanoma: Unravelling the Potential Utility of Their Tracking by Liquid Biopsy. *Cancers (Basel)*. 13:6217. doi: 10.3390/cancers13246217.

Ali Syeda Z, Langden SSS, Munkhzul C, Lee M, Song SJ. (2020). Regulatory Mechanism of MicroRNA Expression in Cancer. *Int J Mol Sci*. 21:1723. doi: 10.3390/ijms21051723.

Al-Ostoot FH, Salah S, Khamees HA, Khanum SA. (2021). Tumor angiogenesis: Current challenges and therapeutic opportunities. *Cancer Treat Res Commun*. 28:100422. doi: 10.1016/j.ctarc.2021.100422.

Alqathama A. (2020). BRAF in malignant melanoma progression and metastasis: potentials and challenges. *Am J Cancer Res*. 10:1103-1114.

Amaral T, Sinnberg T, Meier F, Krepler C, Levesque M, Niessner H, *et al*. (2017). The mitogen-activated protein kinase pathway in melanoma part I - Activation and primary resistance mechanisms to BRAF inhibition. *Eur J Cancer*. 73:85-92. doi: 10.1016/j.ejca.2016.12.010.

Anderson NM, Simon MC. (2020). The tumor microenvironment. *Curr Biol*. 30:R921-R925. doi: 10.1016/j.cub.2020.06.081.

Angeloni A, Bogdanovic O. (2021). Sequence determinants, function, and evolution of CpG islands. *Biochem Soc Trans*. 49:1109-1119. doi: 10.1042/BST20200695.

Aoude LG, Bonazzi VF, Brosda S, Patel K, Koufariotis LT, Oey H, *et al*. (2020). Pathogenic germline variants are associated with poor survival in stage III/IV melanoma patients. *Sci Rep*. 10:17687. doi: 10.1038/s41598-020-74956-3.

Arisi M, Zane C, Caravello S, Rovati C, Zanca A, Venturini M, *et al*. (2018). Sun Exposure and Melanoma, Certainties and Weaknesses of the Present Knowledge. *Front Med (Lausanne)*. 5:235. doi: 10.3389/fmed.2018.00235.

Arnold M, Singh D, Laversanne M, Vignat J, Vaccarella S, Meheus F, *et al*. (2022). Global Burden of Cutaneous Melanoma in 2020 and Projections to 2040. *JAMA Dermatol*. 158:495-503. doi: 10.1001/jamadermatol.2022.0160.

Auclair G, Guibert S, Bender A, Weber M. (2014). Ontogeny of CpG island methylation and specificity of DNMT3 methyltransferases during embryonic development in the mouse. *Genome Biol*. 15:545. doi: 10.1186/s13059-014-0545-5.

Baldea I, Giurgiu L, Teacoe ID, Olteanu DE, Olteanu FC, Clichici S, *et al*. (2018). Photodynamic Therapy in Melanoma - Where do we Stand? *Curr Med Chem*. 25:5540-5563. doi: 10.2174/0929867325666171226115626.

Barros-Silva D, Marques CJ, Henrique R, Jerónimo C. (2018). Profiling DNA Methylation Based on Next-Generation Sequencing Approaches: New Insights and Clinical Applications. *Genes (Basel)*. 9:429. doi: 10.3390/genes9090429.

Battaglia AM, Chirillo R, Aversa I, Sacco A, Costanzo F, Biamonte F. (2020). Ferroptosis and Cancer: Mitochondria Meet the "Iron Maiden" Cell Death. *Cells*. 9:1505. doi: 10.3390/cells9061505.

Becevic M, Smith E, Golzy M, Bysani R, Rosenfeld A, Mutrux ER, *et al*. (2021). Melanoma Extension for Community Healthcare Outcomes: A Feasibility Study of Melanoma Screening Implementation in Primary Care Settings. *Cureus*. 13:e15322. doi: 10.7759/cureus.15322.

Behrens CL, Thorgaard C, Philip A, Bentzen J. (2013). Sunburn in children and adolescents: associations with parents' behaviour and attitudes. *Scand J Public Health*. 41:302-310. doi: 10.1177/1403494813476158.

Belhabib I, Zaghdoudi S, Lac C, Bousquet C, Jean C. (2021). Extracellular Matrices and Cancer-Associated Fibroblasts: Targets for Cancer Diagnosis and Therapy? *Cancers (Basel)*. 13:3466. doi: 10.3390/cancers13143466.

Berger SL, Kouzarides T, Shiekhattar R, Shilatifard A. (2009). An operational definition of epigenetics. *Genes Dev*. 23:781-783. doi: 10.1101/gad.1787609.

Bergoug M, Doudeau M, Godin F, Mosrin C, Vallée B, Bénédetti H. (2020). Neurofibromin Structure, Functions and Regulation. *Cells*. 9:2365. doi: 10.3390/cells9112365.

Bermudez Y. (2014). Ultraviolet involvement in melanocyte transformation to melanoma. *Br J Dermatol*. 171:1289. doi: 10.1111/bjd.13452.

Bhatt M, Nabatian A, Kriegel D, Khorasani H. (2016). Does an increased number of moles correlate to a higher risk of melanoma? *Melanoma Manag*. 3:85-87. doi: 10.2217/mmt-2016-0001.

Bouras E, Karakioulaki M, Bougioukas KI, Aivaliotis M, Tzimagiorgis G, Chourdakis M. (2019). Gene promoter methylation and cancer: An umbrella review. *Gene*. 710:333-340. doi: 10.1016/j.gene.2019.06.023.

Braicu C, Buse M, Busuioc C, Drula R, Gulei D, Raduly L, *et al*. (2019). A Comprehensive Review on MAPK: A Promising Therapeutic Target in Cancer. *Cancers (Basel)*. 11:1618. doi: 10.3390/cancers11101618.

Bray F, Ferlay J, Soerjomataram I, Siegel RL, Torre LA, Jemal A. (2018). Global cancer statistics 2018: GLOBOCAN estimates of incidence and mortality

worldwide for 36 cancers in 185 countries. *CA Cancer J Clin*. 68:394-424. doi: 10.3322/caac.21492.

Breslow A. (1970). Thickness, cross-sectional areas and depth of invasion in the prognosis of cutaneous melanoma. *Ann Surg*. 172:902-908. doi: 10.1097/00000658-197011000-00017.

Briatico G, Mancuso P, Argenziano G, Longo C, Mangone L, Moscarella E, *et al*. (2022). Trends in cutaneous melanoma mortality in Italy from 1982 to 2016. *Int J Dermatol*. 61:1237-1244. doi: 10.1111/ijd.16173.

Burke EE, Sondak VK. (2018). Surgical management of melanoma. *Semin Cutan Med Surg*. 37:101-108. doi: 10.12788/j.sder.2018.018.

Cabrita R, Mitra S, Sanna A, Ekedahl H, Lövgren K, Olsson H, *et al*. (2020). The Role of PTEN Loss in Immune Escape, Melanoma Prognosis and Therapy Response. *Cancers (Basel)*. 12:742. doi: 10.3390/cancers12030742.

Cain JA, Montibus B, Oakey RJ. (2022). Intragenic CpG Islands and Their Impact on Gene Regulation. *Front Cell Dev Biol*. 10:832348. doi: 10.3389/fcell.2022.832348.

Candido S, Rapisarda V, Marconi A, Malaponte G, Bevelacqua V, Gangemi P, *et al*. (2014). Analysis of the B-RafV600E mutation in cutaneous melanoma patients with occupational sun exposure. *Oncol Rep*. 31:1079-1082. doi: 10.3892/or.2014.2977.

Candido S, Abrams SL, Steelman LS, Lertpiriyapong K, Fitzgerald TL, Martelli AM, *et al*. (2016). Roles of NGAL and MMP-9 in the tumor microenvironment and sensitivity to targeted therapy. *Biochim Biophys Acta*. 1863:438-448. doi: 10.1016/j.bbamcr.2015.08.010.

Candido S, Salemi R, Piccinin S, Falzone L, Libra M. (2022a). The PIK3CA H1047R Mutation Confers Resistance to BRAF and MEK Inhibitors in A375 Melanoma Cells through the Cross-Activation of MAPK and PI3K-Akt Pathways. *Pharmaceutics*. 14:590. doi: 10.3390/pharmaceutics14030590.

Candido S, Tomasello B, Lavoro A, Falzone L, Gattuso G, Russo A, *et al*. (2022b). Bioinformatic analysis of the LCN2-SLC22A17-MMP9 network in cancer: The role of DNA methylation in the modulation of tumor microenvironment. *Front Cell Dev Biol*. 10:945586. doi: 10.3389/fcell.2022.945586.

Carbone M, Harbour JW, Brugarolas J, Bononi A, Pagano I, Dey A, *et al*. (2020). Biological Mechanisms and Clinical Significance of BAP1 Mutations in Human Cancer. *Cancer Discov*. 10:1103-1120. doi: 10.1158/2159-8290.CD-19-1220.

Castellani G, Buccarelli M, Arasi MB, Rossi S, Pisanu ME, Bellenghi M, *et al*., (2023). BRAF Mutations in Melanoma: Biological Aspects, Therapeutic Implications, and Circulating Biomarkers. *Cancers (Basel)*. 15:4026. doi: 10.3390/cancers15164026.

Chamcheu JC, Roy T, Uddin MB, Banang-Mbeumi S, Chamcheu RN, Walker AL, *et al*. (2019). Role and Therapeutic Targeting of the PI3K/Akt/mTOR Signaling Pathway in Skin Cancer: A Review of Current Status and Future Trends on Natural and Synthetic Agents Therapy. *Cells*. 8:803. doi: 10.3390/cells8080803.

Chan SH, Chiang J, Ngeow J. (2021). CDKN2A germline alterations and the relevance of genotype-phenotype associations in cancer predisposition. *Hered Cancer Clin Pract*. 19:21. doi: 10.1186/s13053-021-00178-x.

Chaudhary N, Choudhary BS, Shah SG, Khapare N, Dwivedi N, Gaikwad A, *et al*. (2021). Lipocalin 2 expression promotes tumor progression and therapy resistance by inhibiting ferroptosis in colorectal cancer. *Int J Cancer*. 149:1495-1511. doi: 10.1002/ijc.33711.

Chen C, Wang Z, Ding Y, Wang L, Wang S, Wang H, *et al*. (2022). DNA Methylation: From Cancer Biology to Clinical Perspectives. *Front Biosci (Landmark Ed)*. 27:326. doi: 10.31083/j.fbl2712326.

Chen X, Yu C, Kang R, Tang D. (2020). Iron Metabolism in Ferroptosis. *Front Cell Dev Biol*. 8:590226. doi: 10.3389/fcell.2020.590226.

Chen Z, Zhang Y. (2020). Role of Mammalian DNA Methyltransferases in Development. *Annu Rev Biochem*. 89:135-158. doi: 10.1146/annurev-biochem-103019-102815.

Chen Z, Wang W, Abdul Razak SR, Han T, Ahmad NH, Li X. (2023). Ferroptosis as a potential target for cancer therapy. *Cell Death Dis*. 14:460. doi: 10.1038/s41419-023-05930-w.

Chiappetta C, Proietti I, Soccodato V, Puggioni C, Zaralli R, Pacini L, *et al*. (2015). BRAF and NRAS mutations are heterogeneous and not mutually exclusive in nodular melanoma. *Appl Immunohistochem Mol Morphol*. 23:172-177. doi: 10.1097/PAI.0000000000000071.

Cho JH, Robinson JP, Arave RA, Burnett WJ, Kircher DA, Chen G, *et al*. (2015). AKT1 Activation Promotes Development of Melanoma Metastases. *Cell Rep*. 13:898-905. doi: 10.1016/j.celrep.2015.09.057.

Clark WH Jr, From L, Bernardino EA, Mihm MC. (1969). The histogenesis and biologic behavior of primary human malignant melanomas of the skin. *Cancer Res*. 29:705-727.

Collier V, Musicante M, Patel T, Liu-Smith F. (2021). Sex disparity in skin carcinogenesis and potential influence of sex hormones. *Skin Health Dis*. 1:e27. doi: 10.1002/ski2.27.

Conforti C, Zalaudek I. (2021). Epidemiology and Risk Factors of Melanoma: A Review. *Dermatol Pract Concept*. 11:e2021161S. doi: 10.5826/dpc.11S1a161S.

Conic RZ, Cabrera CI, Khorana AA, Gastman BR. (2018). Determination of the impact of melanoma surgical timing on survival using the National Cancer Database. *J Am Acad Dermatol*. 78:40-46.e7. doi: 10.1016/j.jaad.2017.08.039.

Connolly KL, Nehal KS, Busam KJ. (2015). Lentigo maligna and lentigo maligna melanoma: contemporary issues in diagnosis and management. *Melanoma Manag*. 2:171-178. doi: 10.2217/mmt.15.3.

Crescenzi E, Leonardi A, Pacifico F. (2021). NGAL as a Potential Target in Tumor Microenvironment. *Int J Mol Sci*. 22:12333. doi: 10.3390/ijms222212333.

Crescenzi E, Leonardi A, Pacifico F. (2023). Iron Metabolism in Cancer and Senescence: A Cellular Perspective. *Biology (Basel)*. 12:989. doi: 10.3390/biology12070989.

Czyz M. (2018). HGF/c-MET Signaling in Melanocytes and Melanoma. *Int J Mol Sci*. 19:3844. doi: 10.3390/ijms19123844.

Dabestani PJ, Dawson AJ, Neumeister MW, Bradbury CM. (2021). Radiation Therapy for Local Cutaneous Melanoma. *Clin Plast Surg*. 48:643-649. doi: 10.1016/j.cps.2021.05.008.

Davalos V, Esteller M. (2023). Cancer epigenetics in clinical practice. *CA Cancer J Clin*. 73:376-424. doi: 10.3322/caac.21765.

Davis EJ, Johnson DB, Sosman JA, Chandra S. (2018). Melanoma: What do all the mutations mean? *Cancer*. 124:3490-3499. doi: 10.1002/cncr.31345.

Davis S, Piggott C, Lyon C, DeSanto K. (2020). Effectiveness of dermoscopy in skin cancer diagnosis. *Can Fam Physician*. 66:739-740.

Day CP, Marchalik R, Merlino G, Michael H. (2017). Mouse models of UV-induced melanoma: genetics, pathology, and clinical relevance. *Lab Invest*. 97:698-705. doi: 10.1038/labinvest.2016.155.

Deaton AM, Bird A. (2011). CpG islands and the regulation of transcription. *Genes Dev*. 25:1010-1022. doi: 10.1101/gad.2037511.

De Giorgi V, Gori A, Savarese I, D'Errico A, Scarfì F, Papi F, *et al*. (2017). Role of BMI and hormone therapy in melanoma risk: a case-control study. *J Cancer Res Clin Oncol*. 143:1191-1197. doi: 10.1007/s00432-017-2387-5.

Deichmann U. (2016). Epigenetics: The origins and evolution of a fashionable topic. *Dev Biol*. 416:249-254. doi: 10.1016/j.ydbio.2016.06.005.

Delyon J, Lebbe C, Dumaz N. (2020). Targeted therapies in melanoma beyond BRAF: targeting NRAS-mutated and KIT-mutated melanoma. *Curr Opin Oncol*. 32:79-84. doi: 10.1097/CCO.0000000000000606.

De Simone P, Valiante M, Silipo V. (2017). Familial melanoma and multiple primary melanoma. *G Ital Dermatol Venereol*. 152:262-265. doi: 10.23736/S0392-0488.17.05554-7.

Dessinioti C, Geller AC, Whiteman DC, Garbe C, Grob JJ, Kelly JW, *et al*. (2021). Not all melanomas are created equal: a review and call for more research into nodular melanoma. *Br J Dermatol*. 185:700-710. doi: 10.1111/bjd.20388.

Dessinioti C, Stratigos AJ. (2022). An Epidemiological Update on Indoor Tanning and the Risk of Skin Cancers. *Curr Oncol*. 29:8886-8903. doi: 10.3390/curroncol29110699.

Devireddy LR, Gazin C, Zhu X, Green MR. (2005). A cell-surface receptor for lipocalin 24p3 selectively mediates apoptosis and iron uptake. *Cell*. 123:1293-1305. doi: 10.1016/j.cell.2005.10.027.

De Visser KE, Joyce JA. (2023). The evolving tumor microenvironment: From cancer initiation to metastatic outgrowth. *Cancer Cell*. 41:374-403. doi: 10.1016/j.ccell.2023.02.016.

Dinnes J, Deeks JJ, Saleh D, Chuchu N, Bayliss SE, Patel L, *et al*. (2018). Reflectance confocal microscopy for diagnosing cutaneous melanoma in adults. *Cochrane Database Syst Rev*. 12:CD013190. doi: 10.1002/14651858.CD013190.

Dobbins M, Decorby K, Choi BC. (2013). The Association between Obesity and Cancer Risk: A Meta-Analysis of Observational Studies from 1985 to 2011. *ISRN Prev Med*. 2013:680536. doi: 10.5402/2013/680536.

Dogan NU, Dogan S, Favero G, Köhler C, Dursun P. (2019). The Basics of Sentinel Lymph Node Biopsy: Anatomical and Pathophysiological Considerations and Clinical Aspects. *J Oncol*. 2019:3415630. doi: 10.1155/2019/3415630.

Dong Y, Wan Z, Gao X, Yang G, Liu L. (2021). Reprogramming Immune Cells for Enhanced Cancer Immunotherapy: Targets and Strategies. *Front Immunol*. 12:609762. doi: 10.3389/fimmu.2021.609762.

Duarte AF, Sousa-Pinto B, Azevedo LF, Barros AM, Puig S, Malvehy J, *et al*. (2021). Clinical ABCDE rule for early melanoma detection. *Eur J Dermatol*. 31:771-778. doi: 10.1684/ejd.2021.4171.

Du Q, Luu PL, Stirzaker C, Clark SJ. (2015). Methyl-CpG-binding domain proteins: readers of the epigenome. *Epigenomics*. 7:1051-1073. doi: 10.2217/epi.15.39.

Du Q, Smith GC, Luu PL, Ferguson JM, Armstrong NJ, Caldon CE, *et al*. (2021). DNA methylation is required to maintain both DNA replication timing precision and 3D genome organization integrity. *Cell Rep*. 36:109722. doi: 10.1016/j.celrep.2021.109722.

Du X, Wu L, Ur Rahman MS, Teng X, Teng L, Ye J, *et al*. (2019). Promoter Hypomethylation Is Responsible for Upregulated Expression of HAI-1 in Hepatocellular Carcinoma. *Dis Markers*. 2019:9175215. doi: 10.1155/2019/9175215.

Ebeling S, Kowalczyk A, Perez-Vazquez D, Mattiola I. (2023). Regulation of tumor angiogenesis by the crosstalk between innate immunity and endothelial cells. *Front Oncol*. 13:1171794. doi: 10.3389/fonc.2023.1171794.

Eble JA, Niland S. (2019). The extracellular matrix in tumor progression and metastasis. *Clin Exp Metastasis*. 36:171-198. doi: 10.1007/s10585-019-09966-1.

Ehrlich M, Lacey M. (2013). DNA methylation and differentiation: silencing, upregulation and modulation of gene expression. *Epigenomics*. 5:553-568. doi: 10.2217/epi.13.43.

Elhamamsy AR. (2017). Role of DNA methylation in imprinting disorders: an updated review. *J Assist Reprod Genet*. 34:549-562. doi: 10.1007/s10815-017-0895-5.

El Sharouni MA, van Diest PJ, Witkamp AJ, Sigurdsson V, van Gils CH. (2020). Subtyping Cutaneous Melanoma Matters. *JNCI Cancer Spectr*. 4:pkaa097. doi: 10.1093/jncics/pkaa097.

Emri G, Paragh G, Tósaki Á, Janka E, Kollár S, Hegedűs C, *et al*. (2018). Ultraviolet radiation-mediated development of cutaneous melanoma: An update. *J Photochem Photobiol B*. 185:169-175. doi: 10.1016/j.jphotobiol.2018.06.005.

Eroglu Z, Ribas A. (2016). Combination therapy with BRAF and MEK inhibitors for melanoma: latest evidence and place in therapy. *Ther Adv Med Oncol*. 8:48-56. doi: 10.1177/1758834015616934.

Ersahin T, Tuncbag N, Cetin-Atalay R. (2015). The PI3K/AKT/mTOR interactive pathway. *Mol Biosyst*. 11:1946-1954. doi: 10.1039/c5mb00101c.

Esteller M. (2007). Epigenetic gene silencing in cancer: the DNA hypermethylome. *Hum Mol Genet*. 16 :R50-R59. doi: 10.1093/hmg/ddm018.

Facciolà A, Venanzi Rullo E, Ceccarelli M, D'Andrea F, Coco M, Micali C, *et al*. (2020). Malignant melanoma in HIV: Epidemiology, pathogenesis, and management. *Dermatol Ther*. 33:e13180. doi: 10.1111/dth.13180.

Fajuyigbe D, Young AR. (2016). The impact of skin colour on human photobiological responses. *Pigment Cell Melanoma Res*. 29:607-618. doi: 10.1111/pcmr.12511.

Falzone L, Salemi R, Travali S, Scalisi A, McCubrey JA, Candido S, *et al*. (2016). MMP-9 overexpression is associated with intragenic hypermethylation of MMP9 gene in melanoma. *Aging (Albany NY)*. 8:933-944. doi: 10.18632/aging.100951.

Fang J, Lu Y, Zheng J, Jiang X, Shen H, Shang X, *et al*. (2023). Exploring the crosstalk between endothelial cells, immune cells, and immune checkpoints in the tumor microenvironment: new insights and therapeutic implications. *Cell Death Dis*. 14:586. doi: 10.1038/s41419-023-06119-x.

Fang WK, Xu LY, Lu XF, Liao LD, Cai WJ, Shen ZY, *et al*. (2007). A novel alternative spliced variant of neutrophil gelatinase-associated lipocalin receptor in oesophageal carcinoma cells. *Biochem J*. 403:297-303. doi: 10.1042/BJ20060836.

Fournier A, Sasai N, Nakao M, Defossez PA. (2012). The role of methyl-binding proteins in chromatin organization and epigenome maintenance. *Brief Funct Genomics*. 11:251-264. doi: 10.1093/bfgp/elr040.

Fruman DA, Chiu H, Hopkins BD, Bagrodia S, Cantley LC, Abraham RT. (2017). The PI3K Pathway in Human Disease. *Cell*. 170:605-635. doi: 10.1016/j.cell.2017.07.029.

Fu Y, Zhuang X, Xia X, Li X, Xiao K, Liu X. (2021). Correlation Between Promoter Hypomethylation and Increased Expression of Syncytin-1 in Non-Small Cell Lung Cancer. *Int J Gen Med*. 14:957-965. doi: 10.2147/IJGM.S294392.

Garbe C, Amaral T, Peris K, Hauschild A, Arenberger P, Basset-Seguin N, *et al*. (2022). European consensus-based interdisciplinary guideline for melanoma. Part 1: Diagnostics: Update 2022. *Eur J Cancer*. 170:236-255. doi: 10.1016/j.ejca.2022.03.008.

García-Lozano JA, Salerni G, Cuellar-Barboza A, la Garza JAC, Ocampo-Candiani J. (2019). Rapid Dermoscopic Changes in Nodular Melanoma. *Dermatol Pract Concept*. 10:e2020016. doi: 10.5826/dpc.1001a16.

Gassenmaier M, Lenders MM, Forschner A, Leiter U, Weide B, Garbe C, *et al*. (2021). Serum S100B and LDH at Baseline and During Therapy Predict the Outcome of Metastatic Melanoma Patients Treated with BRAF Inhibitors. *Target Oncol*. 16:197-205. doi: 10.1007/s11523-021-00792-8.

Gelmi MC, Houtzagers LE, Strub T, Krossa I, Jager MJ. (2022). MITF in Normal Melanocytes, Cutaneous and Uveal Melanoma: A Delicate Balance. *Int J Mol Sci*. 23:6001. doi: 10.3390/ijms23116001.

Giunta EF, Arrichiello G, Curvietto M, Pappalardo A, Bosso D, Rosanova M, *et al*. (2021). Epigenetic Regulation in Melanoma: Facts and Hopes. *Cells*. 10:2048. doi: 10.3390/cells10082048.

Goldstein AM, Tucker MA. (2013). Dysplastic nevi and melanoma. *Cancer Epidemiol Biomarkers Prev*. 22:528-532. doi: 10.1158/1055-9965.EPI-12-1346.

Goydos JS, Shoen SL. (2016). Acral Lentiginous Melanoma. *Cancer Treat Res*. 167:321-329. doi: 10.1007/978-3-319-22539-5_14.

Greenwood JD, Merry SP, Boswell CL. (2022). Skin Biopsy Techniques. *Prim Care*. 49:1-22. doi: 10.1016/j.pop.2021.10.001.

Grigore M, Furtunescu F, Minca D, Costache M, Garbe C, Simionescu O. (2018). The iris signal: blue periphery, tan collaret and freckles pattern - strong indicators for epidermal skin cancer in South-Eastern Europe. *J Eur Acad Dermatol Venereol*. 32:1662-1667. doi: 10.1111/jdv.14929.

Grimaldi AM, Simeone E, Festino L, Vanella V, Strudel M, Ascierto PA. (2017). MEK Inhibitors in the Treatment of Metastatic Melanoma and Solid Tumors. *Am J Clin Dermatol*. 18:745-754. doi: 10.1007/s40257-017-0292-y.

Guibert S, Weber M. (2013). Functions of DNA methylation and hydroxymethylation in mammalian development. *Curr Top Dev Biol*. 104:47-83. doi: 10.1016/B978-0-12-416027-9.00002-4.

Guo L, Qi J, Wang H, Jiang X, Liu Y. (2020). Getting under the skin: The role of CDK4/6 in melanomas. *Eur J Med Chem*. 204:112531. doi: 10.1016/j.ejmech.2020.112531.

Guo W, Wu Z, Chen J, Guo S, You W, Wang S, *et al*. (2022). Nanoparticle delivery of miR-21-3p sensitizes melanoma to anti-PD-1 immunotherapy by promoting ferroptosis. *J Immunother Cancer*. 10:e004381. doi: 10.1136/jitc-2021-004381.

Guo YJ, Pan WW, Liu SB, Shen ZF, Xu Y, Hu LL. (2020). ERK/MAPK signalling pathway and tumorigenesis. *Exp Ther Med*. 19:1997-2007. doi: 10.3892/etm.2020.8454.

Gupta V, Sharma VK. (2019). Skin typing: Fitzpatrick grading and others. *Clin Dermatol*. 37:430-436. doi: 10.1016/j.clindermatol.2019.07.010.

Haddadi N, Lin Y, Travis G, Simpson AM, Nassif NT, McGowan EM. (2018). PTEN/PTENP1: 'Regulating the regulator of RTK-dependent PI3K/Akt signalling', new targets for cancer therapy. *Mol Cancer*. 17:37. doi: 10.1186/s12943-018-0803-3.

Han L, Su B, Li WH, Zhao Z. (2008). CpG island density and its correlations with genomic features in mammalian genomes. *Genome Biol*. 9:R79. doi: 10.1186/gb-2008-9-5-r79.

Hartman ML, Czyz M. (2015). MITF in melanoma: mechanisms behind its expression and activity. *Cell Mol Life Sci*. 72:1249-1260. doi: 10.1007/s00018-014-1791-0.

Hartman RI, Lin JY. (2019). Cutaneous Melanoma-A Review in Detection, Staging, and Management. *Hematol Oncol Clin North Am*. 33:25-38. doi: 10.1016/j.hoc.2018.09.005.

Hayes AJ, Larkin J. (2018). BMI and outcomes in melanoma: more evidence for the obesity paradox. *Lancet Oncol*. 19:269-270. doi: 10.1016/S1470-2045(18)30077-9.

Hoffmann F, Zarbl R, Niebel D, Sirokay J, Fröhlich A, Posch C, *et al*. (2020). Prognostic and predictive value of PD-L2 DNA methylation and mRNA expression in melanoma. *Clin Epigenetics*. 12:94. doi: 10.1186/s13148-020-00883-9.

Holmes GA, Vassantachart JM, Limone BA, Zumwalt M, Hirokane J, Jacob SE. (2018). Using Dermoscopy to Identify Melanoma and Improve Diagnostic Discrimination. *Fed Pract*. 35:S39-S45.

Hornung A, Steeb T, Wessely A, Brinker TJ, Breakell T, Erdmann M, *et al*. (2021). The Value of Total Body Photography for the Early Detection of Melanoma: A Systematic Review. *Int J Environ Res Public Health*. 18:1726. doi: 10.3390/ijerph18041726.

Huang H. (2018). Matrix Metalloproteinase-9 (MMP-9) as a Cancer Biomarker and MMP-9 Biosensors: Recent Advances. *Sensors (Basel)*. 18:3249. doi: 10.3390/s18103249.

Huang J, Zhang L, Wan D, Zhou L, Zheng S, Lin S, *et al*. (2021). Extracellular matrix and its therapeutic potential for cancer treatment. *Signal Transduct Target Ther*. 6:153. doi: 10.1038/s41392-021-00544-0.

Hugdahl E, Kalvenes MB, Mannelqvist M, Ladstein RG, Akslen LA. (2018). Prognostic impact and concordance of TERT promoter mutation and protein expression in matched primary and metastatic cutaneous melanoma. *Br J Cancer*. 118:98-105. doi: 10.1038/bjc.2017.384.

Hunt BG, Glastad KM, Yi SV, Goodisman MA. (2013). The function of intragenic DNA methylation: insights from insect epigenomes. *Integr Comp Biol*. 53:319-328. doi: 10.1093/icb/ict003.

Hvidberg V, Jacobsen C, Strong RK, Cowland JB, Moestrup SK, Borregaard N. (2005). The endocytic receptor megalin binds the iron transporting neutrophil-gelatinase-associated lipocalin with high affinity and mediates its cellular uptake. *FEBS Lett*. 579:773-777. doi: 10.1016/j.febslet.2004.12.031.

Iannetti A, Pacifico F, Acquaviva R, Lavorgna A, Crescenzi E, Vascotto C, *et al*. (2008). The neutrophil gelatinase-associated lipocalin (NGAL), a NF-kappaB-regulated gene, is a survival factor for thyroid neoplastic cells. *Proc Natl Acad Sci USA*. 105:14058-14063. doi: 10.1073/pnas.0710846105.

Ilango S, Paital B, Jayachandran P, Padma PR, Nirmaladevi R. (2020). Epigenetic alterations in cancer. *Front Biosci (Landmark Ed)*. 25:1058-1109. doi: 10.2741/4847.

Ito S, Wakamatsu K, Sarna T. (2018). Photodegradation of Eumelanin and Pheomelanin and Its Pathophysiological Implications. *Photochem Photobiol*. 94:409-420. doi: 10.1111/php.12837.

Ivashko IN, Kolesar JM. (2016). Pembrolizumab and nivolumab: PD-1 inhibitors for advanced melanoma. *Am J Health Syst Pharm*. 73:193-201. doi: 10.2146/ajhp140768.

Jain S, Clark JI. (2015). Ipilimumab for the treatment of melanoma. Melanoma *Manag*. 2:33-39. doi: 10.2217/mmt.14.25.

Janka EA, Várvölgyi T, Sipos Z, Soós A, Hegyi P, Kiss S, *et al*. (2021). Predictive Performance of Serum S100B Versus LDH in Melanoma Patients: A Systematic Review and Meta-Analysis. *Front Oncol*. 11:772165. doi: 10.3389/fonc.2021.772165.

Jankowska AM, Millward CL, Caldwell CW. (2015). The potential of DNA modifications as biomarkers and therapeutic targets in oncology. *Expert Rev Mol Diagn*. 15:1325-1337. doi: 10.1586/14737159.2015.1084229.

Jayasinghe D, Nufer KL, Betz-Stablein B, Soyer HP, Janda M. (2022). Body Site Distribution of Acquired Melanocytic Naevi and Associated Characteristics in the General Population of Caucasian Adults: A Scoping Review. *Dermatol Ther (Heidelb)*. 12:2453-2488. doi: 10.1007/s13555-022-00806-x.

Jenkins NC, Grossman D. (2013). Role of melanin in melanocyte dysregulation of reactive oxygen species. *Biomed Res Int*. 2013:908797. doi: 10.1155/2013/908797.

Jeziorska DM, Murray RJS, De Gobbi M, Gaentzsch R, Garrick D, Ayyub H, *et al*. (2017). DNA methylation of intragenic CpG islands depends on their transcriptional activity during differentiation and disease. *Proc Natl Acad Sci U S A*. 114:E7526-E7535. doi: 10.1073/pnas.1703087114.

Jitian Mihulecea CR, Rotaru M. (2023). Review: The Key Factors to Melanomagenesis. *Life (Basel)*. 13:181. doi: 10.3390/life13010181.

Jones PA. (2012). Functions of DNA methylation: islands, start sites, gene bodies and beyond. *Nat Rev Genet*. 13:484-492. doi: 10.1038/nrg3230.

Jørgensen N, Sayed A, Jeppesen HB, Persson G, Weisdorf I, Funck T, *et al*. (2020). Characterization of HLA-G Regulation and HLA Expression in Breast Cancer and Malignant Melanoma Cell Lines upon IFN-γ Stimulation and Inhibition of DNA Methylation. *Int J Mol Sci*. 21:4307. doi: 10.3390/ijms21124307.

Juric V, O'Sullivan C, Stefanutti E, Kovalenko M, Greenstein A, Barry-Hamilton V, *et al*. (2018). MMP-9 inhibition promotes anti-tumor immunity through disruption of biochemical and physical barriers to T-cell trafficking to tumors. *PLoS One*. 13:e0207255. doi: 10.1371/journal.pone.0207255.

Karagianni F, Pavlidis A, Malakou LS, Piperi C, Papadavid E. (2022). Predominant Role of mTOR Signaling in Skin Diseases with Therapeutic Potential. *Int J Mol Sci*. 23:1693. doi: 10.3390/ijms23031693.

Karami Fath M, Azargoonjahromi A, Soofi A, Almasi F, Hosseinzadeh S, Khalili S, *et al*. (2022). Current understanding of epigenetics role in melanoma treatment and resistance. *Cancer Cell Int*. 22:313. doi: 10.1186/s12935-022-02738-0.

Karran P, Brem R. (2016). Protein oxidation, UVA and human DNA repair. *DNA Repair (Amst)*. 44:178-185. doi: 10.1016/j.dnarep.2016.05.024.

Kee D, McArthur G. (2014). Targeted therapies for cutaneous melanoma. *Hematol Oncol Clin North Am*. 28:491-505. doi: 10.1016/j.hoc.2014.02.003.

Khan AQ, Travers JB, Kemp MG. (2018). Roles of UVA radiation and DNA damage responses in melanoma pathogenesis. *Environ Mol Mutagen*. 59:438-460. doi: 10.1002/em.22176.

Klemm SL, Shipony Z, Greenleaf WJ. (2019). Chromatin accessibility and the regulatory epigenome. *Nat Rev Genet*. 20:207-220. doi: 10.1038/s41576-018-0089-8.

Kollmann K, Briand C, Bellutti F, Schicher N, Blunder S, Zojer M, *et al*. (2019). The interplay of CDK4 and CDK6 in melanoma. *Oncotarget*. 10:1346-1359. doi: 10.18632/oncotarget.26515.

Kong BY, Carlino MS, Menzies AM. (2016). Biology and treatment of BRAF mutant metastatic melanoma. *Melanoma Manag*. 3:33-45. doi: 10.2217/mmt.15.38.

Kulis M, Queirós AC, Beekman R, Martín-Subero JI. (2013). Intragenic DNA methylation in transcriptional regulation, normal differentiation and cancer. *Biochim Biophys Acta*. 1829:1161-1174. doi: 10.1016/j.bbagrm.2013.08.001.

Kumar R, Taylor M, Miao B, Ji Z, Njauw JC, Jönsson G, *et al*. (2015). BAP1 has a survival role in cutaneous melanoma. *J Invest Dermatol*. 135:1089-1097. doi: 10.1038/jid.2014.528.

Lacal I, Ventura R. (2018). Epigenetic Inheritance: Concepts, Mechanisms and Perspectives. *Front Mol Neurosci*. 11:292. doi: 10.3389/fnmol.2018.00292.

Lagacé F, Noorah BN, Conte S, Mija LA, Chang J, Cattelan L, *et al*. (2023). Assessing Skin Cancer Risk Factors, Sun Safety Behaviors and Melanoma Concern in Atlantic Canada: A Comprehensive Survey Study. *Cancers (Basel)*. 15:3753. doi: 10.3390/cancers15153753.

Lake D, Corrêa SA, Müller J. (2016). Negative feedback regulation of the ERK1/2 MAPK pathway. *Cell Mol Life Sci*. 73:4397-4413. doi: 10.1007/s00018-016-2297-8.

Lakshminarasimhan R, Liang G. (2016). The Role of DNA Methylation in Cancer. *Adv Exp Med Biol*. 945:151-172. doi: 10.1007/978-3-319-43624-1_7.

Lavie D, Ben-Shmuel A, Erez N, Scherz-Shouval R. (2022). Cancer-associated fibroblasts in the single-cell era. *Nat Cancer*. 3:793-807. doi: 10.1038/s43018-022-00411-z.

Lavoro A, Falzone L, Tomasello B, Conti GN, Libra M, Candido S. (2023). In silico analysis of the solute carrier (SLC) family in cancer indicates a link among

DNA methylation, metabolic adaptation, drug response, and immune reactivity. *Front Pharmacol*. 14:1191262. doi: 10.3389/fphar.2023.1191262.

Law MH, Macgregor S, Hayward NK. (2012). Melanoma genetics: recent findings take us beyond well-traveled pathways. *J Invest Dermatol*. 132:1763-1774. doi: 10.1038/jid.2012.75.

Lee SM, Choi WY, Lee J, Kim YJ. (2015). The regulatory mechanisms of intragenic DNA methylation. *Epigenomics*. 7:527-531. doi: 10.2217/epi.15.38. PMID: 26111026.

Lei X, Lei Y, Li JK, Du WX, Li RG, Yang J, *et al*. (2020). Immune cells within the tumor microenvironment: Biological functions and roles in cancer immunotherapy. *Cancer Lett*. 470:126-133. doi: 10.1016/j.canlet.2019.11.009.

Leonardi GC, Falzone L, Salemi R, Zanghì A, Spandidos DA, Mccubrey JA, *et al*. (2018). Cutaneous melanoma: From pathogenesis to therapy (Review). *Int J Oncol*. 52:1071-1080. doi: 10.3892/ijo.2018.4287.

Leu JI, Murphy ME, George DL. (2022). Targeting ErbB3 and Cellular NADPH/NADP+ Abundance Sensitizes Cutaneous Melanomas to Ferroptosis Inducers. *ACS Chem Biol*. 17:1038-1044. doi: 10.1021/acschembio.2c00113.

Li FJ, Long HZ, Zhou ZW, Luo HY, Xu SG, Gao LC. (2022). System Xc-/GSH/GPX4 axis: An important antioxidant system for the ferroptosis in drug-resistant solid tumor therapy. *Front Pharmacol*. 13:910292. doi: 10.3389/fphar.2022.910292.

Li J, Cao F, Yin HL, Huang ZJ, Lin ZT, Mao N, *et al*. (2020). Ferroptosis: past, present and future. *Cell Death Dis*. 11:88. doi: 10.1038/s41419-020-2298-2.

Li S, He Y, Chen K, Sun J, Zhang L, He Y, *et al*. (2021). RSL3 Drives Ferroptosis through NF-κB Pathway Activation and GPX4 Depletion in Glioblastoma. *Oxid Med Cell Longev*. 2021:2915019. doi: 10.1155/2021/2915019.

Liao Y, Jia X, Ren Y, Deji Z, Gesang Y, Ning N, *et al*. (2021). Suppressive role of microRNA-130b-3p in ferroptosis in melanoma cells correlates with DKK1 inhibition and Nrf2-HO-1 pathway activation. *Hum Cell*. 34:1532-1544. doi: 10.1007/s13577-021-00557-5.

Lin X, Ping J, Wen Y, Wu Y. (2020). The Mechanism of Ferroptosis and Applications in Tumor Treatment. *Front Pharmacol*. 11:1061. doi: 10.3389/fphar.2020.01061.

Liu F, Li N, Yang W, Wang R, Yu J, Wang X. (2018). The expression analysis of NGAL and NGALR in clear cell renal cell carcinoma. *Gene*. 676:269-278. doi: 10.1016/j.gene.2018.08.060.

Liu J, Song X, Kuang F, Zhang Q, Xie Y, Kang R, *et al*. (2021). NUPR1 is a critical repressor of ferroptosis. *Nat Commun*. 12:647. doi: 10.1038/s41467-021-20904-2.

Liu T, Han C, Wang S, Fang P, Ma Z, Xu L, *et al*. (2019). Cancer-associated fibroblasts: an emerging target of anti-cancer immunotherapy. *J Hematol Oncol*. 12:86. doi: 10.1186/s13045-019-0770-1.

Long GV, Swetter SM, Menzies AM, Gershenwald JE, Scolyer RA. (2023). Cutaneous melanoma. *Lancet*. 402:485-502. doi: 10.1016/S0140-6736(23)00821-8.

Lopes J, Rodrigues CMP, Gaspar MM, Reis CP. (2022). Melanoma Management: From Epidemiology to Treatment and Latest Advances. *Cancers (Basel)*. 14:4652. doi: 10.3390/cancers14194652.

Loras A, Gil-Barrachina M, Marqués-Torrejón MÁ, Perez-Pastor G, Martinez-Cadenas C. (2022). UV-Induced Somatic Mutations Driving Clonal Evolution in Healthy Skin, Nevus, and Cutaneous *Melanoma. Life (Basel)*. 12:1339. doi: 10.3390/life12091339.

Lo Russo PM. (2016). Inhibition of the PI3K/AKT/mTOR Pathway in Solid Tumors. *J Clin Oncol*. 34:3803-3815. doi: 10.1200/JCO.2014.59.0018.

Luke JJ, Schwartz GK. (2013). Chemotherapy in the management of advanced cutaneous malignant melanoma. *Clin Dermatol*. 31:290-297. doi: 10.1016/j.clindermatol.2012.08.016.

Luo M, Wu L, Zhang K, Wang H, Zhang T, Gutierrez L, *et al*. (2018). miR-137 regulates ferroptosis by targeting glutamine transporter SLC1A5 in melanoma. *Cell Death Differ*. 25:1457-1472. doi: 10.1038/s41418-017-0053-8.

Lyko F. (2018). The DNA methyltransferase family: a versatile toolkit for epigenetic regulation. *Nat Rev Genet*. 19:81-92. doi: 10.1038/nrg.2017.80.

Lynch HT, Shaw TG. (2016). Familial atypical multiple mole melanoma (FAMMM) syndrome: history, genetics, and heterogeneity. *Fam Cancer*. 15:487-491. doi: 10.1007/s10689-016-9888-2.

Mahamat-Saleh Y, Hughes MCB, Miura K, Malt MK, von Schuckmann L, Khosrotehrani K, *et al*. (2020). Patterns of Omega-3 and Omega-6 Fatty Acid Dietary Intake and Melanoma Thickness at Diagnosis. *Cancer Epidemiol Biomarkers Prev*. 29:1647-1653. doi: 10.1158/1055-9965.EPI-20-0319.

Malagoli C, Malavolti M, Farnetani F, Longo C, Filippini T, Pellacani G, *et al*. (2019). Food and Beverage Consumption and Melanoma Risk: A Population-Based Case-Control Study in Northern Italy. *Nutrients*. 11:2206. doi: 10.3390/nu11092206.

Manganelli M, Guida S, Ferretta A, Pellacani G, Porcelli L, Azzariti A, *et al*. (2021). Behind the Scene: Exploiting MC1R in Skin Cancer Risk and Prevention. *Genes (Basel)*. 12:1093. doi: 10.3390/genes12071093.

Manzano JL, Layos L, Bugés C, de Los Llanos Gil M, Vila L, Martínez-Balibrea E, *et al*. (2016). Resistant mechanisms to BRAF inhibitors in melanoma. *Ann Transl Med*. 4:237. doi: 10.21037/atm.2016.06.07.

Marra A, Scognamiglio G, Peluso I, Botti G, Fusciello C, Filippelli A, *et al*. (2017). Immune Checkpoint Inhibitors in Melanoma and HIV Infection. *Open AIDS J*. 11:91-100. doi: 10.2174/1874613601711010091.

Maresca V, Flori E, Picardo M. (2015). Skin phototype: a new perspective. *Pigment Cell Melanoma Res*. 28:378-389. doi: 10.1111/pcmr.12365.

Martin JM, Ghaferi JM, Cummins DL, Mamelak AJ, Schmults CD, Parikh M, *et al*. (2009). Changes in skin tanning attitudes. Fashion articles and advertisements in the early 20th century. *Am J Public Health*. 99:2140-2146. doi: 10.2105/AJPH.2008.144352.

Maunakea AK, Chepelev I, Zhao K. (2010). Epigenome mapping in normal and disease States. *Circ Res*. 107:327-339. doi: 10.1161/CIRCRESAHA.110.222463.

McKenzie C, Nahm WJ, Kearney CA, Zampella JG. (2023). Sun-protective behaviors and sunburn among US adults. *Arch Dermatol Res*. 315:1665-1674. doi: 10.1007/s00403-023-02547-z.

Mendizabal I, Zeng J, Keller TE, Yi SV. (2017). Body-hypomethylated human genes harbor extensive intragenic transcriptional activity and are prone to cancer-associated dysregulation. *Nucleic Acids Res*. 45:4390-4400. doi: 10.1093/nar/gkx020.

Meng D, Carvajal RD. (2019). KIT as an Oncogenic Driver in Melanoma: An Update on Clinical Development. *Am J Clin Dermatol*. 20:315-323. doi: 10.1007/s40257-018-0414-1.

Merkel A, Esteller M. (2022). Experimental and Bioinformatic Approaches to Studying DNA Methylation in Cancer. *Cancers (Basel)*. 14:349. doi: 10.3390/cancers14020349.

Micevic G, Theodosakis N, Bosenberg M. (2017). Aberrant DNA methylation in melanoma: biomarker and therapeutic opportunities. *Clin Epigenetics*. 9:34. doi: 10.1186/s13148-017-0332-8.

Ming Z, Lim SY, Rizos H. (2020). Genetic Alterations in the INK4a/ARF Locus: Effects on Melanoma Development and Progression. *Biomolecules*. 10:1447. doi: 10.3390/biom10101447.

Moarii M, Boeva V, Vert JP, Reyal F. (2015). Changes in correlation between promoter methylation and gene expression in cancer. *BMC Genomics*. 16:873. doi: 10.1186/s12864-015-1994-2.

Moore LD, Le T, Fan G. (2013). DNA methylation and its basic function. *Neuropsychopharmacology*. 38:23-38. doi: 10.1038/npp.2012.112.

Morales S, Monzo M, Navarro A. (2017). Epigenetic regulation mechanisms of microRNA expression. *Biomol Concepts*. 8:203-212. doi: 10.1515/bmc-2017-0024.

Motwani J, Eccles MR. (2021). Genetic and Genomic Pathways of Melanoma Development, Invasion and Metastasis. *Genes (Basel)*. 12:1543. doi: 10.3390/genes12101543.

Muñoz-Couselo E, Adelantado EZ, Ortiz C, García JS, Perez-Garcia J. (2017). NRAS-mutant melanoma: current challenges and future prospect. *Onco Targets Ther*. 10:3941-3947. doi: 10.2147/OTT.S117121.

Nagl L, Horvath L, Pircher A, Wolf D. (2020). Tumor Endothelial Cells (TECs) as Potential Immune Directors of the Tumor Microenvironment - New Findings and Future Perspectives. *Front Cell Dev Biol*. 8:766. doi: 10.3389/fcell.2020.00766.

Nagore E, Rachakonda S, Kumar R. (2019). TERT promoter mutations in melanoma survival. *Oncotarget*. 10:1546-1548. doi: 10.18632/oncotarget.26688.

Naidoo C, Kruger CA, Abrahamse H. (2018). Photodynamic Therapy for Metastatic Melanoma Treatment: A Review. *Technol Cancer Res Treat*. 17:1533033818791795. doi: 10.1177/1533033818791795.

Naik PP. (2021). Role of Biomarkers in the Integrated Management of Melanoma. *Dis Markers*. 2021:6238317. doi: 10.1155/2021/6238317.

Neri F, Rapelli S, Krepelova A, Incarnato D, Parlato C, Basile G, *et al*. (2017). Intragenic DNA methylation prevents spurious transcription initiation. *Nature*. 543:72-77. doi: 10.1038/nature21373.

Niebel D, Fröhlich A, Zarbl R, Fietz S, de Vos L, Vogt TJ, *et al*. (2022). DNA methylation regulates TIGIT expression within the melanoma microenvironment, is prognostic for overall survival, and predicts progression-free survival in patients treated with anti-PD-1 immunotherapy. *Clin Epigenetics*. 14:50. doi: 10.1186/s13148-022-01270-2.

Nikolouzakis TK, Falzone L, Lasithiotakis K, Krüger-Krasagakis S, Kalogeraki A, Sifaki M, *et al*. (2020). Current and Future Trends in Molecular Biomarkers for Diagnostic, Prognostic, and Predictive Purposes in Non-Melanoma Skin Cancer. *J Clin Med*. 9:2868. doi: 10.3390/jcm9092868.

Nishiyama A, Nakanishi M. (2021). Navigating the DNA methylation landscape of cancer. *Trends Genet*. 37:1012-1027. doi: 10.1016/j.tig.2021.05.002.

Noel SE, Stoneham AC, Olsen CM, Rhodes LE, Green AC. (2014). Consumption of omega-3 fatty acids and the risk of skin cancers: a systematic review and meta-analysis. *Int J Cancer*. 135:149-156. doi: 10.1002/ijc.28630.

Obrador E, Liu-Smith F, Dellinger RW, Salvador R, Meyskens FL, Estrela JM. (2019). Oxidative stress and antioxidants in the pathophysiology of malignant melanoma. *Biol Chem*. 400:589-612. doi: 10.1515/hsz-2018-0327

Olsen CM, Knight LL, Green AC. (2014). Risk of melanoma in people with HIV/AIDS in the pre- and post-HAART eras: a systematic review and meta-analysis of cohort studies. *PLoS One*. 9:e95096. doi: 10.1371/journal.pone.0095096.

Ostrowski SM, Fisher DE. (2021). Biology of Melanoma. *Hematol Oncol Clin North Am*. 35:29-56. doi: 10.1016/j.hoc.2020.08.010.

Ottaviano M, Giunta EF, Tortora M, Curvietto M, Attademo L, Bosso D, *et al*. (2021). BRAF Gene and Melanoma: Back to the Future. *Int J Mol Sci*. 22:3474. doi: 10.3390/ijms22073474.

Paluncic J, Kovacevic Z, Jansson PJ, Kalinowski D, Merlot AM, Huang ML, *et al*. (2016). Roads to melanoma: Key pathways and emerging players in

melanoma progression and oncogenic signaling. *Biochim Biophys Acta*. 1863:770-784. doi: 10.1016/j.bbamcr.2016.01.025.

Pan Y, Liu G, Zhou F, Su B, Li Y. (2018). DNA methylation profiles in cancer diagnosis and therapeutics. *Clin Exp Med*. 18:1-14. doi: 10.1007/s10238-017-0467-0.

Panning A, Samlowski W, Allred G. (2023). Lack of Influence of Non-Overlapping Mutations in BRAF, NRAS, or NF1 on 12-Month Best Objective Response and Long-Term Survival after Checkpoint Inhibitor-Based Treatment for Metastatic Melanoma. *Cancers (Basel)*. 15:3527. doi: 10.3390/cancers15133527.

Parry L, Clarke AR. (2011). The Roles of the Methyl-CpG Binding Proteins in Cancer. *Genes Cancer*. 2:618-630. doi: 10.1177/1947601911418499.

Patty BJ, Hainer SJ. (2020). Non-Coding RNAs and Nucleosome Remodeling Complexes: An Intricate Regulatory Relationship. *Biology (Basel)*. 9:213. doi: 10.3390/biology9080213.

Pavlidis ET, Pavlidis TE. (2022). Diagnostic biopsy of cutaneous melanoma, sentinel lymph node biopsy and indications for lymphadenectomy. *World J Clin Oncol*. 13:861-865. doi: 10.5306/wjco.v13.i10.861.

Pham DDM, Guhan S, Tsao H. (2020). KIT and Melanoma: Biological Insights and Clinical Implications. *Yonsei Med J*. 61:562-571. doi: 10.3349/ymj.2020.61.7.562.

Philpott C, Tovell H, Frayling IM, Cooper DN, Upadhyaya M. (2017). The NF1 somatic mutational landscape in sporadic human cancers. *Hum Genomics*. 11:13. doi: 10.1186/s40246-017-0109-3.

Pinault L, Fioletov V. (2017). Sun exposure, sun protection and sunburn among Canadian adults. *Health Rep*. 28:12-19.

Pizzagalli MD, Bensimon A, Superti-Furga G. (2021). A guide to plasma membrane solute carrier proteins. *FEBS J*. 288:2784-2835. doi: 10.1111/febs.15531.

Ponti G, Manfredini M, Greco S, Pellacani G, Depenni R, Tomasi A, *et al*. (2017). BRAF, NRAS and C-KIT Advanced Melanoma: Clinico-pathological Features, Targeted-Therapy Strategies and Survival. *Anticancer Res*. 37:7043-7048. doi: 10.21873/anticanres.12175.

Proietti I, Skroza N, Michelini S, Mambrin A, Balduzzi V, Bernardini N, *et al*. (2020). BRAF Inhibitors: Molecular Targeting and Immunomodulatory Actions. *Cancers (Basel)*. 12:1823.

Qayoom H, Sofi S, Mir MA. (2023). Targeting tumor microenvironment using tumor-infiltrating lymphocytes as therapeutics against tumorigenesis. *Immunol Res*. 71:588-599. doi: 10.1007/s12026-023-09376-2.

Rajabi-Estarabadi A, Bittar JM, Zheng C, Nascimento V, Camacho I, Feun LG, *et al*. (2019). Optical coherence tomography imaging of melanoma skin cancer. *Lasers Med Sci*. 34:411-420. doi: 10.1007/s10103-018-2696-1.

Ralli M, Botticelli A, Visconti IC, Angeletti D, Fiore M, Marchetti P, *et al*. (2020). Immunotherapy in the Treatment of Metastatic Melanoma: Current Knowledge and Future Directions. *J Immunol Res*. 2020:9235638. doi: 10.1155/2020/9235638.

Randic T, Kozar I, Margue C, Utikal J, Kreis S. (2021). NRAS mutant melanoma: Towards better therapies. *Cancer Treat Rev*. 99:102238. doi: 10.1016/j.ctrv.2021.102238.

Rashed H, Flatman K, Bamford M, Teo KW, Saldanha G. (2017). Breslow density is a novel prognostic feature in cutaneous malignant melanoma. *Histopathology*. 70:264-272. doi: 10.1111/his.13060.

Rashid K, Ahmad A, Liang L, Liu M, Cui Y, Liu T. (2021). Solute carriers as potential oncodrivers or suppressors: their key functions in malignant tumor formation. *Drug Discov Today*. 26:1689-1701. doi: 10.1016/j.drudis.2021.03.004.

Rashid S, Shaughnessy M, Tsao H. (2023). Melanoma classification and management in the era of molecular medicine. *Dermatol Clin*. 41:49-63. doi: 10.1016/j.det.2022.07.017.

Rastrelli M, Tropea S, Rossi CR, Alaibac M. (2014). Melanoma: epidemiology, risk factors, pathogenesis, diagnosis and classification. *In Vivo*. 28:1005-1011.

Read J, Wadt KA, Hayward NK. (2016). Melanoma genetics. *J Med Genet*. 53:1-14. doi: 10.1136/jmedgenet-2015-103150.

Recillas-Targa F. (2022). Cancer Epigenetics: An Overview. *Arch Med Res*. 53:732-740. doi: 10.1016/j.arcmed.2022.11.003.

Rochette L, Dogon G, Rigal E, Zeller M, Cottin Y, Vergely C. (2022). Lipid Peroxidation and Iron Metabolism: Two Corner Stones in the Homeostasis Control of Ferroptosis. *Int J Mol Sci*. 24:449. doi: 10.3390/ijms24010449.

Rivera CM, Ren B. (2013). Mapping human epigenomes. *Cell*. 155:39-55. doi: 10.1016/j.cell.2013.09.011.

Ross SE, Bogdanovic O. (2019). TET enzymes, DNA demethylation and pluripotency. *Biochem Soc Trans*. 47:875-885. doi: 10.1042/BST20180606.

Saginala K, Barsouk A, Aluru JS, Rawla P, Barsouk A. (2021). Epidemiology of Melanoma. *Med Sci (Basel)*. 9:63. doi: 10.3390/medsci9040063.

Saghafinia S, Mina M, Riggi N, Hanahan D, Ciriello G. (2018). Pan-Cancer Landscape of Aberrant DNA Methylation across Human Tumors. *Cell Rep*. 25:1066-1080.e8. doi: 10.1016/j.celrep.2018.09.082.

Saida T. (2019). Histogenesis of cutaneous malignant melanoma: The vast majority do not develop from melanocytic nevus but arise de novo as melanoma in situ. *J Dermatol*. 46:80-94. doi: 10.1111/1346-8138.14737.

Sample A, He YY. (2018). Mechanisms and prevention of UV-induced melanoma. *Photodermatol Photoimmunol Photomed*. 34:13-24. doi: 10.1111/phpp.12329.

Sandru F, Dumitrascu MC, Petca A, Carsote M, Petca RC, Ghemigian A. (2022). Melanoma in patients with Li-Fraumeni syndrome (Review). *Exp Ther Med*. 23:75. doi: 10.3892/etm.2021.10998.

Sargen MR, Calista D, Elder DE, Massi D, Chu EY, Potrony M, *et al*. (2020). Histologic features of melanoma associated with germline mutations of CDKN2A, CDK4, and POT1 in melanoma-prone families from the United States, Italy, and Spain. *J Am Acad Dermatol*. 83:860-869. doi: 10.1016/j.jaad.2020.03.100.

Sarkar D, Leung EY, Baguley BC, Finlay GJ, Askarian-Amiri ME. (2015). Epigenetic regulation in human melanoma: past and future. *Epigenetics*. 10:103-121. doi: 10.1080/15592294.2014.1003746.

Savoia P, Fava P, Casoni F, Cremona O. (2019). Targeting the ERK Signaling Pathway in Melanoma. *Int J Mol Sci*. 20:1483. doi: 10.3390/ijms20061483.

Sawada Y, Nakamura M. (2021). Daily Lifestyle and Cutaneous Malignancies. *Int J Mol Sci*. 22:5227. doi: 10.3390/ijms22105227.

Schwartz MR, Luo L, Berwick M. (2019). Sex Differences in Melanoma. *Curr Epidemiol Rep*. 6:112-118. doi: 10.1007/s40471-019-00192-7.

Scolyer RA, Rawson RV, Gershenwald JE, Ferguson PM, Prieto VG. (2020). Melanoma pathology reporting and staging. *Mod Pathol*. 33:15-24. doi: 10.1038/s41379-019-0402-x.

Seidel JA, Otsuka A, Kabashima K. (2018). Anti-PD-1 and Anti-CTLA-4 Therapies in Cancer: Mechanisms of Action, Efficacy, and Limitations. *Front Oncol*. 8:86. doi: 10.3389/fonc.2018.00086.

Serman N, Vranic S, Glibo M, Serman L, Bukvic Mokos Z. (2022). Genetic risk factors in melanoma etiopathogenesis and the role of genetic counseling: A concise review. *Bosn J Basic Med Sci*. 22:673-682. doi: 10.17305/bjbms.2021.7378.

Sharp AJ, Stathaki E, Migliavacca E, Brahmachary M, Montgomery SB, Dupre Y, *et al*. (2011). DNA methylation profiles of human active and inactive X chromosomes. *Genome Res*. 21:1592-600. doi: 10.1101/gr.112680.110.

Shellenberger RA, Fayyaz F, Sako Z, Schaeffer M, Tawagi K, Scheidel C, *et al*. (2020). Impact of Biopsy Technique on Clinically Important Outcomes for Cutaneous Melanoma: A Systematic Review and Meta-analysis. *Mayo Clin Proc Innov Qual Outcomes*. 4:373-383. doi: 10.1016/j.mayocpiqo.2020.04.005.

Shenker N, Flanagan JM. (2012). Intragenic DNA methylation: implications of this epigenetic mechanism for cancer research. *Br J Cancer*. 106:248-253. doi: 10.1038/bjc.2011.550.

Shibata Y, Yasui H, Higashikawa K, Miyamoto N, Kuge Y. (2019). Erastin, a ferroptosis-inducing agent, sensitized cancer cells to X-ray irradiation via glutathione starvation in vitro and in vivo. *PLoS One*. 14:e0225931. doi: 10.1371/journal.pone.0225931.

Shreberk-Hassidim R, Ostrowski SM, Fisher DE. (2023). The Complex Interplay between Nevi and Melanoma: Risk Factors and Precursors. *Int J Mol Sci*. 24:3541. doi: 10.3390/ijms24043541.

Sizemore ST, Sizemore GM, Booth CN, Thompson CL, Silverman P, Bebek G, *et al*. (2014). Hypomethylation of the MMP7 promoter and increased expression of MMP7 distinguishes the basal-like breast cancer subtype from other triple-negative tumors. *Breast Cancer Res Treat*. 146:25-40. doi: 10.1007/s10549-014-2989-4.

Skvortsova K, Iovino N, Bogdanović O. (2018). Functions and mechanisms of epigenetic inheritance in animals. *Nat Rev Mol Cell Biol*. 19:774-790. doi: 10.1038/s41580-018-0074-2.

Skvortsova K, Stirzaker C, Taberlay P. (2019). The DNA methylation landscape in cancer. *Essays Biochem*. 63:797-811. doi: 10.1042/EBC20190037.

Slingluff CL Jr, Lee S, Zhao F, Chianese-Bullock KA, Olson WC, Butterfield LH, *et al*. (2013). A randomized phase II trial of multiepitope vaccination with melanoma peptides for cytotoxic T cells and helper T cells for patients with metastatic melanoma (E1602). *Clin Cancer Res*. 19:4228-4238. doi: 10.1158/1078-0432.CCR-13-0002.

Smith LK, Arabi S, Lelliott EJ, McArthur GA, Sheppard KE. (2020). Obesity and the Impact on Cutaneous Melanoma: Friend or Foe? *Cancers (Basel)*. 12:1583. doi: 10.3390/cancers12061583.

Smith ZD, Meissner A. (2013). DNA methylation: roles in mammalian development. *Nat Rev Genet*. 14:204-220. doi: 10.1038/nrg3354.

Sobierajska K, Ciszewski WM, Sacewicz-Hofman I, Niewiarowska J. (2020). Endothelial Cells in the Tumor Microenvironment. *Adv Exp Med Biol*. 1234:71-86. doi: 10.1007/978-3-030-37184-5_6.

Solano F. (2020). Photoprotection and Skin Pigmentation: Melanin-Related Molecules and Some Other New Agents Obtained from Natural Sources. *Molecules*. 25:1537. doi: 10.3390/molecules25071537.

Song W, Li D, Tao L, Luo Q, Chen L. (2020). Solute carrier transporters: the metabolic gatekeepers of immune cells. *Acta Pharm Sin B*. 10:61-78. doi: 10.1016/j.apsb.2019.12.006.

Soura E, Eliades PJ, Shannon K, Stratigos AJ, Tsao H. (2016). Hereditary melanoma: Update on syndromes and management: Genetics of familial atypical multiple mole melanoma syndrome. *J Am Acad Dermatol*. 74:395-407; quiz 408-10. doi: 10.1016/j.jaad.2015.08.038.

Statello L, Guo CJ, Chen LL, Huarte M. (2021). Gene regulation by long non-coding RNAs and its biological functions. *Nat Rev Mol Cell Biol*. 22:96-118. doi: 10.1038/s41580-020-00315-9.

Stolarova L, Jelinkova S, Storchova R, Machackova E, Zemankova P, Vocka M, *et al*. (2020). Identification of Germline Mutations in Melanoma Patients with Early Onset, Double Primary Tumors, or Family Cancer History by NGS

Analysis of 217 Genes. *Biomedicines*. 8:404. doi: 10.3390/biomedicines8100404.

Strashilov S, Yordanov A. (2021). Aetiology and Pathogenesis of Cutaneous Melanoma: Current Concepts and Advances. *Int J Mol Sci*. 22:6395. doi: 10.3390/ijms22126395.

Subbiah V, Baik C, Kirkwood JM. (2020). Clinical Development of BRAF plus MEK Inhibitor Combinations. *Trends Cancer*. 6:797-810. doi: 10.1016/j.trecan.2020.05.009.

Sui X, Zhang R, Liu S, Duan T, Zhai L, Zhang M, *et al*. (2018). RSL3 Drives Ferroptosis Through GPX4 Inactivation and ROS Production in Colorectal Cancer. *Front Pharmacol*. 9:1371. doi: 10.3389/fphar.2018.01371.

Sun X, Zhang N, Yin C, Zhu B, Li X. (2020). Ultraviolet Radiation and Melanomagenesis: From Mechanism to Immunotherapy. *Front Oncol*. 10:951. doi: 10.3389/fonc.2020.00951.

Sung H, Ferlay J, Siegel RL, Laversanne M, Soerjomataram I, Jemal A, *et al*. (2021). Global Cancer Statistics 2020: GLOBOCAN Estimates of Incidence and Mortality Worldwide for 36 Cancers in 185 Countries. *CA Cancer J Clin*. 71:209-249. doi: 10.3322/caac.21660.

Tagliabue E, Gandini S, Bellocco R, Maisonneuve P, Newton-Bishop J, Polsky D, *et al*. (2018). MC1R variants as melanoma risk factors independent of at-risk phenotypic characteristics: a pooled analysis from the M-SKIP project. *Cancer Manag Res*. 10:1143-1154. doi: 10.2147/CMAR.S155283.

Tagliaferri L, Lancellotta V, Fionda B, Mangoni M, Casà C, Di Stefani A, *et al*. (2022). Immunotherapy and radiotherapy in melanoma: a multidisciplinary comprehensive review. *Hum Vaccin Immunother*. 18:1903827. doi: 10.1080/21645515.2021.1903827.

Testori AAE, Blankenstein SA, van Akkooi ACJ. (2019). Surgery for Metastatic Melanoma: an Evolving Concept. *Curr Oncol Rep*. 21:98. doi: 10.1007/s11912-019-0847-6.

Thomas L, Puig S. (2017). Dermoscopy, Digital Dermoscopy and Other Diagnostic Tools in the Early Detection of Melanoma and Follow-up of High-risk Skin Cancer Patients. *Acta Derm Venereol*. 218:14-21. doi: 10.2340/00015555-2719.

Tivey A, Britton F, Scott JA, Rothwell D, Lorigan P, Lee R. (2022). Circulating Tumour DNA in Melanoma-Clinic Ready? *Curr Oncol Rep*. 24:363-373. doi: 10.1007/s11912-021-01151-6.

Toussi A, Mans N, Welborn J, Kiuru M. (2020). Germline mutations predisposing to melanoma. *J Cutan Pathol*. 47:606-616. doi: 10.1111/cup.13689.

Trindade FM, de Freitas MLP, Bittencourt FV. (2021). Dermoscopic evaluation of superficial spreading melanoma. *An Bras Dermatol*. 96:139-147. doi: 10.1016/j.abd.2020.06.012.

Tronick E, Hunter RG. (2016). Waddington, Dynamic Systems, and Epigenetics. *Front Behav Neurosci*. 10:107. doi: 10.3389/fnbeh.2016.00107.

Uguen A, Guéguen P, Talagas M, Costa S, De Braekeleer M, Marcorelles P. (2016). BRAF and NRAS Mutations are Not Mutually Exclusive in Melanoma and in Single Melanoma Cells. *Appl Immunohistochem Mol Morphol*. 24:e14-e15. doi: 10.1097/PAI.0000000000000217.

Ullah R, Yin Q, Snell AH, Wan L. (2022). RAF-MEK-ERK pathway in cancer evolution and treatment. *Semin Cancer Biol*. 85:123-154. doi: 10.1016/j.semcancer.2021.05.010.

Uner OE, See TRO, Szalai E, Grossniklaus HE, Stålhammar G. (2021). Estimation of the timing of BAP1 mutation in uveal melanoma progression. *Sci Rep*. 11:8923. doi: 10.1038/s41598-021-88390-6.

Walter FM, Prevost AT, Vasconcelos J, Hall PN, Burrows NP, Morris HC, *et al*. (2013). Using the 7-point checklist as a diagnostic aid for pigmented skin lesions in general practice: a diagnostic validation study. *Br J Gen Pract*. 63:e345-e353. doi: 10.3399/bjgp13X667213.

Wang Q, Xiong F, Wu G, Liu W, Chen J, Wang B, *et al*. (2022). Chen Y. Gene body methylation in cancer: molecular mechanisms and clinical applications. *Clin Epigenetics*. 14:154. doi: 10.1186/s13148-022-01382-9.

Wang Q, Shao X, Zhang Y, Zhu M, Wang FXC, Mu J, *et al*. (2023). Role of tumor microenvironment in cancer progression and therapeutic strategy. *Cancer Med*. 12:11149-11165. doi: 10.1002/cam4.5698.

Wang S, Yi X, Wu Z, Guo S, Dai W, Wang H, *et al*. (2022). CAMKK2 Defines Ferroptosis Sensitivity of Melanoma Cells by Regulating AMPK–NRF2 Pathway. *J Invest Dermatol*. 142:189-200.e8. doi: 10.1016/j.jid.2021.05.025.

Wang X, Xu S, Zhang L, Cheng X, Yu H, Bao J, *et al*. (2021). Vitamin C induces ferroptosis in anaplastic thyroid cancer cells by ferritinophagy activation. *Biochem Biophys Res Commun*. 551:46-53. doi: 10.1016/j.bbrc.2021.02.126.

Ward-Peterson M, Acuña JM, Alkhalifah MK, Nasiri AM, Al-Akeel ES, Alkhaldi TM, *et al*. (2016). Association Between Race/Ethnicity and Survival of Melanoma Patients in the United States Over 3 Decades: A Secondary Analysis of SEER Data. *Medicine (Baltimore)*. 95:e3315. doi: 10.1097/MD.0000000000003315.

Wei EX, Li X, Nan H. (2019). Having a first-degree relative with melanoma increases lifetime risk of melanoma, squamous cell carcinoma, and basal cell carcinoma. *J Am Acad Dermatol*. 81:489-499. doi: 10.1016/j.jaad.2019.04.044.

Wei J, Gao X, Qin Y, Liu T, Kang Y. (2020). An Iron Metabolism-Related SLC22A17 for the Prognostic Value of Gastric Cancer. *Onco Targets Ther*. 13:12763-12775. doi: 10.2147/OTT.S287811.

Wellbrock C, Arozarena I. (2016). The Complexity of the ERK/MAP-Kinase Pathway and the Treatment of Melanoma Skin Cancer. *Front Cell Dev Biol*. 4:33. doi: 10.3389/fcell.2016.00033.

Weyers W. (2018). Screening for malignant melanoma-a critical assessment in historical perspective. *Dermatol Pract Concept*. 8:89-103. doi: 10.5826/dpc.0802a06.

Willsmore ZN, Coumbe BGT, Crescioli S, Reci S, Gupta A, Harris RJ, *et al*. (2021). Combined anti-PD-1 and anti-CTLA-4 checkpoint blockade: Treatment of melanoma and immune mechanisms of action. *Eur J Immunol*. 51:544-556. doi: 10.1002/eji.202048747.

Wilson MA, Schuchter LM. (2016). Chemotherapy for Melanoma. *Cancer Treat Res*. 167:209-229. doi: 10.1007/978-3-319-22539-5_8.

Wong DJ, Ribas A. (2016). Targeted Therapy for Melanoma. *Cancer Treat Res*. 167:251-262. doi: 10.1007/978-3-319-22539-5_10.

Wong JSL, Kwok GGW, Tang V, Li BCW, Leung R, Chiu J, *et al*. (2021). Ipilimumab and nivolumab/pembrolizumab in advanced hepatocellular carcinoma refractory to prior immune checkpoint inhibitors. *J Immunother Cancer*. 9:e001945. doi: 10.1136/jitc-2020-001945.

Wright K, Ly T, Kriet M, Czirok A, Thomas SM. (2023). Cancer-Associated Fibroblasts: Master Tumor Microenvironment Modifiers. *Cancers (Basel)*. 15:1899. doi: 10.3390/cancers15061899.

Wu S, Cho E, Li WQ, Weinstock MA, Han J, Qureshi AA. (2016). History of Severe Sunburn and Risk of Skin Cancer Among Women and Men in 2 Prospective Cohort Studies. *Am J Epidemiol*. 183:824-833. doi: 10.1093/aje/kwv282.

Wu W, Geng Z, Bai H, Liu T, Zhang B. (2021). Ammonium Ferric Citrate induced Ferroptosis in Non-Small-Cell Lung Carcinoma through the inhibition of GPX4-GSS/GSR-GGT axis activity. *Int J Med Sci*. 18:1899-1909. doi: 10.7150/ijms.54860.

Wu X, Zhang Y. (2017). TET-mediated active DNA demethylation: mechanism, function and beyond. *Nat Rev Genet*. 18:517-534. doi: 10.1038/nrg.2017.33.

Wu Y, Yu C, Luo M, Cen C, Qiu J, Zhang S, *et al*. (2020). Ferroptosis in Cancer Treatment: Another Way to Rome. *Front Oncol*. 10:571127. doi: 10.3389/fonc.2020.571127.

Xavier MJ, Roman SD, Aitken RJ, Nixon B. (2019). Transgenerational inheritance: how impacts to the epigenetic and genetic information of parents affect offspring health. *Hum Reprod Update*. 25:518-540. doi: 10.1093/humupd/dmz017.

Xiao X, Yeoh BS, Vijay-Kumar M. (2017). Lipocalin 2: An Emerging Player in Iron Homeostasis and Inflammation. *Annu Rev Nutr*. 37:103-130. doi: 10.1146/annurev-nutr-071816-064559.

Xiao Y, Yu D. (2021). Tumor microenvironment as a therapeutic target in cancer. *Pharmacol Ther*. 221:107753. doi: 10.1016/j.pharmthera.2020.107753.

Xie Z, Zhou Z, Yang S, Zhang S, Shao B. (2023). Epigenetic regulation and therapeutic targets in the tumor microenvironment. *Mol Biomed*. 4:17. doi: 10.1186/s43556-023-00126-2.

Yaeger R, Corcoran RB. (2019). Targeting Alterations in the RAF-MEK Pathway. *Cancer Discov*. 9:329-341. doi: 10.1158/2159-8290.CD-18-1321.

Yamashita K, Hosoda K, Nishizawa N, Katoh H, Watanabe M. (2018). Epigenetic biomarkers of promoter DNA methylation in the new era of cancer treatment. *Cancer Sci*. 109:3695-3706. doi: 10.1111/cas.13812.

Yan HF, Zou T, Tuo QZ, Xu S, Li H, Belaidi AA, *et al*. (2021). Ferroptosis: mechanisms and links with diseases. *Signal Transduct Target Ther*. 6:49. doi: 10.1038/s41392-020-00428-9.

Yang J, Nie J, Ma X, Wei Y, Peng Y, Wei X. (2019). Targeting PI3K in cancer: mechanisms and advances in clinical trials. *Mol Cancer*. 18:26. doi: 10.1186/s12943-019-0954-x.

Yang J, Xu J, Wang W, Zhang B, Yu X, Shi S. (2023). Epigenetic regulation in the tumor microenvironment: molecular mechanisms and therapeutic targets. *Signal Transduct Target Ther*. 8:210. doi: 10.1038/s41392-023-01480-x.

Yang K, Fung TT, Nan H. (2018). An Epidemiological Review of Diet and Cutaneous Malignant Melanoma. *Cancer Epidemiol Biomarkers Prev*. 27:1115-1122. doi: 10.1158/1055-9965.EPI-18-0243.

Yang K, Oak ASW, Slominski RM, Brożyna AA, Slominski AT. (2020). Current Molecular Markers of Melanoma and Treatment Targets. *Int J Mol Sci*. 21:3535. doi: 10.3390/ijms21103535.

Yao F, Deng Y, Zhao Y, Mei Y, Zhang Y, Liu X, *et al*. (2021). A targetable LIFR-NF-κB-LCN2 axis controls liver tumorigenesis and vulnerability to ferroptosis. *Nat Commun*. 12:7333. doi: 10.1038/s41467-021-27452-9.

Yuan Y, Ni S, Zhuge A, Li B, Li L. (2021). Iron Regulates the Warburg Effect and Ferroptosis in Colorectal Cancer. *Front Oncol*. 11:614778. doi: 10.3389/fonc.2021.614778.

Yuan Z, Li Y, Zhang S, Wang X, Dou H, Yu X, *et al*., (2023). Extracellular matrix remodeling in tumor progression and immune escape: from mechanisms to treatments. *Mol Cancer*. 22:48. doi: 10.1186/s12943-023-01744-8.

Zhang M, Qureshi AA, Geller AC, Frazier L, Hunter DJ, Han J. (2012). Use of tanning beds and incidence of skin cancer. *J Clin Oncol*. 30:1588-1593. doi: 10.1200/JCO.2011.39.3652.

Zhang MW, Fujiwara K, Che X, Zheng S, Zheng L. (2017). DNA methylation in the tumor microenvironment. *J Zhejiang Univ Sci B*. 18:365-372. doi: 10.1631/jzus.B1600579.

Zhang XD, Liu ZY, Wang MS, Guo YX, Wang XK, Luo K, *et al*. (2023). Mechanisms and regulations of ferroptosis. *Front Immunol*. 14:1269451. doi: 10.3389/fimmu.2023.1269451.

Zhang Y, Zhang Y, Sun K, Meng Z, Chen L. (2019). The SLC transporter in nutrient and metabolic sensing, regulation, and drug development. *J Mol Cell Biol*. 11:1-13. doi: 10.1093/jmcb/mjy052.

Zhang Y, Sun Z, Jia J, Du T, Zhang N, Tang Y, *et al*. (2021). Overview of Histone Modification. *Adv Exp Med Biol*. 1283:1-16. doi: 10.1007/978-981-15-8104-5_1.

Zhao S, Li P, Wu W, Wang Q, Qian B, Li X, *et al*. (2021). Roles of ferroptosis in urologic malignancies. *Cancer Cell Int*. 21:676. doi: 10.1186/s12935-021-02264-5.

Zhao Y, Li Y, Zhang R, Wang F, Wang T, Jiao Y. (2020). The Role of Erastin in Ferroptosis and Its Prospects in Cancer Therapy. *Onco Targets Ther*. 13:5429-5441. doi: 10.2147/OTT.S254995.

Zhong J, Yan W, Wang C, Liu W, Lin X, Zou Z, *et al*. (2022). BRAF Inhibitor Resistance in Melanoma: Mechanisms and Alternative Therapeutic Strategies. *Curr Treat Options Oncol*. 23:1503-1521. doi: 10.1007/s11864-022-01006-7.

Zhong F, Lin Y, Zhao L, Yang C, Ye Y, Shen Z. (2023). Reshaping the tumour immune microenvironment in solid tumours via tumour cell and immune cell DNA methylation: from mechanisms to therapeutics. *Br J Cancer*. 129:24-37. doi: 10.1038/s41416-023-02292-0.

Zhou Y, Song KY, Giubellino A. (2019). The Role of MET in Melanoma and Melanocytic Lesions. *Am J Pathol*. 189:2138-2148. doi: 10.1016/j.ajpath.2019.08.002.